LEVEL

MECHANICS OF COMPOSITE MATERIALS

WITH DIFFERENT MODULI IN TENSION AND COMPRESSION

by

ROBERT M. JONES

JULY 1978

CIVIL AND MECHANICAL ENGINEERING DEPARTMENT

SCHOOL OF ENGINEERING AND APPLIED SCIENCE

SOUTHERN METHODIST UNIVERSITY

DALLAS, TEXAS 75275

OCT

D

APPROVED FOR PUBLIC RELEASE; DISTRIBUTION UNLIMITED

Qualified requestors may obtain additional
copies from the Defense Documentation Center.
All others should apply to the National Tech-
nical Information Service.

Conditions of Reproduction

Reproduction, translation, publication, use,
and disposal in whole or in part by or for the
United States Government is permitted.

REPORT DOCUMENTATION PAGE	READ INSTRUCTIONS BEFORE COMPLETING FORM

1. REPORT NUMBER AFOSR-TR- 78 - 1 4 0 0	2. GOVT ACCESSION NO.	3. RECIPIENT'S CATALOG NUMBER

4. TITLE (and Subtitle) MECHANICS OF COMPOSITE MATERIALS WITH DIFFERENT MODULI IN TENSION AND COMPRESSION	5. TYPE OF REPORT & PERIOD COVERED FINAL JUNE 1973 - MAY 1978
	6. PERFORMING ORG. REPORT NUMBER

7. AUTHOR(s) ROBERT M. JONES	8. CONTRACT OR GRANT NUMBER(s) AFOSR 73-2532

9. PERFORMING ORGANIZATION NAME AND ADDRESS SOUTHERN METHODIST UNIVERSITY CIVIL AND MECHANICAL ENGINEERING DEPARTMENT DALLAS, TEXAS 75275	10. PROGRAM ELEMENT, PROJECT, TASK AREA & WORK UNIT NUMBERS 61102F 2307B1

11. CONTROLLING OFFICE NAME AND ADDRESS AIR FORCE OFFICE OF SCIENTIFIC RESEARCH/NA BUILDING 410 BOLLING AFB, D.C. 20332	12. REPORT DATE JULY 1978
	13. NUMBER OF PAGES 129

14. MONITORING AGENCY NAME & ADDRESS(if different from Controlling Office)	15. SECURITY CLASS. (of this report) UNCLASSIFIED
	15a. DECLASSIFICATION/DOWNGRADING SCHEDULE

16. DISTRIBUTION STATEMENT (of this Report)

Approved for public release;
distribution unlimited.

17. DISTRIBUTION STATEMENT (of the abstract entered in Block 20, if different from Report)

18. SUPPLEMENTARY NOTES

19. KEY WORDS (Continue on reverse side if necessary and identify by block number)

COMPOSITE MATERIALS, STRESS ANALYSIS, BUCKLING, DIFFERENT STIFFNESSES, ORTHOTROPY, ANISOTROPY, GRAPHITE, CARBON-CARBON, GRAPHITE-EPOXY, BORON-EPOXY, BORON-ALUMINUM

20. ABSTRACT (Continue on reverse side if necessary and identify by block number)
Composite materials have been used for several years in thermal protection systems such as reentry vehicle nosetips and heatshields as well as in more conventional aerospace structures such as laminated wings and stabilizers in the latest aircraft. Many composite materials, e.g., ATJ-S graphite, carbon-carbon, and graphite-epoxy, exhibit different strength and stiffness behavior in tension and compression. The moduli differences range from 20% for ATJ-S graphite to between 100% and 400% for carbon-carbon. The principal objective

DD $_{1\ JAN\ 73}^{FORM}$ 1473 EDITION OF 1 NOV 65 IS OBSOLETE UNCLASSIFIED

BLOCK 20, ABSTRACT, continued

of this research is to model the behavior of solid bodies with different elastic moduli in tension and compression as well as the behavior of laminated plates and shells that have different elastic moduli in tension and compression and lamination asymmetries. The results of this work are coordinated with research sponsored by the Air Force Materials Laboratory on nonlinear stress-strain behavior of reentry vehicle materials. This report is a summary of work done during the last five years.

D D
RECEIVED
OCT 27 1978
D

TABLE OF CONTENTS

1. INTRODUCTION

Composite materials are receiving increasing attention for many aerospace structural applications because of the thermal protection advantages as well as cost and weight savings over competing materials. Rocket nozzles, for example, require materials that exhibit high thermal insulating qualities in addition to maintaining structural integrity. These characteristics are somewhat contradictory because of the peculiar nature of the resulting thermal stress problem. That is, adding more material to increase the thermal insulation increases the thermal stresses and thereby decreases the structural integrity. Thus, the design analysis tools must be quite accurate and hence very representative of the actual nozzle materials. Laminated plates and shells are basic aerospace structural elements. The use of these elements in the latest aircraft and missile structures depends on precise knowledge of their behavior. Accordingly, accurate design analysis tools are essential for all these structural applications of composite materials.

A significant characteristic of composite materials is the difference in behavior under tensile and compressive loads. Both the elastic moduli (stiffnesses) and the strengths in the principal material property directions of these orthotropic materials are different for tensile loading than for compressive loading. This characteristic behavior is shown schematically in the stress-strain curve of Fig. 1. This phenomenon is but one of several differences that make composite materials more difficult to analyze (and hence design) than the more common structural materials such as aluminum.

Both fiber-reinforced and granular composite materials have different moduli in tension and compression as displayed in Table 1.
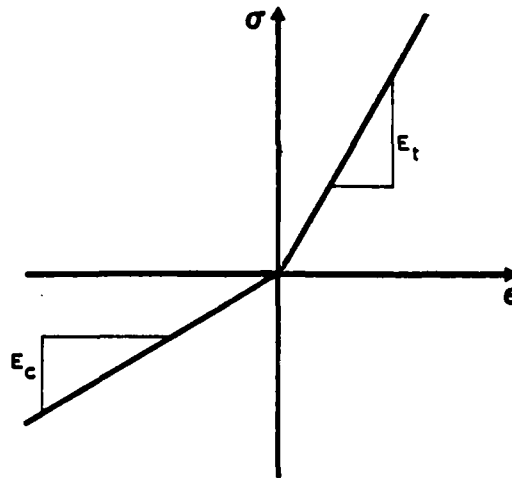
FIGURE 1   STRESS-STRAIN CURVE FOR A MATERIAL WITH
DIFFERENT MODULI IN TENSION AND COMPRESSION

TABLE 1

TENSION AND COMPRESSION MODULI RELATIONSHIPS
FOR SEVERAL COMMON COMPOSITE MATERIALS

MATERIAL	FIBROUS OR GRANULAR	REPRESENTATIVE MODULI RELATIONSHIP
GLASS/EPOXY	FIBROUS	$E_t = 1.2E_c$
BORON/EPOXY	FIBROUS	$E_c = 1.2E_t$
GRAPHITE/EPOXY	FIBROUS	$E_t = 1.4E_c$
CARBON/CARBON	FIBROUS	$E_t = 2\text{-}5E_c$
ZTA GRAPHITE	GRANULAR	$E_c = 1.2E_t$
ATJ-S GRAPHITE	GRANULAR	$E_t = 1.2E_c$

Unidirectional glass fibers in an epoxy matrix have compression moduli 20% lower than the tension moduli [1]. For some unidirectional boron/ epoxy fiber-reinforced laminae, the compression moduli are about 15-20% larger than the tension moduli [2]. In contrast, some unidirectional graphite/epoxy fiber-reinforced laminae have tension moduli up to 40% greater than the compression moduli [2]. Other fiber-reinforced composites such as carbon/carbon have tension moduli from two to five times the compression moduli [3]. Thus, no clear pattern of larger tension than compression moduli or vice versa exists for fiber-reinforced composite materials. A plausible physical explanation for this puzzling circumstance is not available.

For granular composite materials, the picture is no clearer. ZTA graphite has tension moduli as much as 20% lower than the compression moduli [4]. On the other hand, ATJ-S graphite has tension moduli as much as 20% more than the compression moduli [5].

Many other materials have different tension and compression moduli. Which modulus is higher may depend on the fiber or granule stiffness relative to the matrix stiffness. This relationship would influence whether the fibers or granules tend to contact and hence stiffen the composite. A general physical explanation of the reasons for different behavior in tension and compression is not yet available. Investigation of micro-mechanical behavioral aspects of composite materials may lead to a rational explanation of this phenomenon. Until such an explanation is available, the apparent behavior can be used in analyzing the stress-strain behavior of materials. That is, even without knowing why the materials behave as they do, their apparent behavior can be modeled.

Actual stress-strain behavior is probably not as simple as shown

FIGURE 2   COMPARISON OF ACTUAL STRESS-STRAIN BEHAVIOR WITH THE BILINEAR MODEL
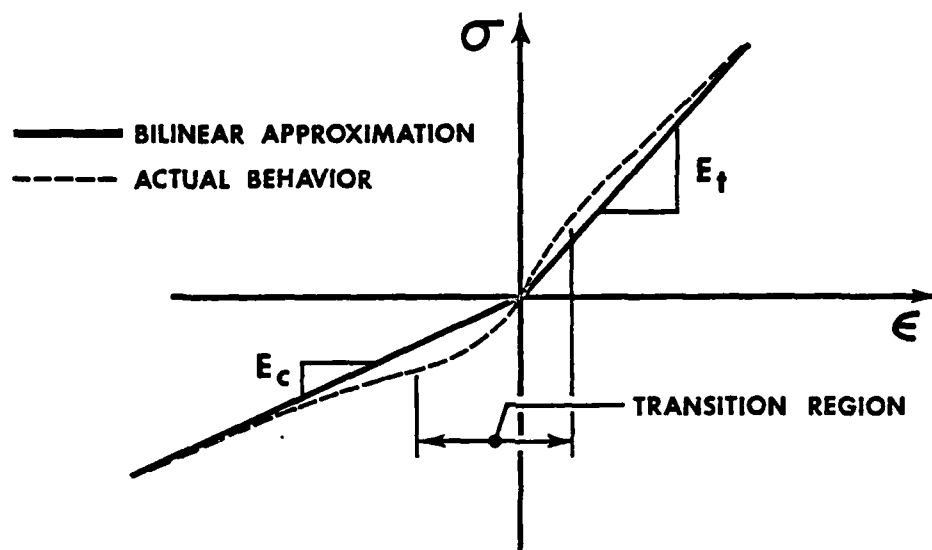
in Fig. 1.   Instead, a nonlinear transition region may exist between
the tension and compression linear portions of the stress-strain curve.
The measurement of strains near zero stress is difficult to perform accu-
rately, but the stress-strain behavior might be as shown in Fig. 2 where-
in replacement of actual behavior with a bilinear model is offered as a
simplification of obviously nonlinear behavior.   For most materials, the
mechanical property data are insufficient to justify use of a more com-
plex material model.   However, one possible disadvantage of the bilinear
stress-strain curve approximation is that a discontinuity in slope
(modulus) occurs at the origin of the stress-strain curve.

Given that the uniaxial stress-strain behavior is approximated with
a bilinear representation, the definition remains of the actual multi-
axial stress-strain, or constitutive, relations that are required in
structural analysis.   Over the past ten years, Ambartsumyan and his co
workers, [References 6 to 9], in the process of obtaining solutions for
stresses in shells and bodies of revolution, defined a set of stress-
strain relations that will be referred to herein as the Ambartsumyan

material model. Tabaddor [10] elaborated somewhat on the Ambartsumyan

material model. Jones [11] applied the model to buckling under biaxial

loading of circular cylindrical shells made of an isotropic material.

However, in application of the Ambartsumyan material model to orthotro-

pic materials, certain characteristics, such as a nonsymmetric compliance

matrix in the stress-strain relations [12], are apparent.

Another significant characteristic of composite materials is non-

linear stress-strain behavior. Not all composites have nonlinear beha-

vior, but for some of the most common such as ATJ-S graphite (a granular

composite) nearly all the stress-strain curves are nonlinear. In addi-

tion, fiber-reinforced composite materials such as graphite/epoxy have

nearly linear stress-strain behavior parallel to and transverse to the

fiber direction, but have highly nonlinear stress - shear strain beha-

vior as shown in Fig. 3. These material nonlinearities can be analyzed

in several fashions. For example, Jones and Nelson [13] present a
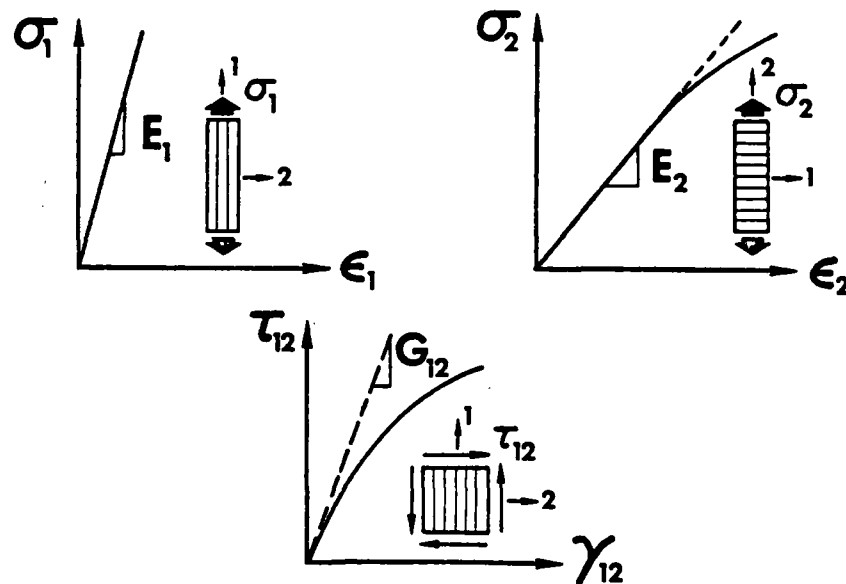
FIGURE 3 TYPICAL STRESS-STRAIN BEHAVIOR OF FIBER-REINFORCED COMPOSITE
         MATERIALS

nonlinear orthotropic model whose strain predictions agree very well with experimental data for ATJ-S graphite which exhibits the biaxial softening phenomenon (larger strains under biaxial tension than are predicted on the basis of usual Poisson effects). Also, Hahn and Tsai [14] describe a nonlinear orthotropic model for the single nonlinear shear stress - shear strain behavior typical of graphite/epoxy.

The study of nonlinear stress-strain behavior of fiber-reinforced composite materials is also motivated by the fact that the stress-strain curve nonlinearities become more pronounced at elevated temperatures and moisture contents [15]. The resin matrix materials boron/epoxy and graphite/epoxy readily absorb moisture, and increases in temperature and in moisture content greatly affect the shear stress - shear strain behavior of these materials as shown with the schematic shear stress - shear strain curves in Fig. 4. At room temperature, boron/epoxy and graphite/epoxy have nonlinear shear behavior, but an increase in temperature to 260°F
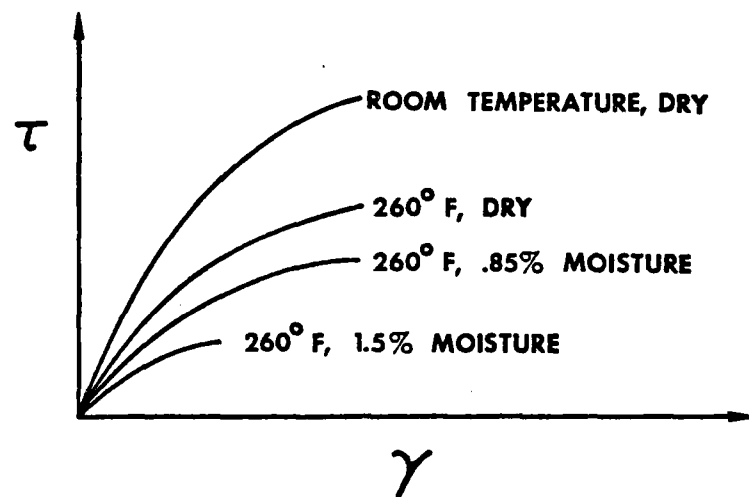
FIGURE 4 EFFECTS OF TEMPERATURE AND MOISTURE ON SHEAR STRESS - SHEAR STRAIN BEHAVIOR

leads to an even greater curvature of the stress-strain curve. As the temperature and moisture content increase from 260°F, dry to 260°F, .85% moisture (by weight of the overall composite), the curvature of the shear stress - shear strain curve again increases. For conditions of 260°F and 1.5% moisture, the stress-strain curve in Fig. 4 is not only highly nonlinear, but the ultimate capacity of the composite to withstand shear loading is greatly reduced. Fiber-reinforced composite materials are often used under conditions similar to those shown in Fig. 4, so provisions for nonlinear stress-strain behavior must be included in the analysis of these materials at elevated temperatures and moisture contents. Sufficient experimental data are not available at this time to investigate the nonlinear behavior of fiber-reinforced composite materials under conditions other than room temperature and no moisture content. However, the ideas developed in this research are applicable to fiber-reinforced composites at high temperatures and moisture contents when such experimental data do become available.

The principal objective of this project is to analyze the behavior of three-dimensional bodies as well as laminated plates and shells with different nonlinear stress-strain behavior in tension and compression. That is, both of the two aforementioned composite material characteristics, different moduli in tension and compression and nonlinear stress-strain behavior, are addressed. A secondary objective is to study the behavior of laminated plates and shells with different elastic moduli in tension and compression as well as with lamination asymmetries. This report is basically a description of the research performed during the past five years along with some of the work done for the Air Force Materials Laboratory.

2. DESCRIPTION OF RESEARCH

This description of research is divided into five parts: (1) an overview of the activities during the five years of the grant; (2) a statement of how the Principal Investigator's research was sponsored; (3) a list of the publications during the grant period; (4) a list of the advanced degrees generated during the grant; and (5) a brief discussion of each research accomplishment. An especially important result of the present research, nonlinear modeling of carbon-carbon materials, is described more fully in Section 3.

2.1 OVERVIEW OF ACTIVITIES DURING THE FIVE YEAR GRANT PERIOD

The research over the past five years under this grant has been concentrated in three related areas:

(1) material models for nonlinear multimodulus behavior of various classes of composite materials.

(2) stress analysis of solid bodies made of nonlinear multimodulus composite materials

(3) analysis of bending, buckling, and vibration behavior of laminated plates and shells including those with nonlinear multimodulus behavior.

The first area of developing appropriate material models for composite materials is an essential precursor to the application of such models in areas (2) and (3). Conversely, any model developed in area (1) must be applied in, for example, areas (2) and (3) to test its validity.

The material models are developed by first observing the physical behavior characteristics of composite materials and then attempting to construct models for stress-strain behavior that reflect those character-

8

istics. The models are applied in the context of usual structural mechanics analysis approaches to treat nonlinear multimodulus materials in various iteration and search schemes. These iteration and search schemes are sometimes multilevel in order to find all the necessary unknowns in these transcendental problems.

The structural mechanics analysis areas in which the material models are applied are, of course, consistent with the Air Force problem areas which originally motivated this research. Specifically, area (2), stress analysis of solid bodies, is now motivated by the need to predict the behavior of carbon-carbon rocket nozzles and was originally motivated by a similar need to predict the behavior of graphite and carbon-carbon re-entry vehicle nosetips. On the other hand, area (3), structural behavior of laminated plates and shells, is motivated by the obviously rapid expansion of the use of composite materials in aerospace applications. In particular, aircraft and spacecraft have many nonconventional structural mechanics design analysis needs.

The specific accomplishments during the five year grant period are described briefly later, but for now a summary or overview statement of the accomplishments is that reasonably accurate material models have been developed to portray not only the nonlinear stress-strain behavior of the most common composite materials but also the character of different stress-strain behavior under tension loading than under compression loading. These material models have been verified or validated by use in structural mechanics analysis problems related to rocket nozzles and reentry vehicle nosetips and to laminated aircraft wings and spacecraft structures. The validations range from correlation of predicted behavior with the measurements in the simplest of laboratory experiments to correlation with more

9

complex experiments and even scaled nosetip test firings.

2.2 STATEMENT OF RESEARCH SPONSORSHIP

The Principal Investigator has conducted the following sponsored research during the grant period:

(1) "Mechanics of Composite Materials with Different Moduli in Tension and Compression," Air Force Office of Scientific Research, June 1973 - May 1978.

(2) "Plastic Volume Change Effects in Deformation of Graphitic Materials," Air Force Materials Laboratory, March 1973 - November 1974.

(3) "Buckling of Shells with Different Moduli in Tension and Compression," Office of Naval Research, April 1973 - July 1974.

(4) "Nonlinear Multiaxial Modeling of Graphitic and Carbon-Carbon Materials," Air Force Materials Laboratory, February 1975 - June 1976.

All four projects are closely related because they are all applicable to problems in Air Force and Navy fiber-reinforced structures. The initial motivation for this work was thermal stress failure problems in reentry vehicle nosetips. Recently, however, the primary motivation has been thermal and mechanical stress problems in rocket nozzles. Throughout the grant period, an additional motivation has been stress analysis problems in laminated aircraft structural parts.

2.3 GRANT-SUPPORTED PUBLICATIONS

(1) "Buckling and Vibration of Unsymmetrically Laminated Cross-Ply Rectangular Plates", AIAA Journal, December 1973, pp. 1626-1632, by Robert M. Jones.

(2) "Buckling and Vibration of Antisymmetrically Laminated Angle-Ply Rectangular Plates", Journal of Applied Mechanics, December 1973, pp. 1143-1144, by Robert M. Jones, Harold S. Morgan, and James M. Whitney.

(3) "Stiffness of Orthotropic Materials and Laminated Fiber-Reinforced Composites", AIAA Journal, January 1974, pp. 112-114, by Robert M. Jones.

(4) "Mechanics of Composite Materials with Different Moduli in Tension and Compression", AFOSR-TR-74-1597, July 1974, by Robert M. Jones.

(5) "A New Material Model for the Nonlinear Biaxial Behavior of ATJ-S Graphite", Journal of Composite Materials, January 1975, pp. 10-27, by Robert M. Jones and Dudley A. R. Nelson, Jr.

(6) "Buckling of Stiffened Laminated Composite Circular Cylindrical Shells with Different Moduli in Tension and Compression", AFOSR-TR-0547, February 1975, by Robert M. Jones and Harold S. Morgan.

(7) "Buckling of Laminated Composite Circular Cylindrical Shells with Different Moduli in Tension and Compression", Proceedings of the 1975 International Conference on Composite Materials, Geneva, Switzerland and Boston, Massachusetts, 7-18 April 1975, Vol.2, pp. 318-343, by Robert M. Jones and Harold S. Morgan.

(8) "Buckling and Vibration of Cross-Ply Laminated Circular Cylindrical Shells", AIAA Journal, May 1975, pp. 664-671, by Robert M. Jones and Harold S. Morgan.

(9) "Further Characteristics of a Nonlinear Material Model for ATJ-S Graphite", Journal of Composite Materials, July 1975, pp. 251-265, by Robert M. Jones and Dudley A. R. Nelson, Jr.

(10) "Mechanics of Composite Materials with Different Moduli in Tension and Compression", AFOSR-TR-75-1519, July 1975, by Robert M. Jones.

(11) "Deflection of Unsymmetrically Laminated Cross-Ply Rectangular Plates", Proceedings of the 12th Annual Meeting of the Society of Engineering Science, 20-22 October 1975, Austin, Texas, pp. 155-167, by Robert M. Jones.

(12) "Bending and Extension of Cross-Ply Laminates with Different Moduli in Tension and Compression", Proceedings of the 17th AIAA/ASME/SAE Structures, Structural Dynamics, and Materials Conference, King of Prussia, Pennsylvania, 5-7 May 1976, pp. 158-167, by Robert M. Jones and Harold S. Morgan.

(13) "Material Models for Nonlinear Deformation of Graphite," AIAA Journal, June 1976, pp. 709-717, by Robert M. Jones and Dudley A. R. Nelson, Jr.

(14) "Theoretical-Experimental Correlation of Material Models for Nonlinear Deformation of Graphite", AIAA Journal, October 1976, pp. 1427-1435, by Robert M. Jones and Dudley A. R. Nelson, Jr.

(15) "Apparent Flexural Modulus and Strength of Multimodulus Materials" Journal of Composite Materials, October 1976, pp. 342-354, by Robert M. Jones.

(16) "Mechanics of Composite Materials with Different Moduli in Tension and Compression", AFOSR Interim Scientific Report, November 1976, by Robert M. Jones.

(17) "Stress-Strain Relations for Materials with Different Moduli in Tension and Compression", AIAA Journal, January 1977, pp. 16-23, by Robert M. Jones.

(18) "JNMDATA, A Preprocessor Computer Program for the Jones-Nelson-Morgan Nonlinear Material Models", Informal AFOSR Report, April 1977, by Robert M. Jones.

(19) "Mechanics of Composite Materials with Different Moduli in Tension and Compression", AFOSR Interim Scientific Report, July 1977, by Robert M. Jones.

(20) "Nonlinear Deformation of a Thermally Stressed Graphite Annular Disk", AIAA Journal, August 1977, pp. 1116-1122, by Robert M. Jones and H. Stuart Starrett.

(21) "A Nonsymmetric Compliance Matrix Approach to Nonlinear Multi-modulus Orthotropic Materials", AIAA Journal, October 1977, pp. 1436-1443, by Robert M. Jones.

(22) "Analysis of Nonlinear Stress-Strain Behavior of Fiber-Reinforced Composite Materials", AIAA Journal, December 1977, pp. 1669-1676, by Robert M. Jones and Harold S. Morgan.

(23) "Effect of Prebuckling Deformations on Buckling of Laminated Composite Circular Cylindrical Shells", Proceedings of the 19th AIAA/ASME Structures, Structural Dynamics, and Materials Conference, Bethesda, Maryland, 3-5 April 1978, by Robert M. Jones and Jose C. F. Henneman. To appear in AIAA Journal.

(24) "Biaxial Strength Characteristics of Fiber-Reinforced Composite Laminae", Proceedings of the Second International Conference on Composite Materials, Toronto, Canada, 16-20 April 1978, by Robert M. Jones and Jose C. F. Henneman.

(25) "Analysis of Nonlinear Deformation Behavior of Laminated Fiber-Reinforced Composite Materials", Proceedings of the Second International Conference on Composite Materials, Toronto, Canada, 16-20 April 1978, by Harold S. Morgan and Robert M. Jones.

(26) "Buckling of Cross-Ply Laminated Rectangular Plates with Nonlinear
Stress-Strain Behavior", Paper No. 78-PVP-64, ASME/CSME Pressure
Vessels and Piping Conference, Montreal, Canada, 25-29 June 1978,
by Harold S. Morgan and Robert M. Jones to appear in _Journal of
Applied Mechanics._

In addition, results from this grant research were presented in:

(1) "Nonlinear Deformation of Graphitic Materials", AFML-TR-74-259,
February 1975, by Robert M. Jones and Dudley A. R. Nelson, Jr.

(2) "Nonlinear Multiaxial Modeling of Graphite and Carbon-Carbon
Materials", AFML-TR-76-215, December 1976, by Robert M. Jones.

(3) _Mechanics of Composite Materials_, McGraw-Hill, 1975, by Robert
M. Jones.

2.4 GRANT-SUPPORTED ADVANCED DEGREES

The following individuals had partial support from this grant during their
pursuit of a degree:

(1) Dudley A. R. Nelson, Jr., Ph.D., February 1975.

(2) Harold S. Morgan, Ph.D., October 1976.

Parviz Moayad was supported during 1976-77 and A. L. Somanath during
1977-78, but they have not completed a degree. In addition, the following
individual was supported by the Brazilian Government but worked on research
for this grant:

Jose C. F. Hennemann, Ph.D., July 1975.

14

2.5 REVIEW OF SPECIFIC RESEARCH ACCOMPLISHMENTS

This review of specific research accomplishments is divided into three areas: (1) material models for nonlinear multimodulus behavior of composite materials; (2) stress analysis of solid bodies made of nonlinear multimodulus materials; and (3) analysis of bending, buckling, and vibration of laminated plates and shells including those with nonlinear multimodulus behavior. The papers and reports generated during the grant period are categorized within those three areas. Some publications are contributions in more than one area, so they are multiply cited. Each of the publications is fully cited in Section 2.3 and will be referenced with that section number and the publication number within that section, e.g., [2.3-1] is the first cited reference in Section 2.3. The material models used in applications in areas (2) and (3) generally progress over the grant period from linear elastic to linear elastic multimodulus or nonlinear elastic and finally to nonlinear multimodulus. The progress in developing and applying this hierarchy of models to various structural mechanics problems is briefly described in the following three subsections.

2.5.1 Material Models for Nonlinear Multimodulus Behavior of Composite Materials

The material models developed start from elastic and progress through nonlinear to multimodulus to, finally, nonlinear multimodulus. Chronologically, the progression is uneven in the sense that contributions were made to the nonlinear multimodulus models prior to full investigation of the nonlinear and multimodulus models. The chronological order of development will be ignored, and the progression itself will be emphasized.

2.5.1.1 Elastic Models

Elastic models serve only as a base from which to develop the

15

ultimate objective. However, two contributions were made which enable better understanding of the baseline elastic models. First, the stiffness of orthotropic materials loaded in nonprincipal material directions was investigated [2.3-3]. The off-axis stiffness is shown to be highly dependent on the shear modulus. Explicit relations are derived to enable the determination of whether the off-axis modulus is lower, higher, or in between the moduli in principal material directions. Of major significance is the observation that the off-axis modulus for a composite lamina is lower than E_2 (the stiffness transverse to the fibers for a unidirectionally reinforced lamina) if the shear modulus is low enough. The second contribution involves the strength of orthotropic materials loaded in nonprincipal material directions [2.3-24]. This problem is the strength analog of the preceding problem. Similar relations between off-axis strength and the strengths in principal material directions are derived for two common strength theories, Tsai-Hill and Tsai-Wu. Of major significance is the observation that the off-axis strength for a composite lamina is lower than Y (the strength transverse to the fibers for a unidirectionally reinforced lamina) if S (the shear strength) is low enough.

2.5.1.2 Nonlinear Models

The most significant development in nonlinear models is the Jones-Nelson-Morgan ronlinear material model. In its original form [2.3-5], the secant moduli in the various principal material directions of a composite material are expressed in terms of the strain energy density (hereafter abbreviated as strain energy) in the form

$$\text{Mechanical Property}_i = A_i \left[1 - B_i (U/U_0)^{C_i} \right] \qquad (2.1)$$

where the strain energy is

16

$$U = (\sigma_x \varepsilon_x + \sigma_y \varepsilon_y + \sigma_z \varepsilon_z + \tau_{yz} \gamma_{yz} + \tau_{zx} \gamma_{zx} + \tau_{xy} \gamma_{xy})/2 \qquad (2.2)$$

and the constants A_i, B_i, and C_i are the initial value of the mechanical property, the initial curvature of the stress-strain curve, and the rate of change of curvature of the stress-strain curve, respectively [2.3-9]. The term U_0 is used to nondimensionalize the term in brackets in Eq. (2.1). This model has been successfully used to predict the nonlinear deformation of graphite [2.3-5, 2.3-9, and 2.3-20].

A basic limitation of the model in Eq. (2.1) is that the implied stress-strain curve [the stress-strain curve that can be back-calculated from Eq. (2.1)] first rises and then falls. The rising takes place at an ever-decreasing rate and finally becomes a negative slope as shown with the short dashed curve in Fig. 2.1. The degree of stress-strain curve nonlinearity inherent to graphites is small enough that the model limitation doesn't influence the behavior. However, the nonlinearities and/or the orthotropy of fiber-reinforced composite materials are high enough that the stress-strain curve must be rationally extended beyond the defined data. An additional reason for the extension is that the energy associated with multiaxial stress states is larger than with the uniaxial stress states in which the mechanical properties are measured. The chosen form of the extension [2.3-22] is a straight line on the stress-strain curve in Fig. 2.1 and has a limit of a constant slope on the mechanical property vs. strain energy curve in Fig. 2.2. This model is tested for boron-epoxy and graphite-epoxy in Ref. 2.3-22.

A key characteristic of the nonlinear models is that the stress and strain states are unknown as are the mechanical properties, and all are transcendentally related. Thus, an iteration procedure [2.3-5] is essential to determine the proper strains and mechanical properties for a
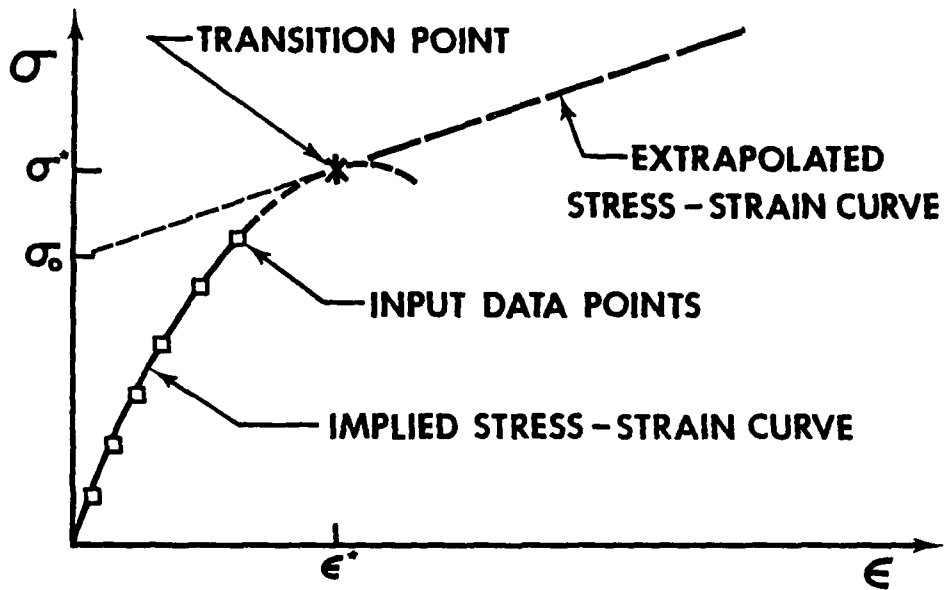
17
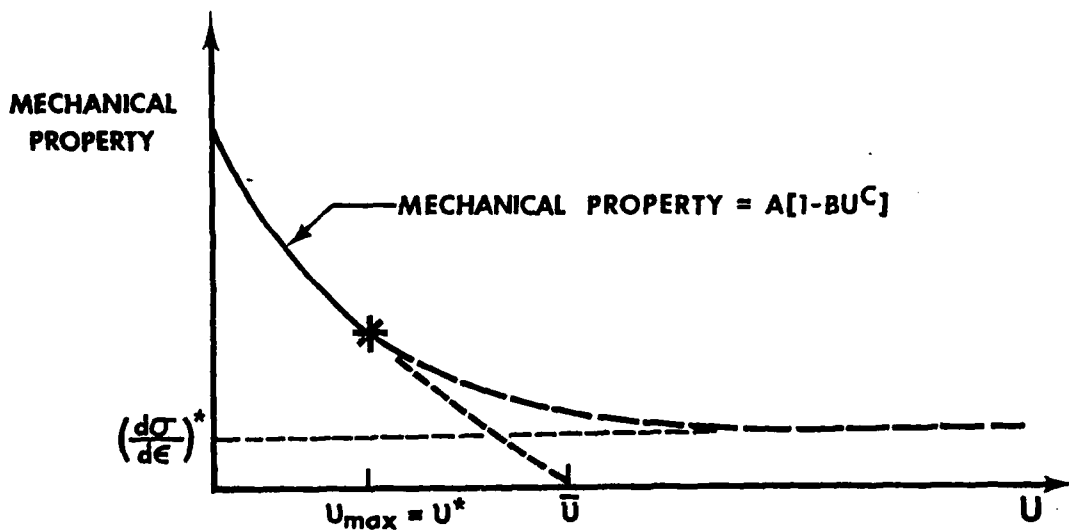
FIGURE 2.1 STRESS-STRAIN CURVE EXTRAPOLATION

FIGURE 2.2 MECHANICAL PROPERTY VERSUS STRAIN ENERGY CURVE EXTRAPOLATION

18

specified stress state.

2.5.1.3 Multimodulus Models

The basis for the multimodulus material models is Ref. 2.3-17.
There, all the logic for choosing the appropriate mechanical properties
from values under tension or compression loading is described including
how cross-compliances (Poisson's ratios) are determined. These choices
are made in principal stress coordinates to avoid any shearing stresses
which are inherently a state of mixed tension and compression. Accord-
ingly, the usual shear moduli of a material are not essential mechanical
properties. Instead, tension and compression moduli at 45° to principal
material directions are used; thus, a set of mechanical characterization
tests different from that for ordinary orthotropic materials is necessary.

The manner of choosing the tension or compression compliances in
Ref. 2.3-17 revolves about an assumption that the resulting compliance
matrix must be symmetric. The effect of relaxing this assumption is
examined in Ref. 2.3-21 where use of a nonsymmetric compliance matrix is
found to be slightly more accurate than use of a symmetric compliance
matrix for deformation of a tubular graphite specimen. However, the
difference between the two approaches is essentially negligible because
it is on the order of only a few percent.

A very simple multimodulus model is used in Ref. 2.3-15 to analyze
the usual ASTM 3-point and 4-point bending specimens when applied for
multimodulus materials. This uniaxial but nonconstant stress state is
especially easy to analyze. The significance of this work is that the
flexural modulus calculated from the prescribed ASTM equations is not the
flexural modulus of a multimodulus material. Perhaps more important is
the fact that the actual flexural modulus is a quantity derived from the
tension and compression moduli, i.e., the flexural modulus is not an

19

independent quantity. Therefore, the flexural modulus should not be the goal of any experimental program for multimodulus materials because it is not basic mechanical characterization information.

2.5.1.4 Nonlinear Multimodulus Models

The original version of the Jones-Nelson-Morgan nonlinear material model, i.e., with no stress-strain curve extrapolation, is coupled with the multimodulus compliance matrix concepts in Ref. 2.3-13 for ATJ-S graphite. The search and iteration procedures for both the nonlinear and the multimodulus elements are nested to accomplish this merger of models. The agreement between predicted and measured strains for a comprehensive hierarchy of experiments is quite impressive as will be seen in Section 2.5.2.

The nonlinear multimodulus model is not needed for the characteristics of boron-epoxy or graphite-epoxy, but is essential to the treatment of carbon-carbon. The straight line extrapolation of the stress-strain curve is necessary to fit the available carbon-carbon data, i.e., the extrapolation is not used in its original sense to arbitrarily extend data beyond their range of validity. As will be seen in Section 3, the application of the Jones-Nelson-Morgan nonlinear multimodulus material model to carbon-carbon is quite successful.

In all applications of the nonlinear material modeling procedure, the JNMDATA program [2.3-18] is essential in the otherwise tedious task of converting reported stress-strain data to mechanical property versus strain energy data and subsequently fitting Eq. (2.1) to the latter data. A nonlinear regression technique was developed for the JNMDATA program to automate the curve fitting operation and to provide the most accurate model. This program is the key to effective use of the Jones-Nelson-Morgan material models.

2.5.2 Stress Analysis of Solid Bodies Made of Nonlinear Multimodulus Materials

The stress analysis of solid bodies made of nonlinear multimodulus composite materials is performed in this grant with two computer programs, SAAS IIIM and MULTIAX, developed or modified during this grant. The SAAS IIIM program is a finite element stress analysis computer program for axisymmetric bodies under axisymmetric loading and for bodies under plane stress or plane strain. The SAAS IIIM program is a modification of the SAAS III program [16] to incorporate the Jones-Nelson-Morgan nonlinear multimodulus material models. The MULTIAX computer program is essentially a one element version of SAAS IIIM used for uniform multiaxial stress states. Neither program is documented in a report, but all changes in input instructions from the SAAS III program are available for the SAAS IIIM program. The input instructions for MULTIAX are listed on comment cards in the program.

A validation of the Jones-Nelson-Morgan material models is now sought in a heirarchy of comparisons between theory and experiment. The Jones-Nelson-Morgan models are defined with data from stress-strain curves in principal material directions and at 45° to principal material directions, but not with shear stress-strain behavior (unless the material does not exhibit multimodulus behavior in which case the shear behavior is substituted for the 45° off-axis behavior in the model definition). The validation should progress from simple, well-controlled laboratory experiments to more complicated, less well-controlled simulation tests. Specifically, for orthotropic materials, the following heirarchy seems appropriate and has been used for at least one material in this grant:

(1) uniaxial off-axis loading tests wherein a uniform stress state

21

is developed in the gage section under highly controlled laboratory conditions.

(2) biaxial loading tests in principal material directions wherein a uniform stress state is developed in the gage section under highly controlled laboratory conditions

(3) biaxial loading tests which are not in principal material directions wherein a uniform stress state is developed in the gage section under highly controlled laboratory conditions

(4) thermal loading tests like (1), (2), or (3) but with the load generated with heat and not with mechanical means. The stress state is not likely to be uniform nor is it usually possible to achieve a thermal loading with the accuracy of most mechanical loadings.

(5) simulation tests such as reentry vehicle nosetip ground tests in a rocket nozzle exhaust wherein both thermal and mechanical stresses are developed throughout the nosetip or rocket nozzle ground test firings wherein both thermal and mechanical stresses are also developed. Neither of these simulation tests can be performed with the accuracy and reliability of any of the foregoing tests.

(6) instrumented flight tests of reentry vehicle nosetips, rockets, aircraft, etc. The loading conditions in all of these tests are generally difficult to define. Moreover, the amount of instrumentation is likely to be much lower than for ground tests.

Obviously, upon progression in the foregoing hierarchy, the quality of experimental information decreases at the same time the quantity increases [although sometimes the quantity decreases too, as in (6)]. Thus, correla-

tions between theory and experiment must be carefully evaluated at all levels in the heirarchy in order to draw appropriate conclusions about the validity or lack of validity of any material models.

In what follows, the almost complete use of the foregoing hierarchy will be described for ATJ-S graphite, as well as partial uses of the hierarchy for boron-epoxy, graphite-epoxy, and carbon-carbon.

2.5.2.1 ATJ-S Graphite Modeling and Response

The Jones-Nelson material model for ATJ-S graphite [2.3-5,9,13] is a nonlinear multimodulus model, but does not have (or need) the stress-strain curve extension character of the Jones-Nelson-Morgan model [2.3-22]. This material is transversely isotropic in cylindrical coordinates with the r-θ plane being the plane of isotropy. The model is defined with data from stress-strain curves for uniaxial loading in principal material directions and at 45° to principal material directions. Then, the model is verified in a four-step process: (1) uniaxial off-axis loading at 70° to principal material directions; (2) biaxial loading of a tubular specimen; (3) biaxial thermal loading of an annular disk; and (4) thermal and mechanical loading of a reentry vehicle nosetip. Each of these four steps is described in the following paragraphs.

Uniaxial Off-Axis Loading at 70°   The measured response of ATJ-S graphite to uniaxial off-axis loading at 70° to the across-grain direction (the z-direction in cylindrical coordinates)[17] is shown for tension loading in Fig. 2.3 and for compression loading in Fig. 2.4. The predicted (with MULTIAX) normal strain [2.3-9,14] for a specified stress is essentially identical to the measured response under both tension and compression loading. The predicted transverse strain under tension loading is not as accurate as the predicted normal strain. However, the predicted transverse
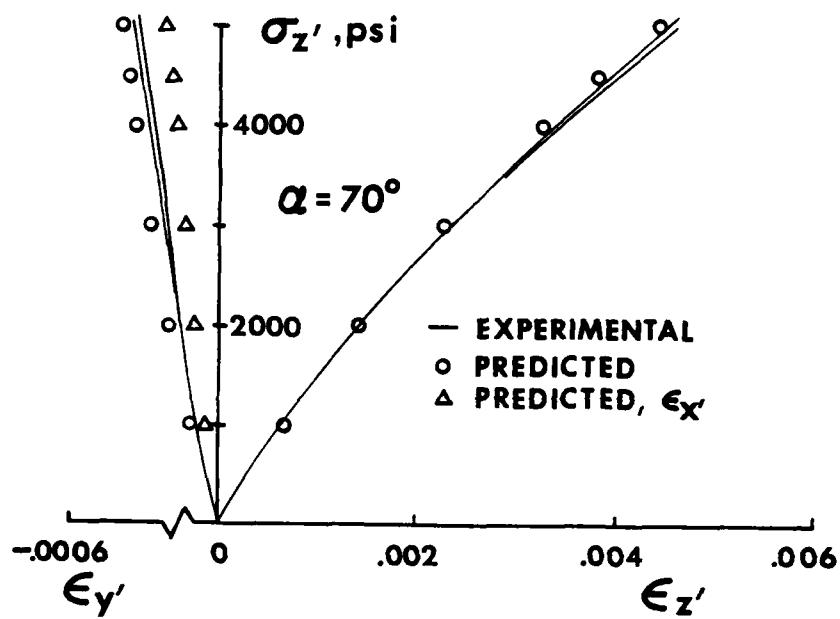
23

FIGURE 2.3   UNIAXIAL OFF-AXIS RESPONSE AT 70°
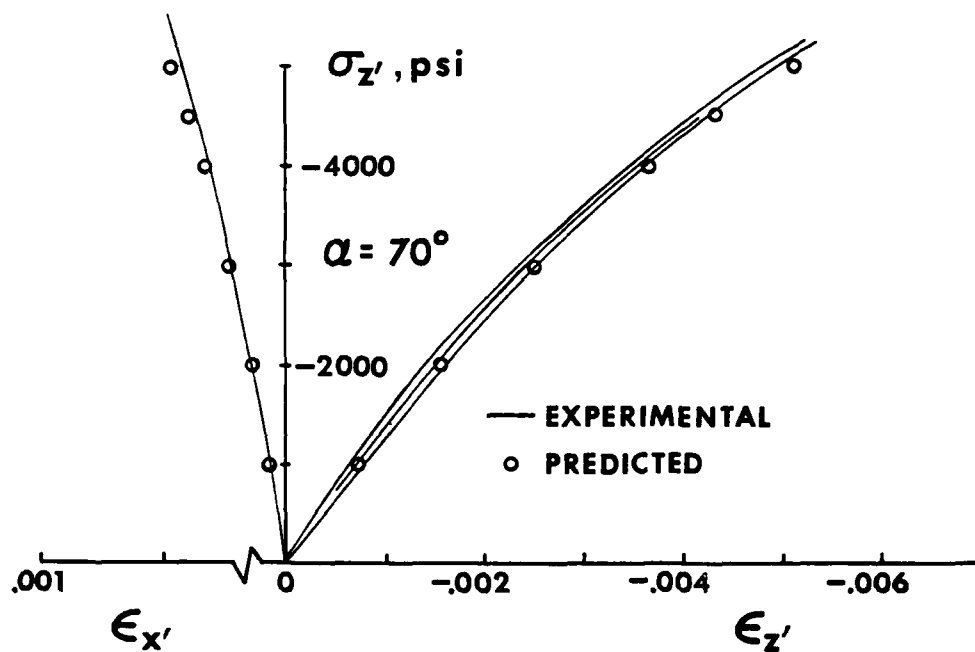FOR ATJ-S GRAPHITE UNDER TENSION

FIGURE 2.4   UNIAXIAL OFF-AXIS RESPONSE AT 70°
FOR ATJ-S GRAPHITE UNDER COMPRESSION

24

strain under compression loading is identical to the measured response. This initial and simplest comparison between predicted and measured response is quite satisfying.

Biaxial Loading of a Tubular Specimen   Jortner [17] measured the axial and circumferential strains in a tubular test specimen under internal pressure and axial tension or compression (hence, a biaxial stress state) for several different billets of ATJ-S graphite. These measured strains for a maximum principal stress of 3550 psi are shown along with the strains predicted with the Jones-Nelson model in MULTIAX and SAAS IIIM in Fig. 2.5 [2.3-5,14]. The predictions are a function of the specific energy value used in Eq. (2.1), namely whether all the energy is used (total), only the tension energy for tension properties and compression energy for compression properties (divided), or a portion of each (weighted). These differences arise only in mixed tension and compression stress states. All predicted strains for this stress level are quite close to the measured values thereby increasing confidence in the Jones-Nelson model for graphite.

Biaxial Thermal Loading of an Annular Disk   Pears and Starrett [18] measure the internal diameter change of a graphite annular disk subjected to rapid heating around the circumference as in Fig. 2.6. The diameter change is measured with laser beams, and the temperature is measured at the inner diameter with a thermocouple and near the outer diameter with a micro-optical spot. The induction coils rapidly heat the specimen so that temperature differences of several thousand degrees exist between the inner and outer diameter. The Jones-Nelson model is defined with data for ATJ-S graphite over the appropriate temperature range [19]. That is, the model must be defined at many discrete temperatures and a procedure developed to interpolate the model behavior between those temperatures for each element
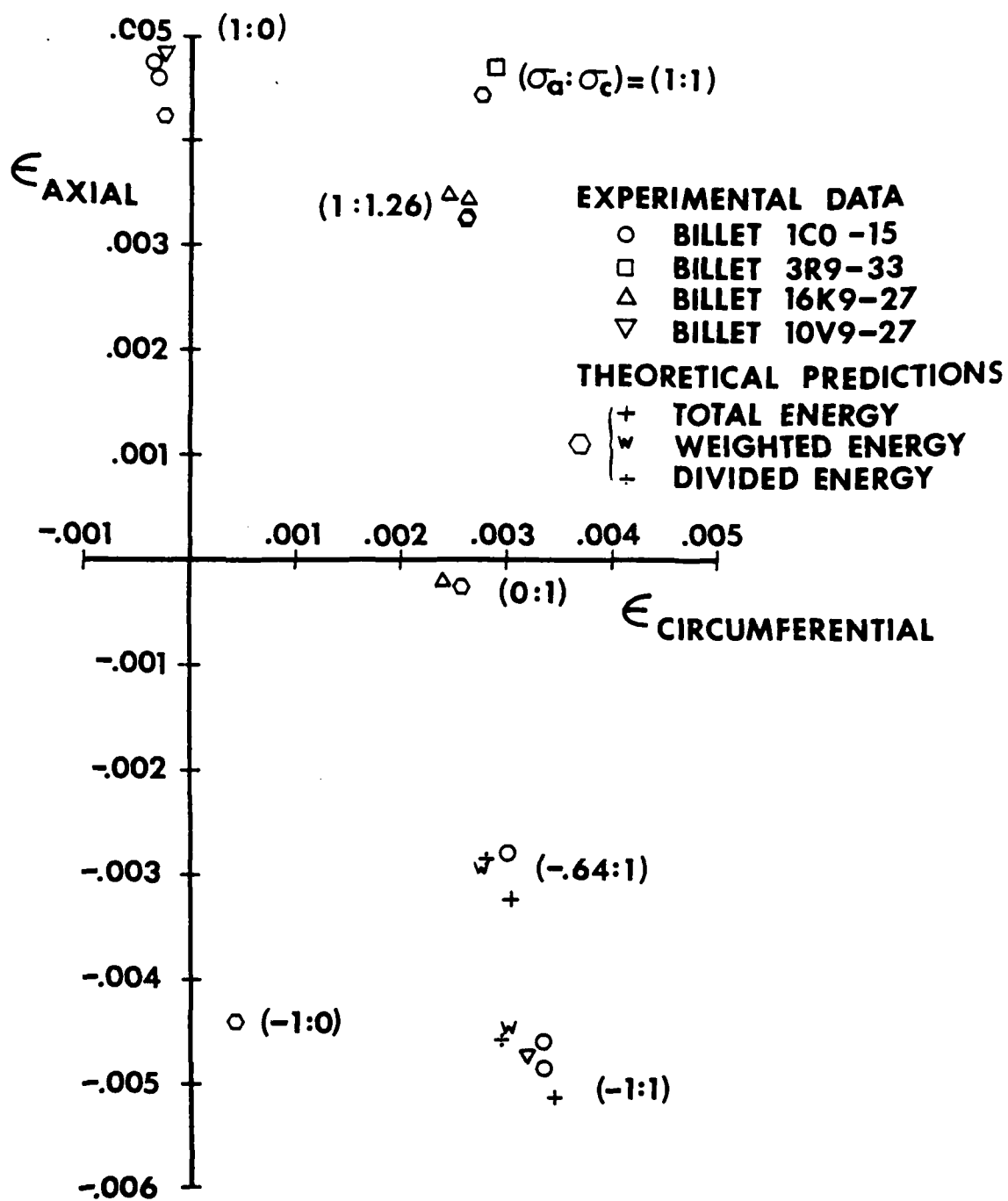
25

FIGURE 2.5 PREDICTED AND MEASURED STRAINS IN A GRAPHITE TUBULAR SPECIMEN
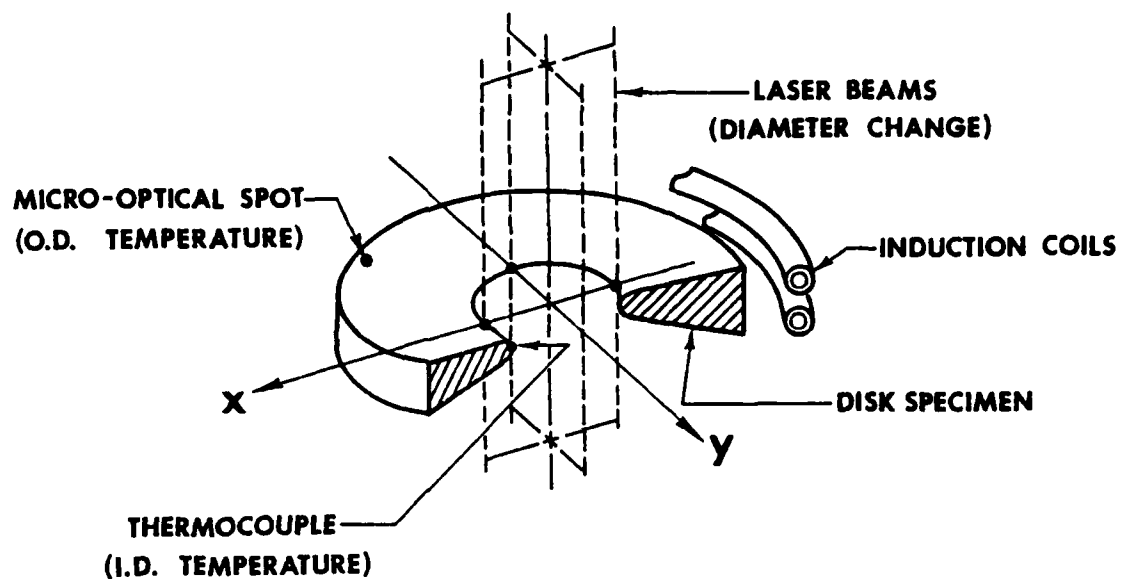
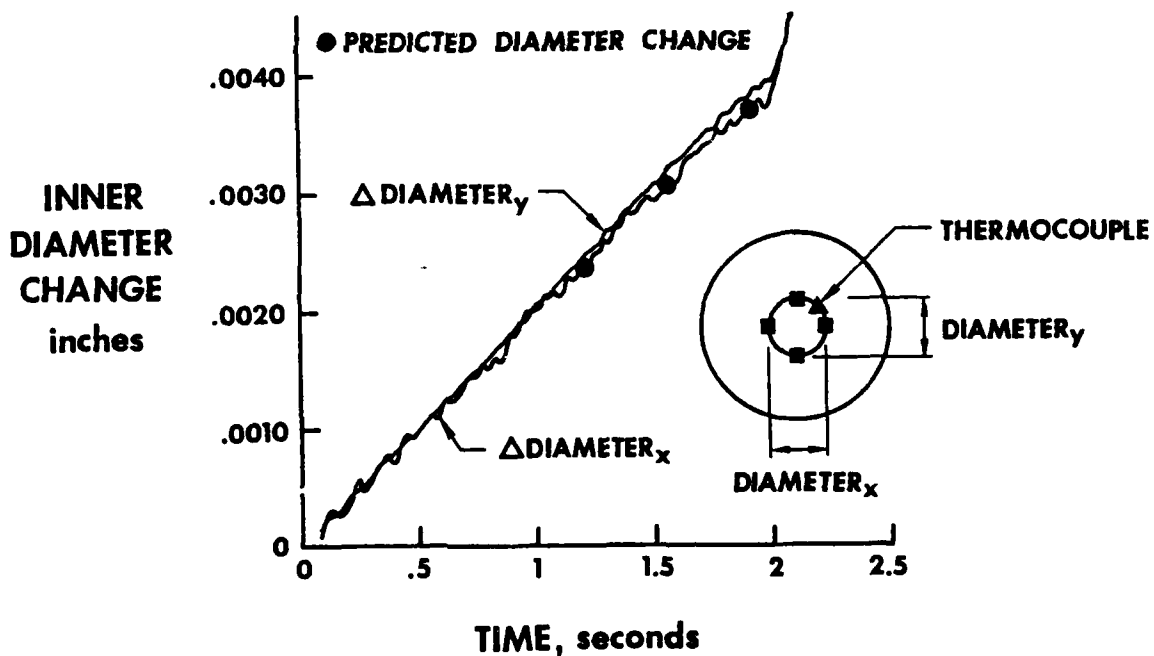FIGURE 2.6   SCHEMATIC OF SoRI THERMAL STRESS DISK TEST

FIGURE 2.7   INNER DIAMETER CHANGE VERSUS TIME

of the finite element idealization of the disk. A quasistatic stress analysis is then performed with SAAS IIIM, i.e., at each time, the temperature distribution (predicted with a heat transfer program and calibrated to the measured inner diameter temperature) is used to predict the thermal stresses and resulting deformations. Thus, the inner diameter change is predicted as a function of time in Fig. 2.7 where the agreement with measured response is excellent. Accordingly, the level of validation of the Jones-Nelson model is raised to yet another level in the heirarchy presented earlier.

Thermal and Mechanical Loading of a Reentry Vehicle Nosetip   The prediction of stresses and strains in a shell-type reentry vehicle nosetip under thermal and mechanical loading from the 50 MW arc jet facility at Wright-Patterson AFB, Ohio was performed under a related AFML contract [20]. The Jones-Nelson-Morgan model (i.e., with an extended stress-strain curve) is essential to obtain convergence of the iteration procedure in SAAS IIIM. The data for the model are obtained from Starrett and Pears [19]. The strains in element 232 on the inner radius of the nosetip in Fig. 2.8 are about 20% higher than the strains predicted with the DOASIS program [21] (this comparison was the objective of the contract), whereas the present stresses are about 15% lower than the DOASIS stresses. Correlation with strains measured in the actual nosetip test was not meaningful (nor in the scope of the contract) because information sufficient to deduce the actual temperature distribution corresponding to the measured strains was not available. A crude and not entirely rational comparison of raw strain predictions with measured strains leads to the conclusion that the predicted strains are higher than the measured strains. However,
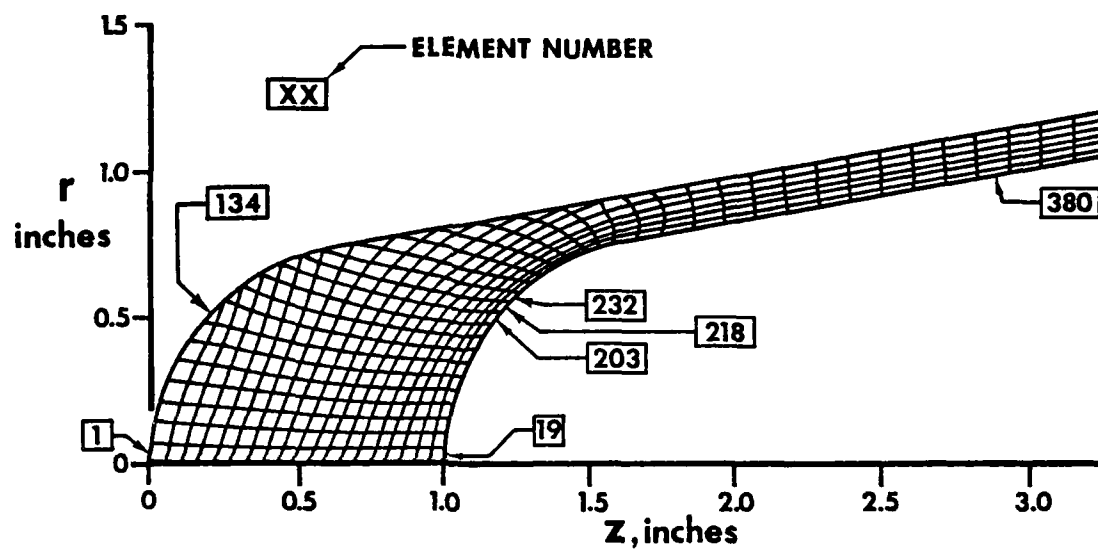
FIGURE 2.8   FINITE ELEMENT IDEALIZATION OF
SHELL-TYPE REENTRY VEHICLE NOSETIP

29

the temperatures at which the predictions were made are not the same as those at which the measurements were made. This step in the validation procedure for the Jones-Nelson-Morgan model is obviously inconclusive, but not discouraging

2.5.2.2 Boron-Epoxy and Graphite-Epoxy Modeling and Response

The Jones-Nelson-Morgan nonlinear model (not multimodulus because the multimodulus character is negligible) is defined for data obtained by Cole and Pipes [22] for both boron-epoxy and graphite-epoxy. The model is then used to predict strains under off-axis tension loading for boron-epoxy in Fig. 2.9 and for graphite-epoxy in Fig. 2.10 [2.3-22]. For boron-epoxy, the Jones-Nelson-Morgan model leads to strains that are sometimes larger and sometimes smaller than both the Cole and Pipes data and the Hahn and Tsai nonlinear model [14]. For graphite-epoxy, the Jones-Nelson-Morgan model leads to essentially the same strains as the Hahn and Tsai model and, as with boron-epoxy, sometimes larger and sometimes smaller than the Cole and Pipes data. This correlation is not entirely satisfying, but the data with which the models are compared are not always consistent because, perhaps, of inconsistent aging of the test specimens.

2.5.2.3 Carbon-Carbon Modeling and Response

The Jones-Nelson-Morgan model for carbon-carbon was defined with data obtained by Starrett, Weiler, and Pears [23] for AVCO Mod 3a carbon-carbon. The model was then used in MULTIAX to predict strains under uniaxial off-axis tension and compression loading as well as under shear loading. For example, see the 22° off-axis (from the x-direction) tension response prediction in Fig. 2.11 along with measured response for that direction, the x-direction, and at 45° to the x-direction (the latter two
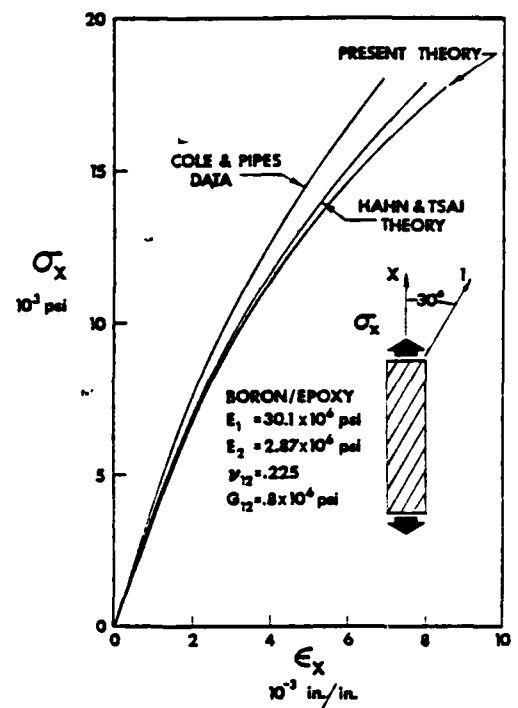
30

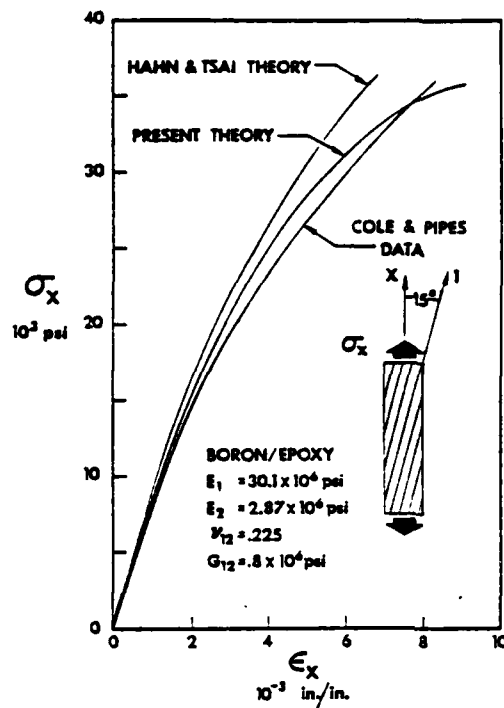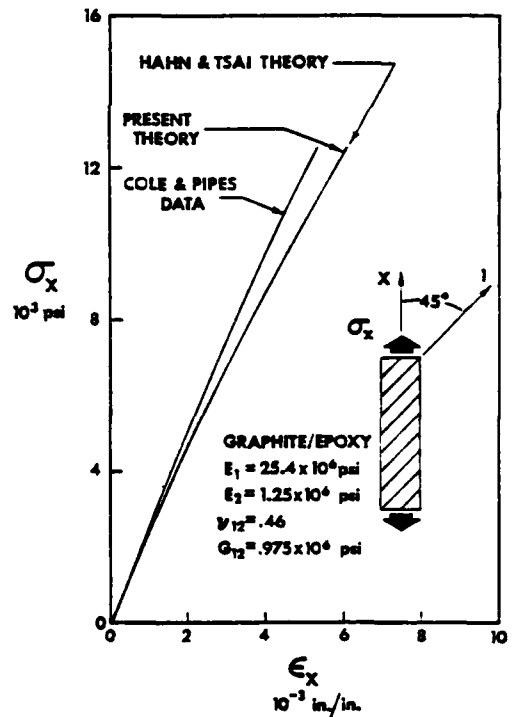FIGURE 2.9 BORON-EPOXY OFF-AXIS LOADING RESULTS
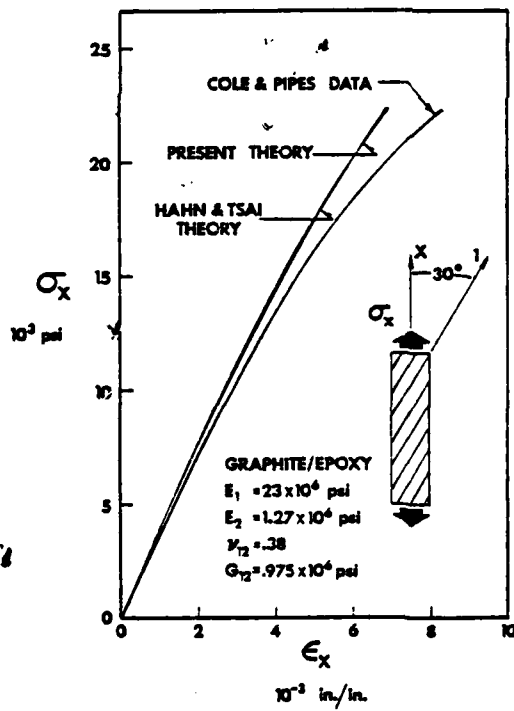
FIGURE 2.10 GRAPHITE-EPOXY OFF-AXIS LOADING RESULTS
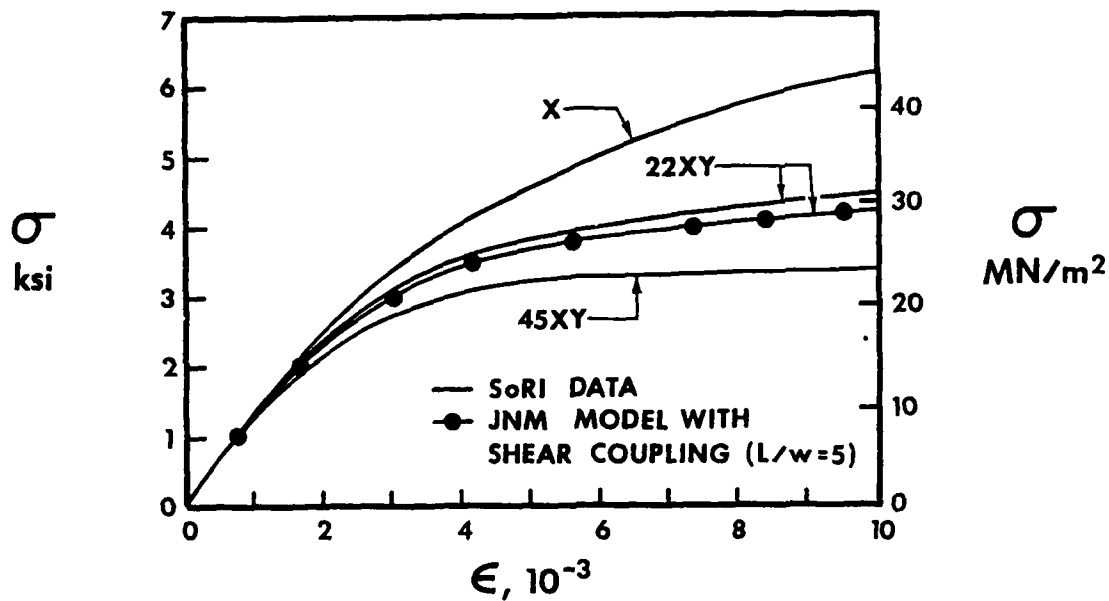
FIGURE 2.11   XY-PLANE TENSION RESPONSE OF AVCO MOD 3a CARBON-CARBON
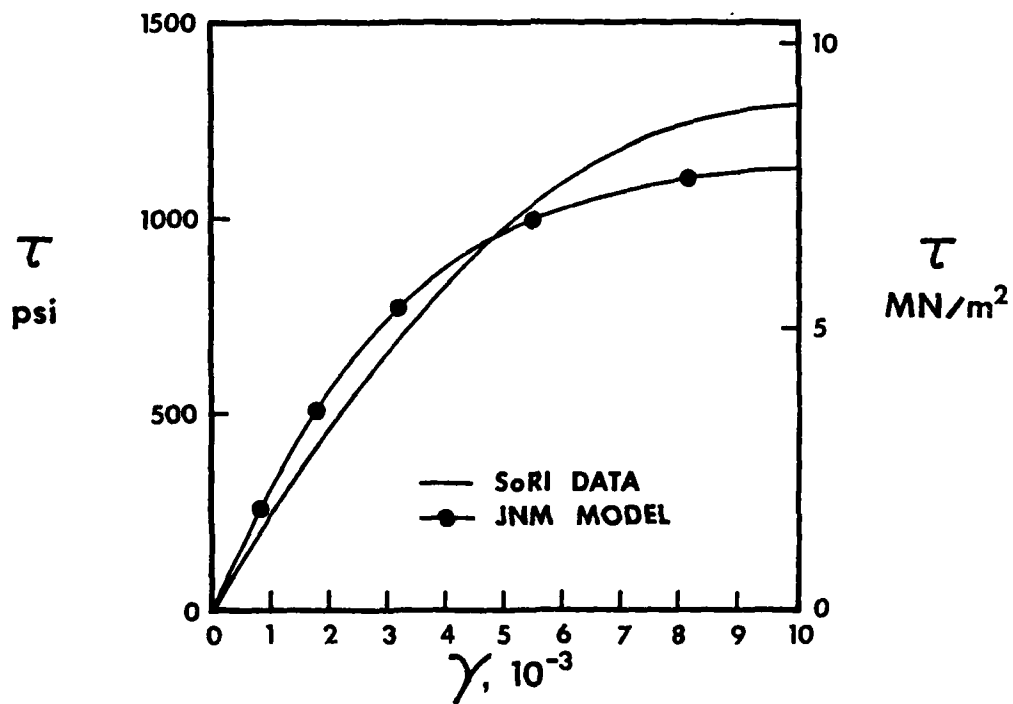
FIGURE 2.12   XZ-PLANE SHEAR RESPONSE OF AVCO MOD 3a CARBON-CARBON

32

responses are used to define the model) in the xy-plane. Also, observe
the predicted and measured shear response in the xz-plane in Fig. 2.12.
Both agreements are very reasonable considering that both the data used
to define the model and that used to compare with the predicted response
are "most probable value" data, i.e., a sort of averaged representation
of a collection of somewhat inconsistent and highly variable (from billet
to billet) stress-strain curves. Thus, agreement between predicted and
measured response is no guarantee of material model validity nor is dis-
agreement an indication of model invalidity. The modeling and response
of carbon-carbon is discussed more fully in Section 3.

2.5.3 Structural Behavior of Laminated Plates and Shells

The various aspects of structural behavior (bending, buckling, and vibration) of laminated plates and shells are discussed in three sub-sections: (1) elastic material behavior; (2) nonlinear material behavior; and (3) multimodulus material behavior. No research was performed for nonlinear multimodulus material behavior of laminated plates and shells because no materials currently used in laminates have different enough stress-strain behavior under tension loading than under compression loading to justify its consideration.

2.5.3.1 Elastic Material Behavior

The major contribution in the present research on elastic material behavior is the proper understanding of analysis of unsymmetrically laminated plates and shells. Prior to this grant, the common belief was that the effect of laminate asymmetry (of material and geometrical parameters) on structural behavior is negligibly small if the laminate has more than six or eight layers. That belief was founded on Whitney and Leissa's correct observation [24] that for antisymmetric laminates the effect of bending-extension coupling on structural behavior does die out very rapidly as the number of layers in the laminate increases. However, the fallacy was in people incorrectly applying the result for the special class of antisymmetric laminates to the general class of unsymmetric laminates. In fact, the effect of bending-extension coupling _can_ be of engineering significance for a fifty-layer laminate!

Buckling and Vibration of Unsymmetrically Laminated Plates   The first vehicle for investigating the unsymmetric laminate problem is buckling and vibration of unsymmetrically laminated cross-ply plates [2.3-1]. First, a new solution is obtained for buckling and vibration of antisym-

34

metrically laminated cross-ply plates. Then, the solution can be generalized to treat unsymmetrically laminated cross-ply plates. For a graphite-epoxy plate in which all unidirectionally reinforced layers are at 0° to the applied load (fibers parallel to load), except for one layer at 90° (fibers perpendicular to the load), the normalized buckling load is plotted against the number of laminate layers in Fig. 2.13. There, the 90° layer is always the second layer from the bottom (and hence it gets thinner and closer to the bottom as the number of layers increases). The solution for all 0° layers is independent of the number of layers and is approached, as the number of layers increases, by the exact solution as well as by the solution in which coupling between bending and extension is ignored ($B_{ij} = 0$). The important point is that the exact solution differs from the $B_{ij} = 0$ solution by nonnegligible amounts even for a 100-layer laminate! This specific laminate example is a counterexample to the statement that laminate symmetry is not important for laminates with many layers. Thus, although laminate asymmetry might not be important for a specific unsymmetric laminate, the mere existence of many layers does not mean laminate asymmetry can be ignored safely. The word safely is significant because the principal effect of lamination asymmetry is to increase deflections, lower buckling loads, and lower vibration frequencies. Thus, neglect of nonnegligible lamination asymmetries is unconservative design analysis. Results for vibration of unsymmetrically laminated cross-ply plates are similar to the buckling results. The only significant difference is that vibration frequencies calculated with the various approaches mentioned are not so different as buckling loads because the vibration frequencies involve the square root of a function of the laminate properties whereas the buckling load involves the function itself.
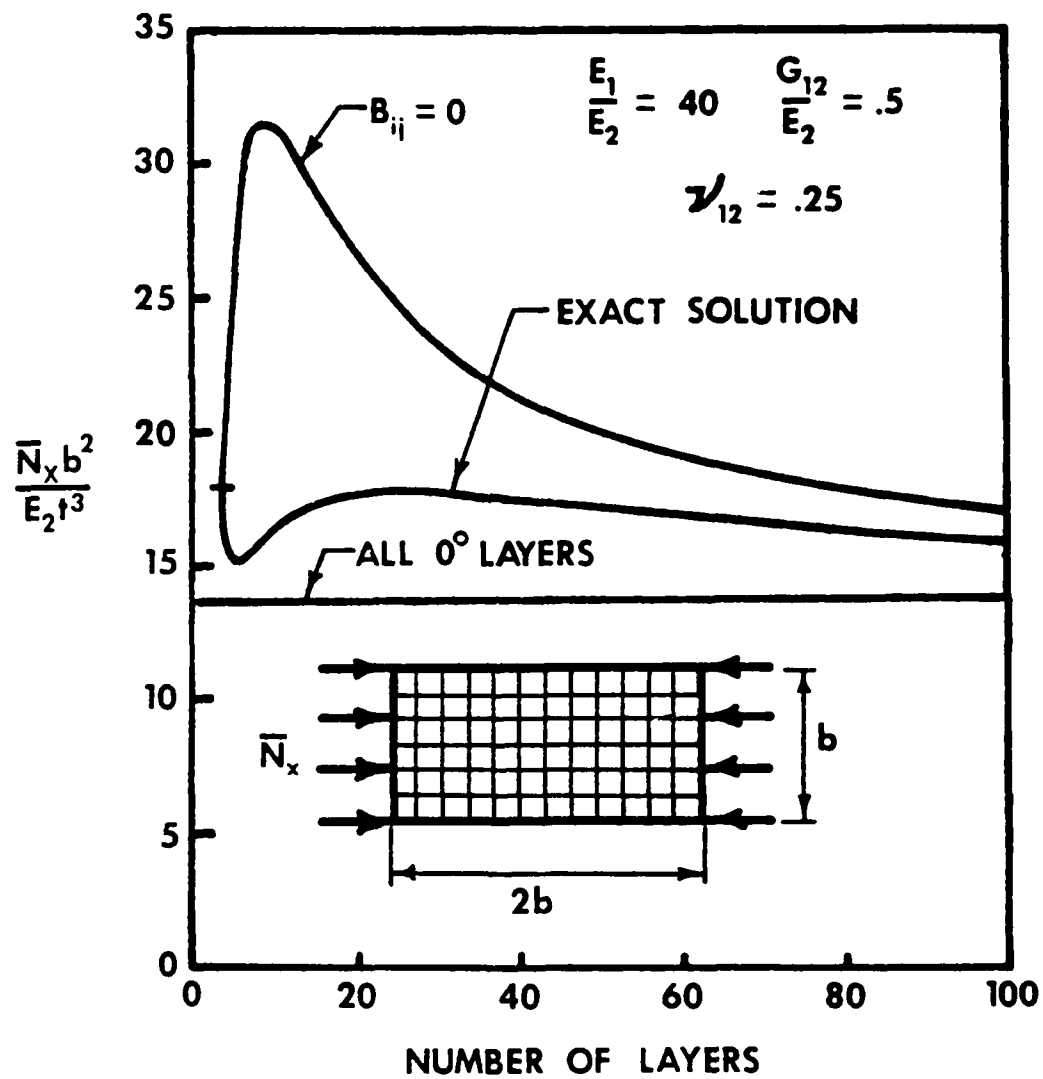
FIGURE 2.13   UNIAXIAL BUCKLING LOADS FOR GRAPHITE-EPOXY
              RECTANGULAR UNSYMMETRIC CROSS-PLY LAMINATED PLATES

36

<u>Deflection of Unsymmetrically Laminated Cross-Ply Plates</u>   The un-

symmetric laminate problem is continued with an investigation of the

specific influence of laminate asymmetry on plate deflection under trans-

verse load. An exact solution is obtained [2.3-11] for response to a

sinusoidal load on a plate with simply supported edges. Solutions for

various sinusoidal loadings can be summed to obtain the solution for a

general loading if a Fourier series is applied. For example, the results

for a uniform transverse load are shown in Fig. 2.14. There, the exact

solution is a much higher deflection than the approximate $B_{ij} = 0$ solution

in which laminate asymmetry is ignored even if the laminate has more than

50 layers! This study complements the study on buckling and vibration

[2.3-1] and completes the basic plates analysis aspect of lamination asym-

metries.

<u>Application of Unsymmetric Plate Analysis to Lightning Strike</u>

<u>Protection Concepts</u>   The unsymmetric plate analyses developed in the

preceding paragraphs are applied to design analysis of three lightning

strike protection concepts for the Space Shuttle payload bay doors. The

baseline configuration is a 20" x 13' panel (20" in the axial direction

between frames and 13' in the circumferential direction). The panel is

composed of a honeycomb core with two layers of graphite-epoxy tape and

one layer of graphite-epoxy cloth on top and bottom of the core. The

mechanical properties and geometry of each layer are listed in Table 2.1.

Also displayed are the mechanical properties and geometry of the three

lightning strike protection concepts: (1) .005 in. aluminum foil on top

of an adhesive layer; (2) 200 x 200 aluminum mesh embedded in adhesive;

and (3) flame sprayed aluminum covered by an adhesive protective layer.

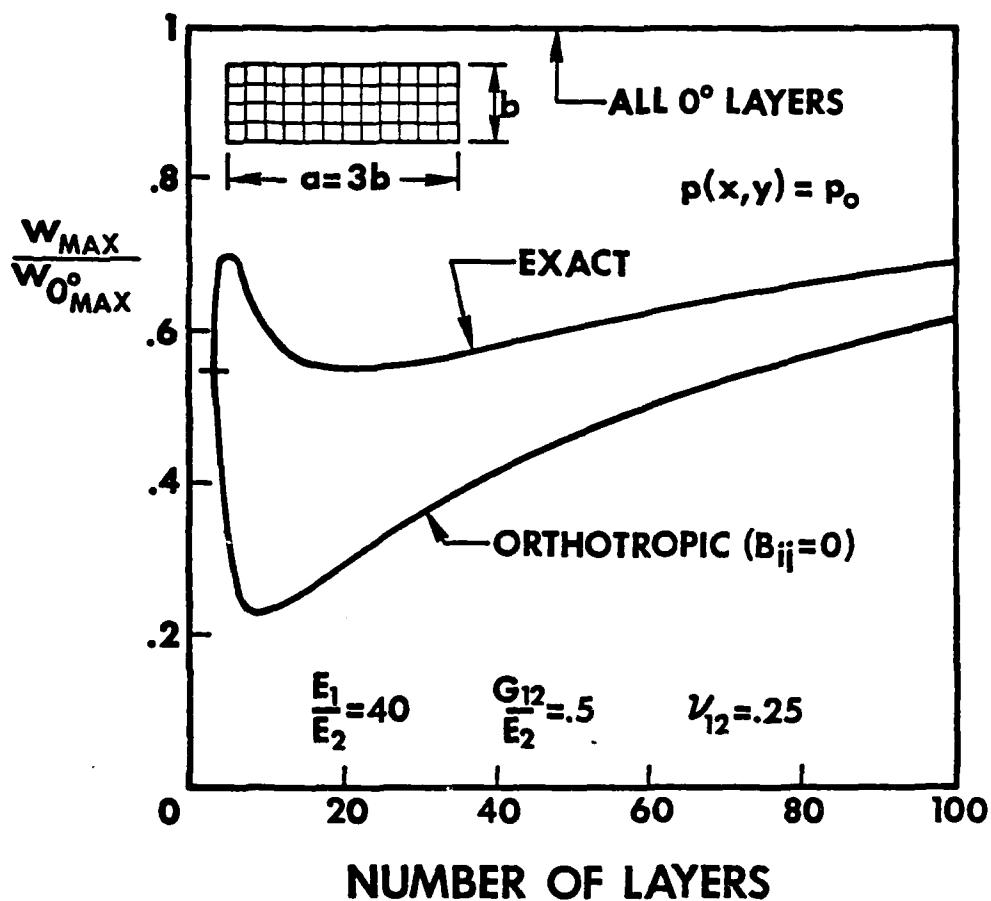The objective of the study is to determine the effect on structural

FIGURE 2.14   EFFECT OF NUMBER OF LAYERS ON DEFLECTION OF
SIMPLY SUPPORTED UNSYMMETRICALLY LAMINATED
CROSS-PLY GRAPHITE-EPOXY RECTANGULAR PLATES
UNDER UNIFORM TRANSVERSE LOAD

38

TABLE 2.1 GEOMETRY AND MECHANICAL PROPERTIES
OF LIGHTNING STRIKE STUDY CONFIGURATIONS
FOR SPACE SHUTTLE PAYLOAD BAY DOORS

CONFIGURATION	LAYER	$E_x, 10^6$ psi	$E_y, 10^6$ psi	ν_{xy}	$G_{xy}, 10^6$ psi	t, in.	ρ, lb/in.^{3}
BASIC PAYLOAD BAY DOOR (THESE SEVEN LAYERS ARE IDENTICAL FOR ALL FOUR CONFIGURATIONS)	1	20.5	1.9	.3	.66	.0044	.060
	2	9.65	9.45	.044	.60	.0073	.060
	3	20.5	1.9	.3	.66	.0044	.060
	4	0	0	0	0	.600	.005
	5	20.5	1.9	.3	.66	.0044	.060
	6	9.65	9.45	.044	.60	.0073	.060
	7	20.5	1.9	.3	.66	.0044	.060
PAYLOAD BAY DOOR WITH .005 in. ALUMINUM FOIL	8	.5	.5	.4	.179	.008	.044
	9	10.0	10.0	.33	3.76	.005	.097
PAYLOAD BAY DOOR WITH 200x200 ALUMINUM MESH	8	1.6	1.6	.3	.2	.006	.054
PAYLOAD BAY DOOR WITH FLAME SPRAYED ALUMINUM	8	10.0	10.0	.33	3.76	.010	.097
	9	.5	.5	.4	.179	.008	.044

TABLE 2.2 DEFLECTION OF PAYLOAD BAY DOOR PANELS WITH
VARIOUS LIGHTNING STRIKE PROTECTION CONCEPTS

CONFIGURATION	MAXIMUM (CENTER) DEFLECTION, w, in.				
	EXACT SOLUTION	$B_{ij} = 0$	ERROR	REDUCED BENDING STIFFNESS	ERROR
BASIC PAYLOAD BAY DOOR	.0223	—	—	--	--
PAYLOAD BAY DOOR WITH ALUMINUM FOIL	.0198	.0196	-1.0%	.0199	+.5%
PAYLOAD BAY DOOR WITH ALUMINUM MESH	.0218	.0218	—	.0218	--
PAYLOAD BAY DOOR WITH FLAME SPRAYED ALUMINUM	.0184	.0177	-3.8%	.0185	+.5%

behavior of ignoring bending-extension coupling caused by the laminate asymmetry induced by the application of lightning strike protection layers. The specific structural behavior measures are maximum panel deflection (at the center), buckling under axial load, and fundamental natural frequency. The analysis approaches compared are the exact solutions discussed earlier, the complete neglect of bending-extension coupling ($B_{ij} = 0$), and the approximate treatment of bending-extension coupling in the form of the reduced bending stiffness approximation. For each concept and each structural behavior aspect, the three analysis approaches are compared in Tables 2.2, 2.3, and 2.4 for deflection, buckling and vibration, respectively. The exact solution is used as the baseline for all calculations of percentage error. The aluminum mesh concept is noteworthy from the standpoint that all analysis approaches yield the same result, i.e., their error is zero. The $B_{ij} = 0$ approximation is from one to five percent in error on the unconservative side for the other two concepts. The reduced bending stiffness approximation is essentially correct with the error being less than ±.5% in all cases.

The principal conclusion to be drawn is that neglecting coupling between bending and extension due to laminate asymmetry in this problem might not be unacceptable. Certainly the reduced bending stiffness approximation is perfectly acceptable. Neither of these two conclusions is necessarily applicable beyond the parameters of the present study.

Buckling and Vibration of Antisymmetrically Laminated Angle-Ply Rectangular Plates   The simplest solution for buckling and vibration of antisymmetrically laminated angle-ply plates is obtained by Whitney and Leissa [24]. In Ref. 2.3-2, the numerical errors uncovered in the investigation of laminated plates are corrected.

40

TABLE 2.3   BUCKLING OF PAYLOAD BAY DOOR PANELS WITH
VARIOUS LIGHTNING STRIKE PROTECTION CONCEPTS

CONFIGURATION	BUCKLING LOAD, N_x, lb/in.				
	EXACT SOLUTION	$B_{ij} = 0$	ERROR	REDUCED BENDING STIFFNESS	ERROR
BASIC PAYLOAD BAY DOOR	1187	—	—	—	—
PAYLOAD BAY DOOR WITH ALUMINUM FOIL	1332	1352	+1.5%	1330	-.2%
PAYLOAD BAY DOOR WITH ALUMINUM MESH	1214	1214	—	1214	—
PAYLOAD BAY DOOR WITH FLAME SPRAYED ALUMINUM	1431	1496	+4.5%	1426	-.3%

TABLE 2.4   VIBRATION OF PAYLOAD BAY DOOR PANELS WITH
VARIOUS LIGHTNING STRIKE PROTECTION CONCEPTS

CONFIGURATION	FUNDAMENTAL VIBRATION FREQUENCY, ω, cps				
	EXACT SOLUTION	$B_{ij} = 0$	ERROR	REDUCED BENDING STIFFNESS	ERROR
BASIC PAYLOAD BAY DOOR	61.3	—	—	—	—
PAYLOAD BAY DOOR WITH ALUMINUM FOIL	60.6	61.1	+ .8%	60.6	—
PAYLOAD BAY DOOR WITH ALUMINUM MESH	60.3	60.3	—	60.3	—
PAYLOAD BAY DOOR WITH FLAME SPRAYED ALUMINUM	60.6	61.9	+2.1%	60.5	-.2%

41

Buckling and Vibration of Cross-Ply Laminated Circular Cylindrical
Shells   The unsymmetric laminate problem is extended from plates to
circular cylindrical shells in this research [2.3-8]. First, for S2
simply supported edge boundary conditions, a closed form (but computer
implemented because of mode shape searching) solution is derived which
leads to new results for both antisymmetrically and unsymmetrically lami-
nated shells. For antisymmetric laminates, both buckling and vibration
results are presented in the form of Batdorf k-Z plots where k is a
normalized buckling load or vibration frequency and Z is the Batdorf shell
curvature parameter. The effect of bending-extension coupling on buckling
loads and vibration frequencies is seen to rapidly die out as the number
of layers increases. However, for unsymmetric laminates (the one specified
for the plate problem earlier in this sub-section), the effect of bending-
extension coupling on lateral pressure buckling loads dies out very slowly
as the number of layers increases as in Fig. 2.15. Similar results are
obtained for axial compression and vibration.

Effect of Prebuckling Deformations on Buckling of Laminated
Composite Shells   A distinctly different problem from the unsymmetric
laminate problem is addressed, namely how the deformations that exist prior
to buckling influence the buckling load [2.3-23]. Two types of deforma-
tion exist prior to buckling: both are a form of bending-extension coup-
ling, but one exists even if the laminate is symmetric about its middle
surface. This type of bending-extension coupling is shown by Almroth
[25] to lower the axial buckling load of isotropic shells by up to 20%
depending on the boundary conditions. Here, the other bending-extension
coupling due to laminate asymmetry (both antisymmetry and general lack of
symmetry) is investigated. For buckling under axial compression of anti-
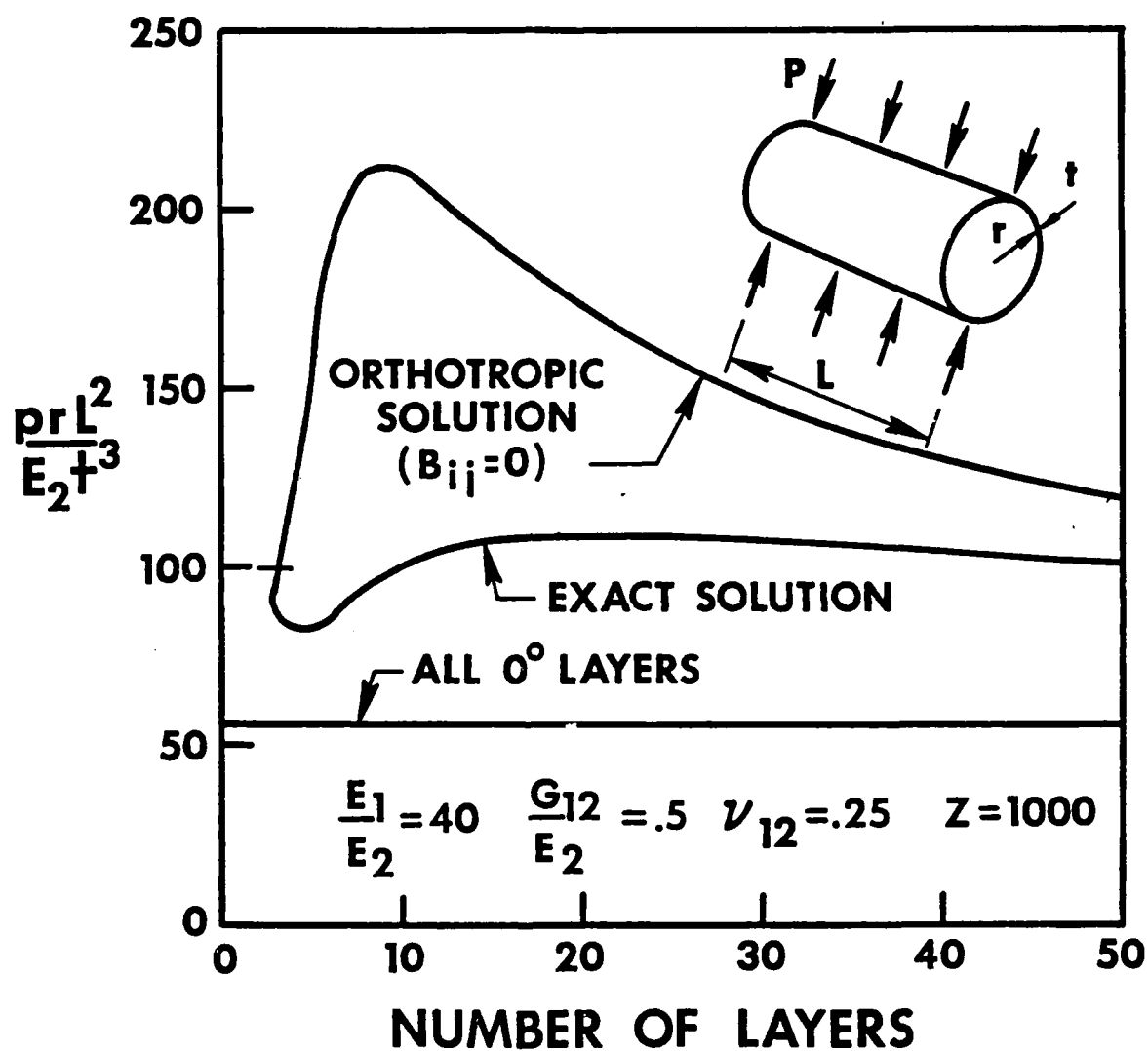symmetric cross-ply laminated circular cylindrical shells, the buckling

42

FIGURE 2.15   NORMALIZED LATERAL PRESSURE BUCKLING LOADS
FOR UNSYMMETRICALLY CROSS-PLY LAMINATED
GRAPHITE-EPOXY CIRCULAR CYLINDRICAL SHELLS

43

load normalized by the buckling load for a laminate with an infinite number of layers is plotted against the orthotropy ratio, E_1/E_2, for several laminates with different numbers of layers in Fig. 2.16. There, the results for membrane prebuckling deformations are shown as solid curves and the results when rigorous prebuckling deformations are considered are shown as discrete points connected with dashed lines. Obviously, the effect of laminate asymmetry is dependent on the level of orthotropy, starting from the 20% effect at isotropy and rapidly decreasing to a few percent as the orthotropy ratio increases. That is, the major influence of laminate asymmetry is captured in a classical buckling analysis with membrane prebuckling deformations for shells. For plates, similar conclusions are anticipated, but the actual numerical results would be much harder to obtain than the present shell results.

2.5.3.2 Nonlinear Material Behavior

Nonlinear material behavior is included in analysis of deformation of laminae and laminates as well as buckling of laminates. Such material behavior is seen in boron-epoxy, graphite-epoxy, and boron-aluminum laminates. These analyses are described in the following paragraphs.

Off-Axis Loading of a Composite Lamina   The nonlinear material behavior that results when stress is applied in nonprincipal material directions is analyzed for boron-epoxy and graphite-epoxy in Ref. 2.3-22. There, as described in Sections 2.5.1.2 and 2.5.2.2, the linear extension of the stress-strain curve is used to model the mechanical behavior. The load or stress applied in nonprincipal material directions excites a combination of nonlinear responses of the material. As seen in Section 2.5.2.2, the agreement between predicted and measured response is quite
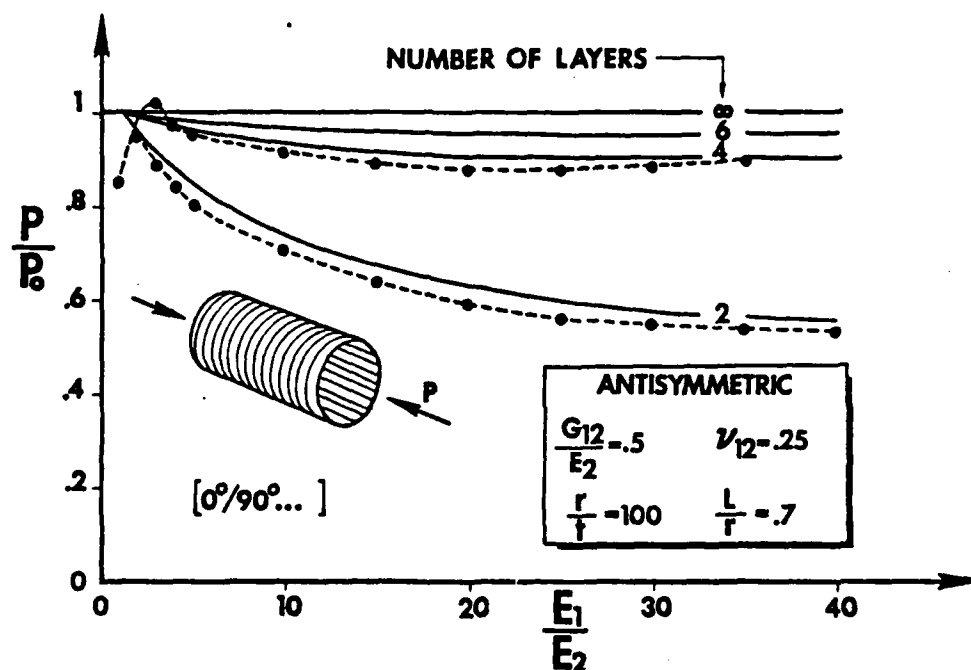
44

FIGURE 2.16   RELATIVE CLASSICAL AND RIGOROUS AXIAL BUCKLING LOADS
FOR SHORT ANTISYMMETRICALLY LAMINATED SHELLS

45

good. This lamina behavior model is used as the basic building block for the laminate analyses described in the next two paragraphs.

Extension of Composite Laminates Application of the nonlinear material model to laminate stress analysis is much more complex than application to lamina stress analysis. When laminae are bonded together to form a laminate, both laminate strain compatibility and laminate force equilibrium must be considered in addition to the nonlinear stress-strain behavior. The basic nonlinear stress-strain model of a lamina is combined with logic to search for the point on a laminate load-deflection curve where the stress-strain relations, strain compatibility, and force equilibrium are all satisfied [2.3-25]. To accomplish this seemingly obvious goal, several search and iteration procedures are developed. Basically, a means is derived of progressing along the load-strain curve in Fig. 2.17 for a symmetric laminate under uniaxial load (hence, strain is directly related to deformation). This means of progressing involves using tangent and secant mechanical properties which are arrived at through several iteration procedures. Typical results for a boron-epoxy laminate are shown in Fig. 2.18 where the agreement between predicted and measured response is quite good.

Buckling of Composite Laminates The problem of laminate buckling when the lamina stress-strain behavior is nonlinear [2.3-26] goes one step further than the laminate extension analysis just described. That step is the evaluation of the stability of equilibrium at every point along the load-deformation curve that we now can obtain. At every point on Fig. 2.19, the tangent mechanical properties are used to calculate a buckling load λ_{c_i} and compare that buckling load with the estimated buckling load λ_{e_i} which is the load at that point on the load-deflection curve. If $\lambda_{c_i} > \lambda_{e_i}$, then the estimated load is too low. If $\lambda_{c_i} < \lambda_{e_i}$, then

46
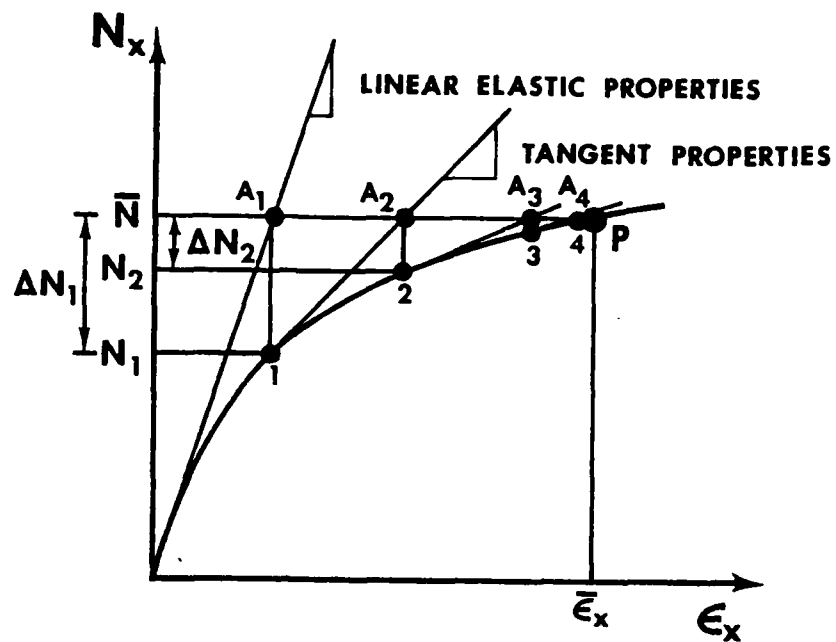
FIGURE 2.17   TANGENT PREDICTOR METHOD FOR ITERATION ALONG
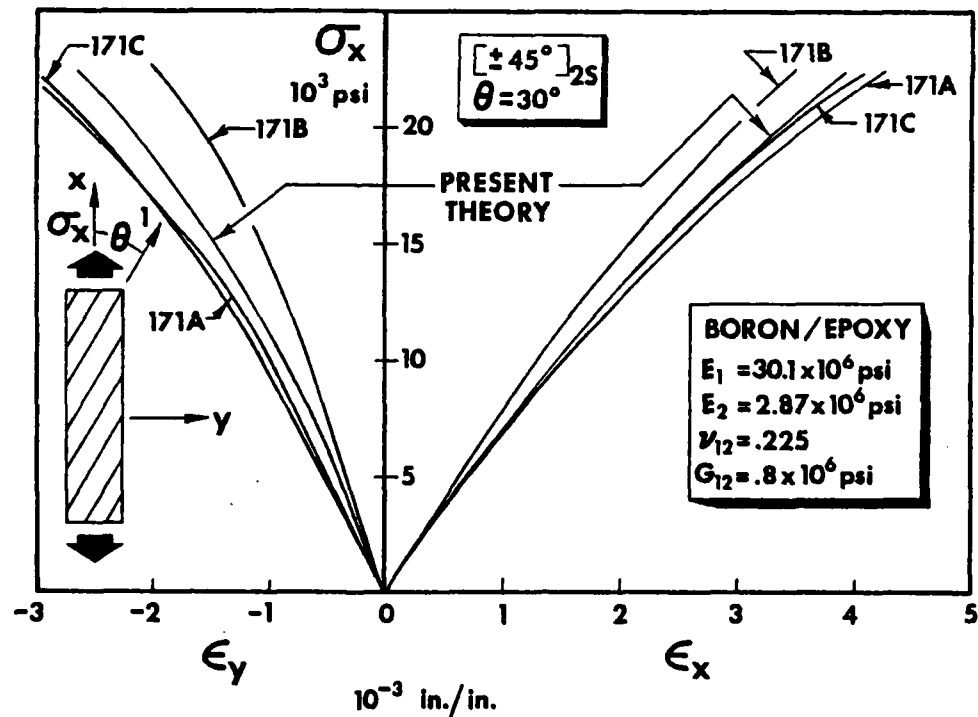THE LOAD-STRAIN CURVE TO A SPECIFIC LOAD

FIGURE 2.18   STRESS-STRAIN BEHAVIOR OF A $[\pm 45°]_{2S}$ BORON-EPOXY LAMINATE
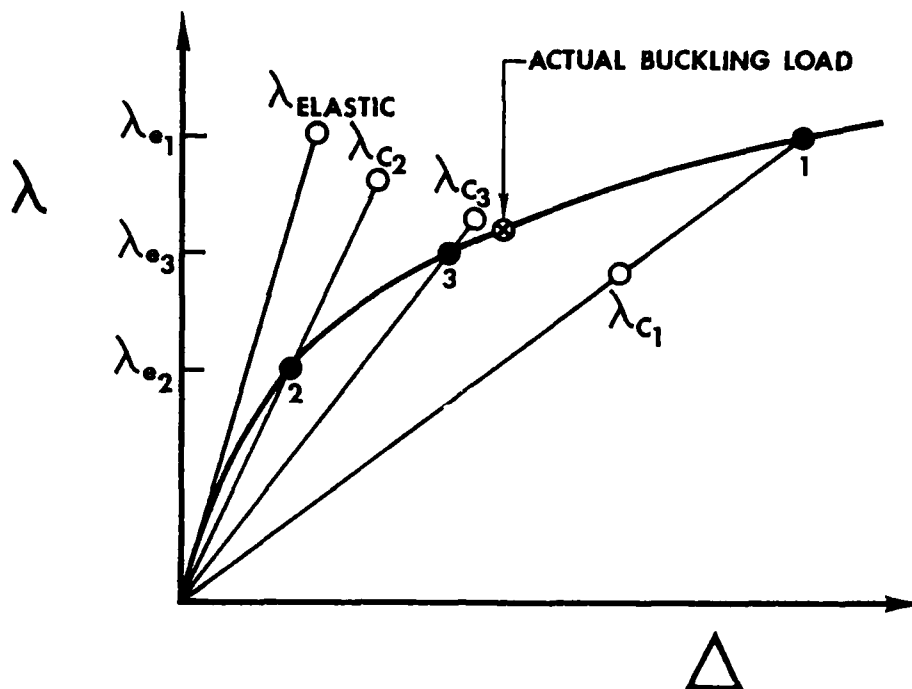LOADED AT 30° TO THE LAMINATE AXES

47

FIGURE 2.19   SEQUENCE OF ESTIMATED AND CALCULATED BUCKLING LOADS
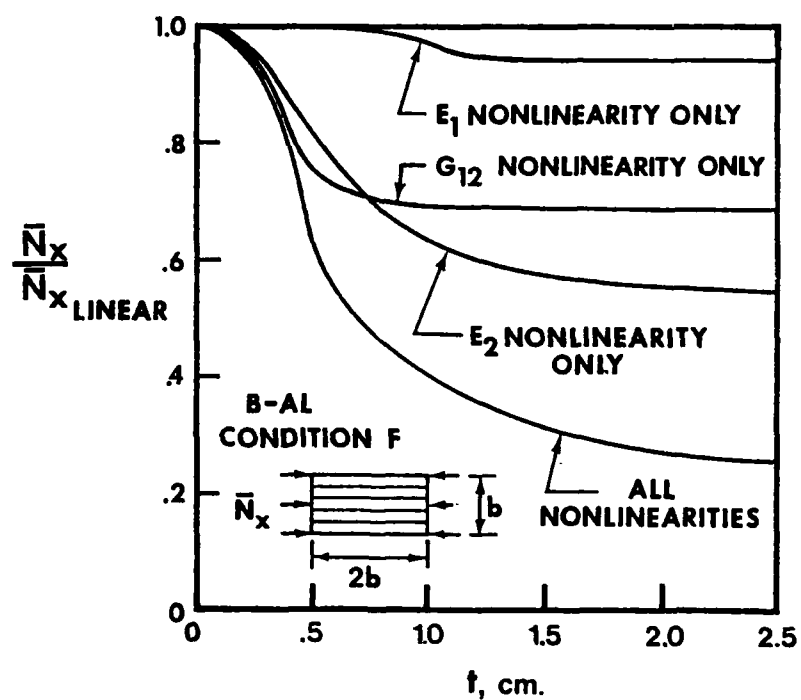

FIGURE 2.20   NORMALIZED AXIAL BUCKLING LOADS FOR
BORON-ALUMINUM UNIDIRECTIONAL LAMINATES

48

the estimated load is too high. These bounds are the basis for an interval halving search procedure to calculate the buckling load to any desired accuracy. For example, the buckling results for unidirectional $0°$ laminates of boron-aluminum are shown in Fig. 2.20 as a function of laminate thickness. There, the thicker the laminate, the more prominent the nonlinear stress-strain behavior is in lowering the buckling load. These effects are separated for the several nonlinear stress-strain behaviors of boron-aluminum, namely nonlinearities in E_1, E_2, and G_{12}. Obviously, these nonlinearities are predicted to be quite influential in determining buckling loads. However, no measured buckling loads are available for comparison with the predictions.

2.5.3.3 Multimodulus Material Behavior

Multimodulus material behavior is generally not a dominant behavioral characteristic for laminated plates and shells. That is, the materials out of which laminated plates and shells are made generally do not have strong multimodulus characteristics. Moreover, these characteristics are somewhat diminished in a structural analysis: a 10% variation between tension and compression moduli does not become a 10% variation in structural behavior, but instead has a somewhat lower influence. Two such structural analyses of laminates from which these conclusions are drawn will be described.

Bending of Cross-Ply Laminates   Cylindrical bending of cross-ply laminates with different moduli in tension and compression [2.3-12] is studied as a vehicle to learn about the influence of multimodulus material behavior on structural behavior. The key unknown is the location of the neutral surface which is determined through an iteration and search procedure. The resulting laminate is not symmetric about the neutral surface,

49

so bending-extension coupling arises. This coupling complicates the determination of the effect of the multimodulus behavior. An example of stresses in a somewhat contrived multimodulus laminate is shown in Fig. 2.21. Considerable difference, percentagewise, is seen between the various stress calculations for the middle layer. However, the stresses in the outer layers for the various approximations are not different from each other by amounts anywhere close to the factor of two difference in tension and compression moduli. The larger differences in the middTe layer could be significant, however, in laminate strength predictions.

Buckling of Laminated Shells   The influence of multimodulus material behavior on buckling loads of laminated shells is investigated in Refs. 2.3-6 and 2.3-7. There, the basic multimodulus material model is included in a buckling analysis with all the appropriate logic, including variation in stress versus variation in strain relations. A physical discontinuity in buckling loads is predicted for biaxial loading of a laminated shell whenever a layer stress changes from tension to compression or vice versa. The size of the discontinuity depends on the multimodulus ratio E_t/E_c. For boron-epoxy, the ratio E_t/E_c is quite close to one. Thus, the discontinuities in Fig. 2.22 are quite small and are, in some cases, almost indistinguishable. The buckling load can be shown to be proportional to the square root of E_t/E_c, so a 10% difference in moduli leads to a 5% difference in buckling load at the corresponding discontinuities. This diminishing of the structural importance of the multimodulus ratio is the most important observation to make in this section.

90° LAYER STRESSES

COMPRESSION →

$E_{1_c} = 20 \times 10^6 \text{psi}$ $E_{2_c} = 10 \times 10^6 \text{psi}$

$\nu_{12_c} = .2$

$E_{1_t} = 40 \times 10^6 \text{psi}$ $E_{2_t} = 20 \times 10^6 \text{psi}$

$\nu_{12_t} = .4$

← TENSION

—— EXACT

—— $B_{ij} = 0$

—·— E_{avg}, E_c, E_t

FIGURE 2.21   STRESS DISTRIBUTION IN A 3-LAYER "SYMMETRIC" LAMINATE WITH MODERATE ORTHOTROPY AND HIGH E_t/E_c

FIGURE 2.22   BUCKLING OF A TWO-LAYERED BORON-EPOXY SHELL

51
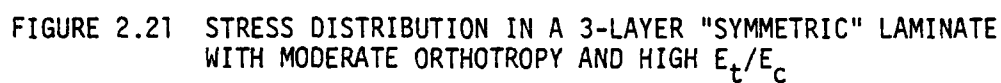
3. MODELING NONLINEAR DEFORMATION OF CARBON-CARBON COMPOSITE MATERIALS

3.1 INTRODUCTION

The process of modeling the nonlinear deformation behavior of carbon-carbon composite materials is quite involved and requires many steps for complete understanding. First, the characteristics of carbon-carbon materials are described in Section 3.2 so the mechanical behavior properties that must be modeled can be observed. Then, the possible comparisons that can be made between theoretically predicted and measured response are discussed in Section 3.3. Next, a specific carbon-carbon model is obtained in Section 3.4 for AVCO Mod 3a three-dimensionally fiber-reinforced carbon-carbon. The effect of how actual test specimens deform in perhaps the simplest test is derived in Section 3.5. Finally, predicted strains under uniaxial off-axis loading and under shear loading are compared in Section 3.6 with measured strains to validate the model displayed in Section 3.4.

3.2 CHARACTERISTICS OF CARBON-CARBON MATERIALS

Carbon-carbon is not a single material, but is instead a broad class of materials. Many types of carbon-carbon are manufactured including various kinds of woven fibers or felt materials both of which are coated or impregnated with a matrix material in a vapor deposition process or a pressure impregnation process. The combination of materials is subsequently carbonized and graphitized to create carbon-carbon.

The steps in a typical pressure impregnation process are illustrated in Fig. 3.1. In the first step, woven graphite fabric in the horizontal plane is pierced with metal rods in the vertical direction while being built up layer by layer in the vertical direction. The warp and fill
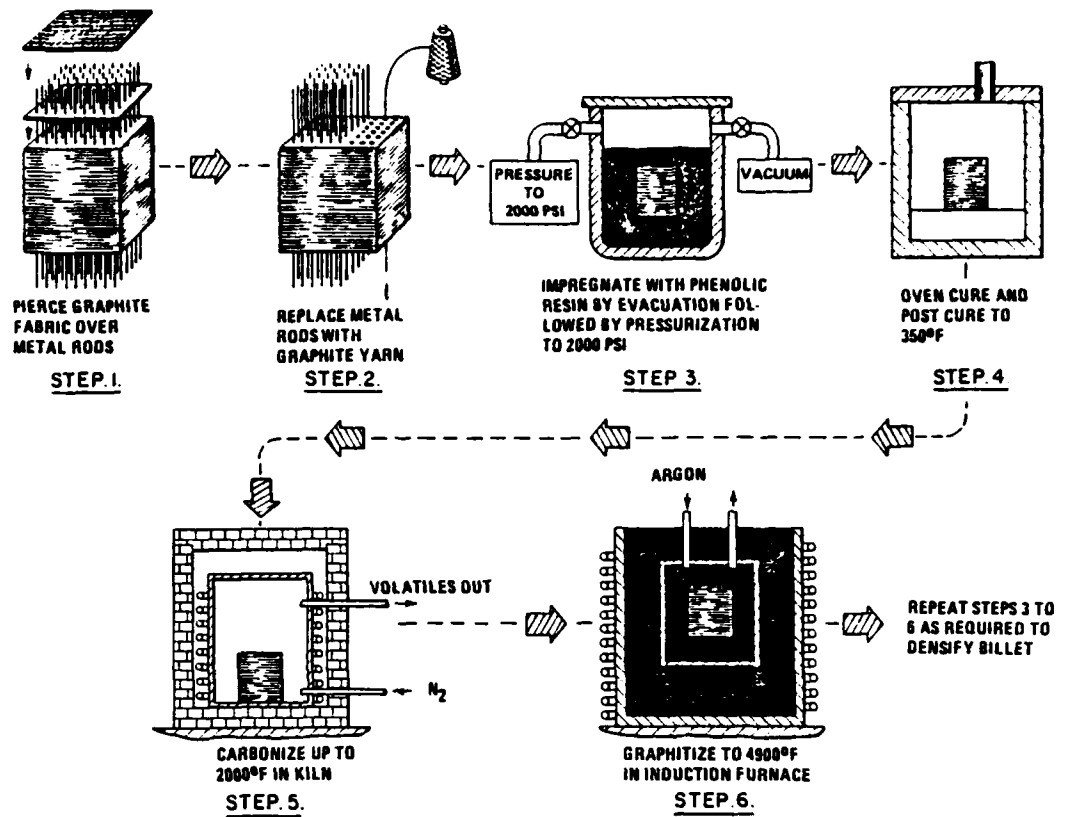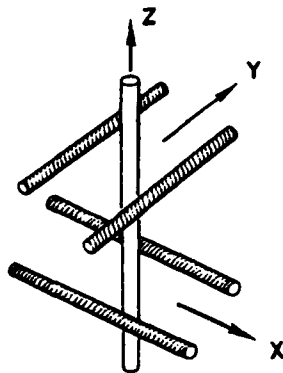
52

Step labels within Figure 3.1:

PIERCE GRAPHITE FABRIC OVER METAL RODS
STEP. I.

REPLACE METAL RODS WITH GRAPHITE YARN
STEP. 2.

IMPREGNATE WITH PHENOLIC RESIN BY EVACUATION FOLLOWED BY PRESSURIZATION TO 2000 PSI

PRESSURE TO 2000 PSI

VACUUM

STEP 3.

OVEN CURE AND POST CURE TO 350°F
STEP. 4

VOLATILES OUT

CARBONIZE UP TO 2000°F IN KILN
STEP. 5.

ARGON

GRAPHITIZE TO 4900°F IN INDUCTION FURNACE
STEP. 6.

REPEAT STEPS 3 TO 6 AS REQUIRED TO DENSIFY BILLET

FIGURE 3.1   AVCO MOD 3a FABRICATION PROCESS

ORTHOGONALLY REINFORCED PARALLEL YARNS
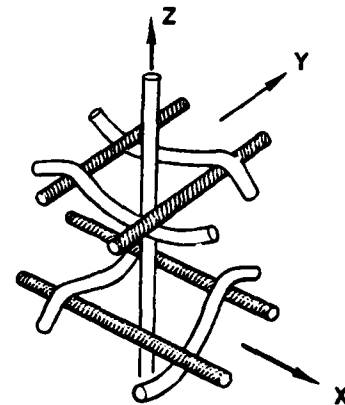
ORTHOGONALLY REINFORCED WOVEN FABRIC

FIGURE 3.2   GEOMETRY OF LAYERS IN xy-PLANE

directions are alternated with each layer. Next, the metal rods are replaced with graphite yarn or graphite fibers. This somewhat loose assembly of layers is impregnated with phenolic resin in step three. The impregnation process takes place first by evacuation of the chamber in which the material is located and then by pressurization to force the phenolic resin into the voids of the woven and pierced fabric. Then, in step four, the material is cured in an oven at 350°F. Next, the material is carbonized at 2000°F in a kiln in step five. Finally, the material is graphitized to 4900°F in an induction furnace in step six. At this stage, the billet of carbon-carbon does not have the degree of density possible, i.e., not all the voids are filled with a graphitized form of the phenolic resin. Accordingly, steps three through six are repeated until the desired density is attained.

Carbon-carbon is made with several different geometries. Each of the layers in Fig. 3.1 can be either woven in the horizontal (x-y) plane or made of parallel fibers as in Fig. 3.2. AVCO 3D is of parallel fiber construction and is shown schematically in Fig. 3.3. One variation on a three-dimensional weave or three-dimensional construction of orthogonal fibers is to add fibers at 45° angles to the x-, y-, and z-directions. The resulting "7D" construction is shown schematically in Fig. 3.4 for fibers with prismatic cross sections. A much simpler carbon-carbon structure is obtained after carbon vapor deposition on carbonized felt. The fibers of uncarbonized felt are shown in the scanning electron photomicrograph in Fig. 3.5 where obviously the fibers have no preferred orientation. The scale of all these possible carbon-carbon constructions is revealed in Fig. 3.6 where the approximate fiber spacings in 7-D carbon-carbon are shown in a nosetip. Obviously, the microscale of carbon-carbon materials is not negligible in comparison to the nosetip dimensions.
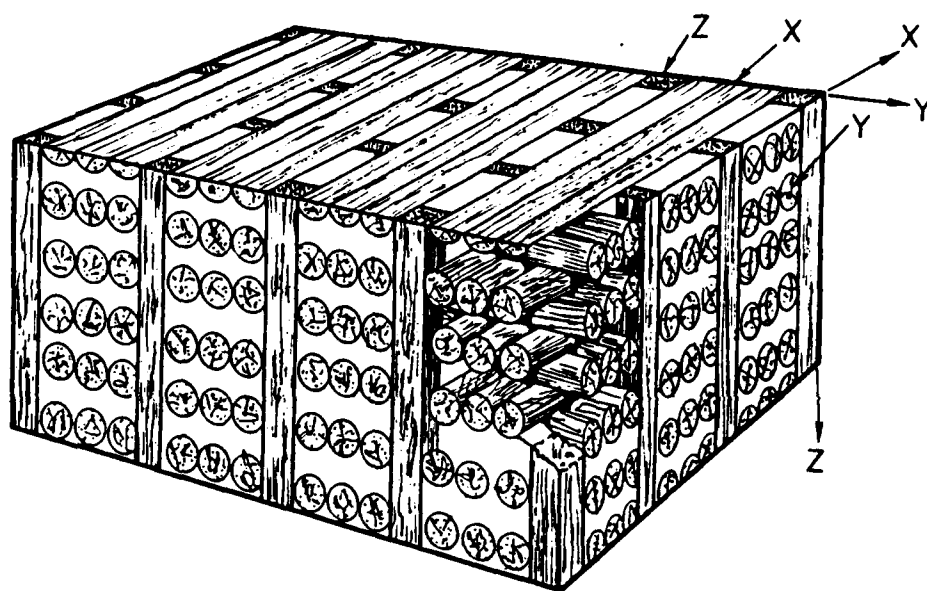
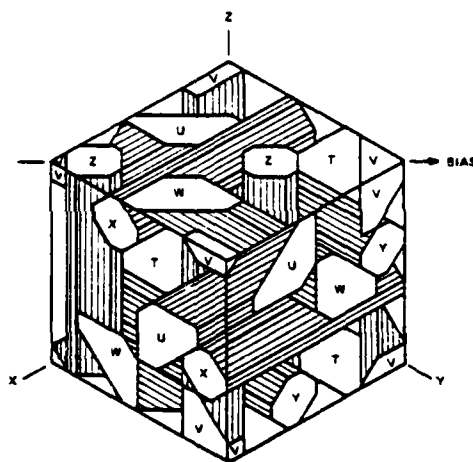FIGURE 3.3   AVCO 3D CONSTRUCTION

FIGURE 3.4   PACKING MODEL OF PRISMS HAVING EQUAL CROSS SECTIONAL AREA
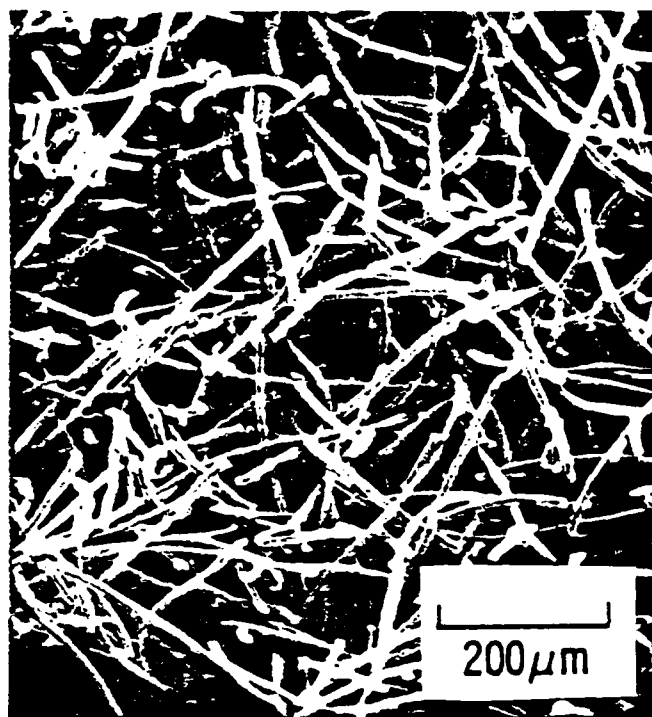IN 7-D CUBIC GEOMETRY

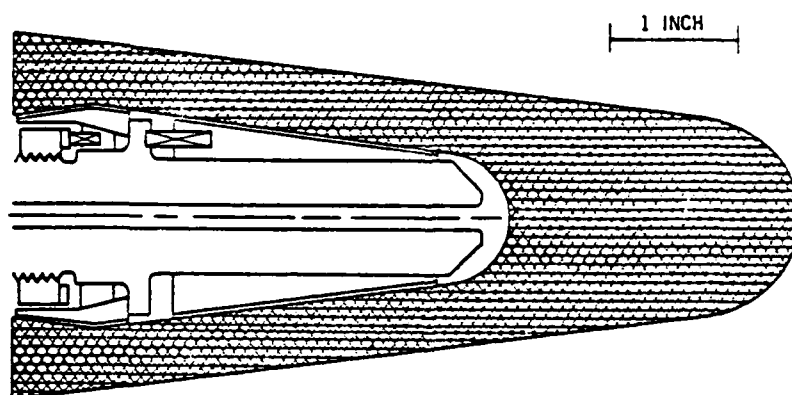55

FIGURE 3.5   UNCARBONIZED VISCOSE-RAYON FELT

FIGURE 3.6   7-D CARBON-CARBON NOSETIP WITH

REPRESENTATIVE FIBER SPACINGS

Generally, the microscale dimensions of graphite, namely the particle size, etc. are negligible for nosetip stress analysis problems. However, the characteristic material dimensions of carbon-carbon are not clearly negligible for nosetip problems although perhaps the answer to this question is dependent on the specific carbon-carbon material to be considered.

The anisotropy of the various carbon-carbon materials depends primarily on the geometry of the fiber construction and secondarily on the manner of incorporating a carbon matrix. For example, the orthogonally reinforced carbon-carbons with parallel fibers such as AVCO 3D (Figs. 3, 3.2 and 3.3) and with woven fabric such as AVCO MOD-3 (Figs. 3.1 and 3.2) are orthotropic with principal material directions in the three fiber directions. In contrast, GE 7-D is not only orthogonally reinforced, but also has fibers at 45° to the x-, y-, and z-directions in which the orthogonal fibers are placed. Accordingly, GE 7-D is anisotropic (although with so many fiber directions, the degree of anisotropy for GE 7-D is lower than the degree of orthotropy for AVCO 3D, i.e., GE 7-D is more like an isotropic material than is AVCO 3D). The manner of incorporating a carbon matrix in carbon-carbon can be an influencing factor for anisotropy only when the process of constructing or depositing the matrix has some directional dependence. For example, a matrix formed by chemical vapor deposition in a shell structural element can have a directional dependence of mechanical properties because of vapor penetration perpendicular to the shell surface and no penetration parallel to the surface. This effect is similar to effects obtained with pyrolytic graphite because of alignment of particles due to direction preferential deposition of material. In summary, the most obvious clue to the degree

57

of anisotropy remains the fiber geometry, but anisotropy is also influenced by the matrix construction.

At least two difficulties arise in analysis of carbon-carbon materials. The first obvious difficulty is the analytical complication due to the many more mechanical properties necessary to characterize carbon-carbons as compared to simpler materials. This analytical complication is handled with relative ease in comparison to the more troublesome problem of measuring the additional mechanical properties. Basically, the problem is that simple strain states do not result from simple imposed stress states. For example, a uniaxial stress at 45° to the fiber directions in Fig. 3.7 leads to both extension in the direction of the load (and the usual Poisson contraction perpendicular to the load) and inplane shearing if the ends of the specimen are not restrained in any way. On the other hand, if the specimen ends are restrained to remain perpendicular to the load, then a complicated nonuniform shearing and extensional response results. The complicated response occurs if the test specimen is short and wide whereas the simpler response occurs if the test specimen is long and narrow. In fact, if the specimen is relatively short and wide, the stiffness being measured is not the Young's modulus in the x-direction of the sketch in Fig. 3.8 but the two-dimensional (transformed reduced) stiffness $\bar{Q}_{11}$. The reason for this discrepancy is that the geometrically admissible state of strain in the specimen depends strongly on the geometry. If the specimen is long and slender, then the boundary conditions at the specimen end grips are of no consequence a la Saint Venant. Accordingly, a pure uniaxial strain is obtained and

$$\sigma_x = E_x \varepsilon_x \qquad (3.1)$$

58
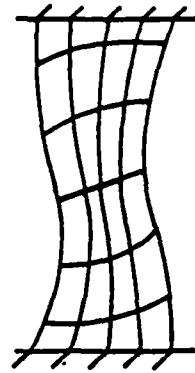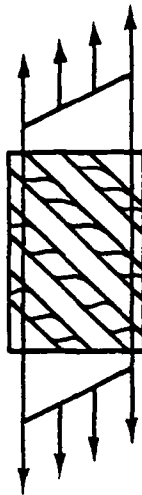
NO END EFFECT   **RESTRAINED ENDS**

FIGURE 3.7   DEFORMATION OF A UNIDIRECTIONALLY REINFORCED LAMINA
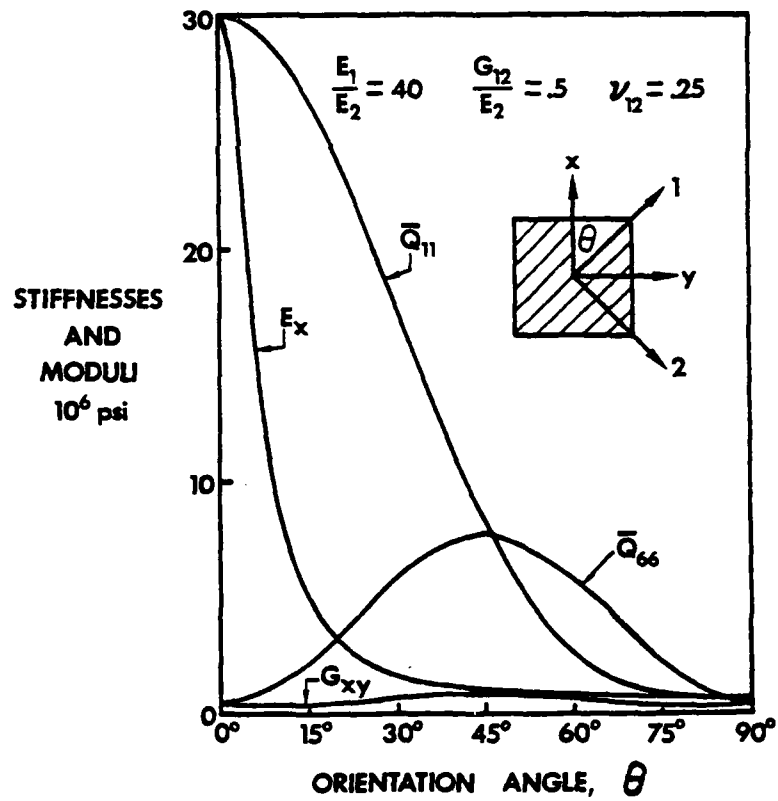LOADED AT 45° TO THE FIBER DIRECTION

FIGURE 3.8   STIFFNESSES $\bar{Q}_{11}$ AND $\bar{Q}_{66}$ VERSUS MODULI E_x AND G_{xy}

59

However, for a short, wide specimen, the end restraint of $\sigma_x \neq 0$, $\varepsilon_y = \gamma_{xy} = 0$ leads to the stress-strain relation

$$\sigma_x = \bar{Q}_{11}\varepsilon_x \qquad (3.2)$$

Similar results are shown in Fig. 3.8 for an applied shear stress resulting in either G_{xy} as desired or $\bar{Q}_{66}$ if the test specimen geometry is not properly chosen.

The foregoing situation is but one example of many complicated mechanics problems which arise in the design of "proper" test specimens. By "proper" test specimens is meant specimens for which the desired response can be measured without undue influence of some unwanted response. For example, even with end restraint in Fig. 3.7, a specimen can be made long enough that the resulting deformation looks like the unrestrained end response. From a practical standpoint, if the response can be made predominantly simple by suitable choice of specimen geometry, then the goal of a proper test specimen is attained. Analysis of specimen response for various geometries to determine the geometry for which simple response occurs is the objective in many mechanics efforts. However, to date, little has been done to apply the principles of mechanics in rational treatment of carbon-carbon materials.

Some of the difficulties in rationally analyzing the mechanical behavior of carbon-carbon materials are related to even more complicated response characteristics than just discussed for a unidirectionally reinforced lamina. For example, anisotropic carbon-carbon under shear loading in one principal material plane will also have shear deformation in the two principal material planes which are perpendicular to the stressed principal material plane. This shear coupling obviously results in very complicated strain response. Moreover, the multimodulus characteristic

60

of carbon-carbon materials is yet another complicating factor in addition to the nonlinear stress-strain behavior in every principal material direction.

If we ignore for a moment both the multimodulus character and the nonlinear character of carbon-carbon materials, the strain-stress equations for linear elastic behavior of orthotropic materials are (in orthogonal x, y, z coordinates aligned with the principal material directions):

$$
\begin{Bmatrix} \varepsilon_x \\ \varepsilon_y \\ \varepsilon_z \\ \gamma_{yz} \\ \gamma_{zx} \\ \gamma_{xy} \end{Bmatrix}
=
\begin{bmatrix}
\frac{1}{E_x} & -\frac{\nu_{xy}}{E_x} & -\frac{\nu_{xz}}{E_x} & 0 & 0 & 0 \\
-\frac{\nu_{xy}}{E_x} & \frac{1}{E_y} & -\frac{\nu_{yz}}{E_y} & 0 & 0 & 0 \\
-\frac{\nu_{xz}}{E_x} & -\frac{\nu_{yz}}{E_y} & \frac{1}{E_z} & 0 & 0 & 0 \\
0 & 0 & 0 & \frac{1}{G_{yz}} & 0 & 0 \\
0 & 0 & 0 & 0 & \frac{1}{G_{zx}} & 0 \\
0 & 0 & 0 & 0 & 0 & \frac{1}{G_{xy}}
\end{bmatrix}
\begin{Bmatrix} \sigma_x \\ \sigma_y \\ \sigma_z \\ \tau_{yz} \\ \tau_{zx} \\ \tau_{xy} \end{Bmatrix}
\tag{3.3}
$$

Obviously, nine independent constants

E_x, E_y, E_z = Young's moduli in x-, y-, and z-directions, respectively

ν_{ij} = Poisson's ratio for transverse strain in the j-direction when stress exists in the i-directions, i.e.,

$$
\nu_{ij} = -\frac{\varepsilon_j}{\varepsilon_i}
$$

for $\sigma_i = \sigma$ and all other stresses are zero.

G_{yz}, G_{zx}, G_{xy} = shear moduli in the y-z, z-x, and x-y planes, respectively. must be measured.

61

We now recognize that the strain-stress relations in Eq. (3.3) must be modified to account for multimodulus behavior. Hence, in the manner Jones [2.3-17], the shear moduli are replaced with Young's moduli at 45° to principal material directions. We then have the following nine independent mechanical properties:

$$E_x, \ E_y, \ E_z, \ \nu_{yz}, \ \nu_{zx}, \ \nu_{xy}, \ E_{yz}^{45}, \ E_{zx}^{45}, \ E_{xy}^{45} \tag{3.4}$$

when the carbon-carbon composite has three orthogonal principal material directions with unequal fiber volumes or unequal fiber sizes in the three directions. If the fiber volumes or fiber sizes are equal in two directions (as in AVCO 3D shown in Fig. 3.3), the six independent mechanical properties are:

$$E_x, \ E_y = E_x, \ E_z, \ \nu_{yz}, \ \nu_{zx} = \nu_{zy}, \ \nu_{xy} \quad E_{yz}^{45}, \ E_{zx}^{45} = E_{zy}^{45}, \ E_{xy}^{45} \tag{3.5}$$

Finally, if equal fiber volumes or fiber sizes exist in all three directions, the three independent mechanical properties are:

$$E_x = E_y = E_z \qquad \nu_{yz} = \nu_{zx} = \nu_{xy} \qquad E_{yz}^{45} = E_{zx}^{45} = E_{xy}^{45} \tag{3.6}$$

(Note, however, that because of the three fiber directions the modulus at 45° is _independent_ of the direct moduli and Poisson's ratios because the shear behavior is independent). All of the properties in Eqs. (3.4), (3.5), and (3.6) must be measured both in tension and in compression. Moreover, these properties must be measured at many stress levels to account for the nonlinear stress-strain behavior in the manner of the Jones-Nelson-Morgan material models discussed in Section 2.

We examine orthotropic and anisotropic carbon-carbon mechanical behavior which is representative of that found in References 23 and 26 through 34. Those references are the primary body of information on carbon-carbon mechanical properties although other information exists

in the Journal of Composite Materials and in other classified and unclass-
ified reports. Typical stress-strain curves are shown in Figs. 3.9 and
3.10 for the materials examined in the CCAP program (Carbon-Carbon Assess-
ment Program). All of the stress-strain curves displayed have some degree
of nonlinearity ranging from mild to strong. Notice how the shapes of
the actual stress-strain curves are similar to the basic shape of the
Jones-Nelson-Morgan nonlinear material model stress-strain curve in Fig.
2.1 on p. 18. The Jones-Nelson-Morgan model was developed to treat carbon-
carbon behavior in addition to ATJ-S graphite as well as boron/epoxy,
graphite/epoxy, and boron/aluminum.

The multimodulus characteristic of carbon-carbon is a manufacturer-
dependent phenomenon. Early materials had drastic differences in tension
and compression moduli. For example, the MDAC low modulus block course
weave material [26] has a ratio of tension modulus to compression modulus
in the z-direction ranging from 4 to 5! More recent materials have closer
tension and compression moduli - for example, AVCO MOD 3 [29] has a ten-
sion modulus greater than the compression modulus by about 60% in both
the x-direction and the z-direction.

Another behavioral characteristic worthy of note is the classical
viscoplastic behavior of carbon-carbon at high temperatures. For example,
AVCO MOD 3a exhibits this behavior at 5000°F in Fig. 3.11. The stress
rate is increased by factors of ten and the stress-strain curve rises in
the usual viscoplastic manner.

Some carbon-carbon materials have a characteristic of rectangular
orthotropy which is quite different from the transverse isotropy of ATJ-S
graphite. The practical significance of this difference is that in a
reentry vehicle nosetip application, ATJ-S graphite is axisymmetric
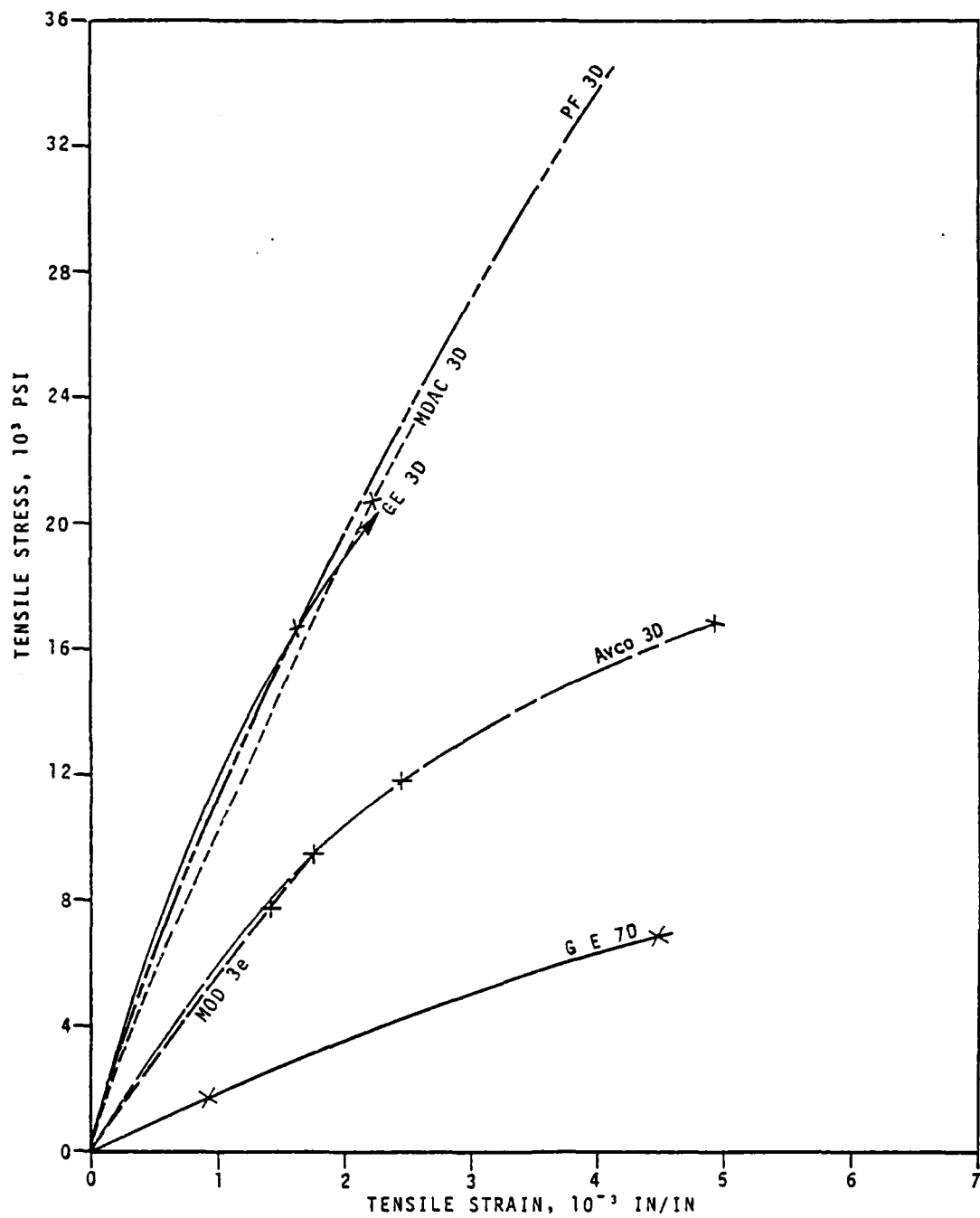whereas carbon-carbon is not. This important distinction is quite sig-

FIGURE 3.9 PROBABLE VALUE TENSION STRESS-STRAIN CURVES FOR
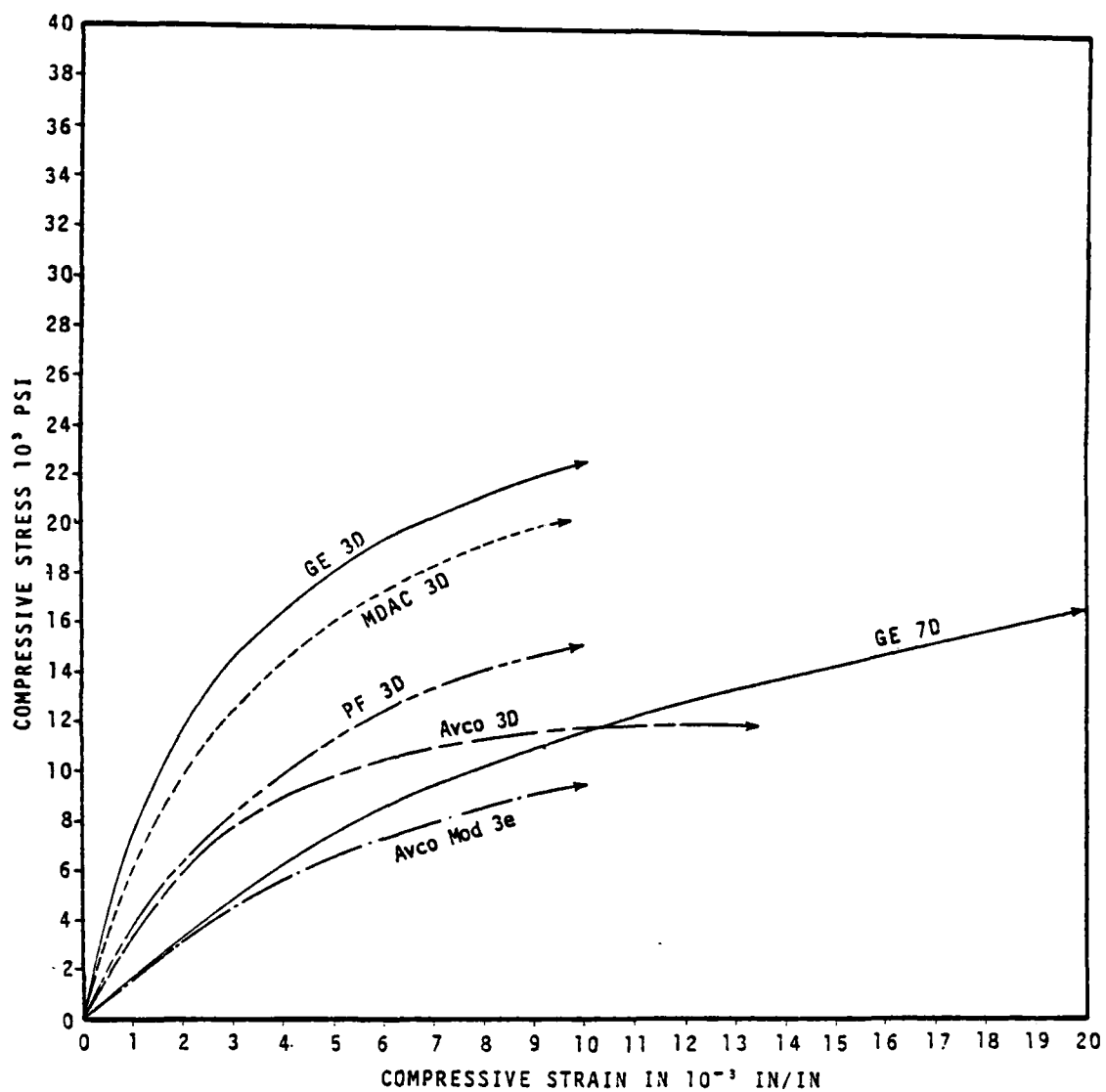CCAP MATERIALS AT 70°F IN THE Z-DIRECTION [30]

64

FIGURE 3.10   PROBABLE VALUE COMPRESSION STRESS-STRAIN CURVES FOR

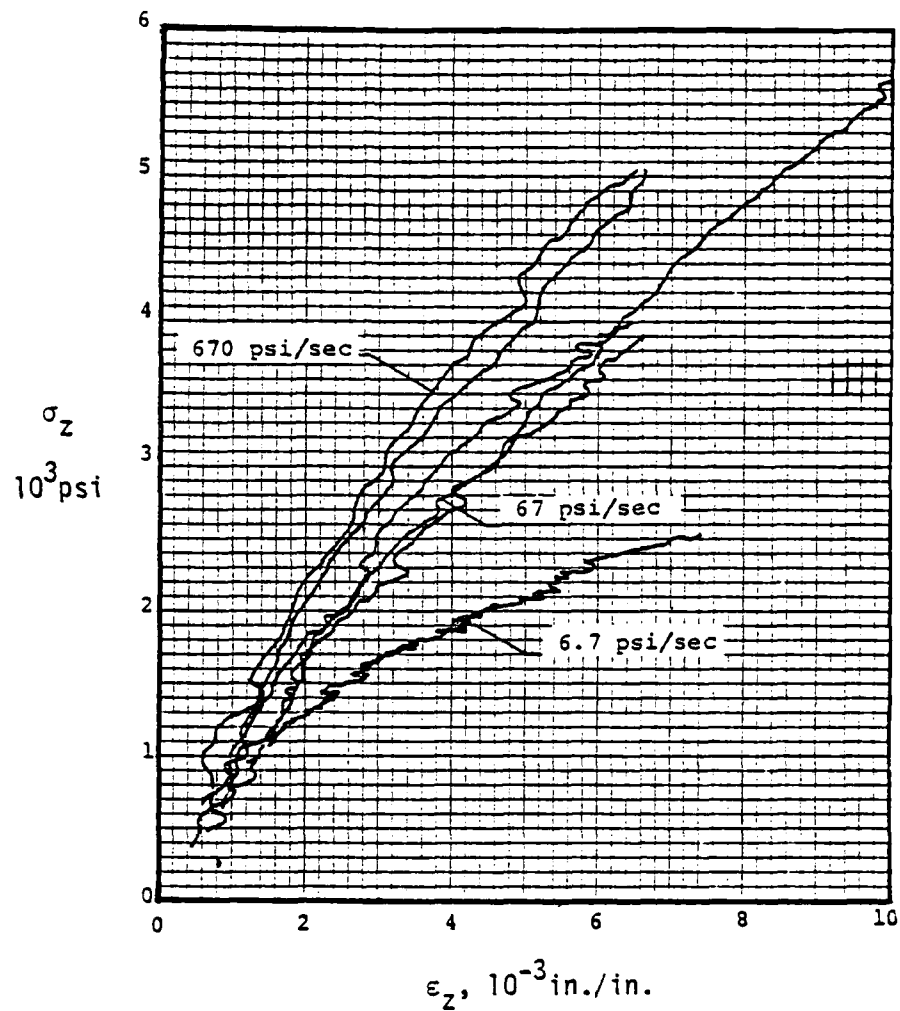CCAP MATERIALS AT 5000°F IN THE Z-DIRECTION [30]

65

FIGURE 3.11   COMPRESSION STRESS-STRAIN CURVES FOR AVCO MOD 3a

AT 5000°F IN THE Z-DIRECTION

FOR VARIOUS STRESS RATES [29]

nificant from the point of view of the nosetip stress analyst.

On the other hand, many different carbon-carbon fiber geometries are used in rocket nozzle applications. The most common orientations are shown in Fig. 3.12. There, five orientations of two-dimensionally woven carbon-carbon are displayed along with a three-dimensional carbon-carbon with fibers in the radial and circumferential direction as opposed to the rectangularly orthotropic three-dimensional carbon-carbon in Fig. 3.3. Four of the orientations in Fig. 3.2 are cylindrically orthotropic, namely 90° to $\mathcal{C}$, 45° to $\mathcal{C}$, 0° to $\mathcal{C}$, and 3-D weave, and are reasonably easy to characterize and analyze. However, the remaining two orientations, tangential and rosette, are anisotropic and present considerable difficulty in both characterization and analysis.

In summary, carbon-carbon materials have mechanical behavioral characteristics which are a substantial escalation in degree of complication over the characteristics of graphite materials. The carbon-carbon analysis problem is very difficult and complex. Hence, the progress will be slow because of the many mechanics problems that must be addressed.

3.3 POSSIBLE THEORETICAL-EXPERIMENTAL RESPONSE COMPARISONS

The types of experiments for which behavior can be meaningfully predicted will be discussed. The objective is to obtain sufficient validation of a material model for carbon-carbon by successful prediction of measured behavior of representative materials under representative loading conditions (both mechanical and thermal). Thus, a multilevel theoretical-experimental correlation effort must be addressed. This effort will be discussed by comparison with a similar effort for ATJ-S Graphite, a transversely isotropic polycrystaline particulate composite material. First, the mechanical property characteristics of various carbon-carbon

67

90° TO ℄   45° TO ℄   0° TO ℄

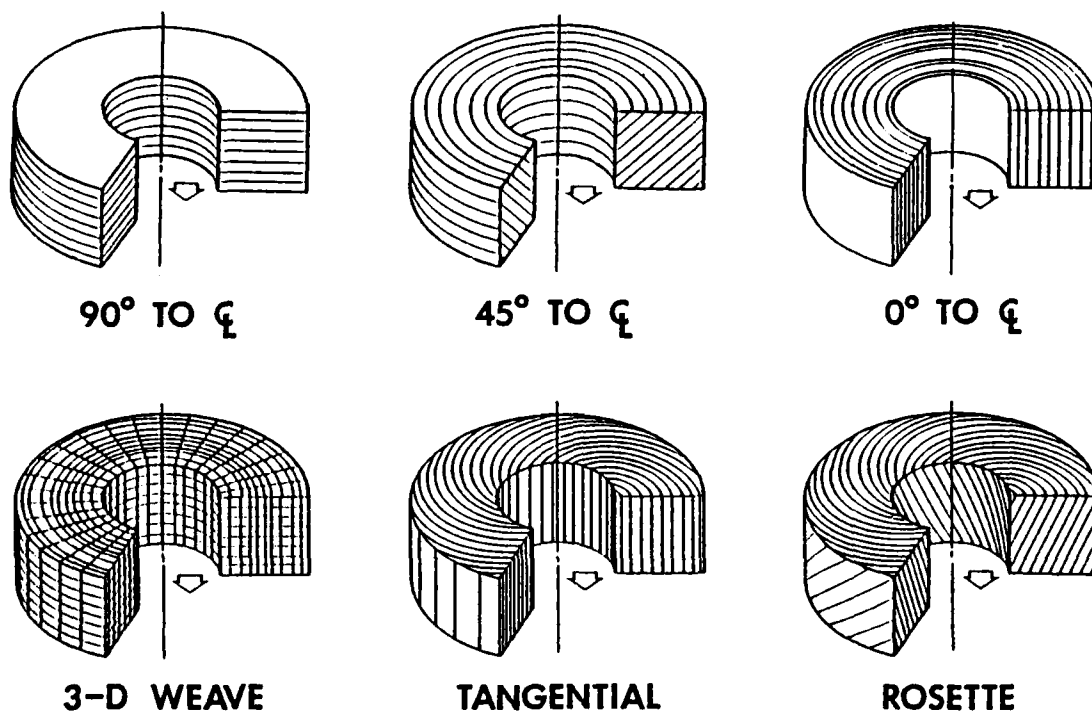3-D WEAVE   TANGENTIAL   ROSETTE

FIGURE 3.12   CARBON-CARBON ROCKET NOZZLE MATERIAL ORIENTATIONS

materials will be categorized. Then, the heirarchy correlation efforts

for ATJ-S Graphite will be described. Finally, possible correlation efforts

for carbon-carbon materials will be discussed.

3.3.1 Mechanical Property Anisotropy Classes for Carbon-Carbon Materials

Carbon-carbon materials are made in many forms with the primary

difference between the various forms being the direction of the fibers.

Unidirectional fibers are not common for carbon-carbons, but two-dimensional

woven fibers are a very common form. See Fig. 3.12 for various two-

dimensional fiber orientation relative to the body geometry of a rocket

nozzle. Moreover, three-dimensionally woven fibers such as the 3-D weave

in Figs. 3.3 or 3.12 are used. Finally, multidirectional weaves are

possible, e.g., the 7-D weave in Figs. 3.4 and 3.6. We will categorize

these various forms of carbon-carbon according to the type of anisotropy

they exhibit. For convenience, we will concentrate on three broad classes:

anisotropic, rectangularly orthotropic, and cylindrically orthotropic.

Anisotropic Carbon-Carbon Materials   Anisotropic carbon-carbon

materials are made of multidirectionally woven fibers that are not per-

pendicular to one another and do not exhibit any planes of mechanical

property symmetry. Examples of anisotropic carbon-carbons include the

GE 7-D carbon-carbon in Figs. 3.4 and 3.6 and the tangential and rosette

weaves in Fig. 3.12. The latter materials are two-dimensional woven

fabric that has been reoriented such that the fibers no longer lie in

a single plane nor are they all parallel to one another as they were

when they were formed in a single plane.

Rectangularly Orthotropic Carbon-Carbon Materials   For rectangu-

larly orthotropic carbon-carbon materials, the fiber directions are always

parallel to one of the three rectangular coordinate directions. Moreover,

the material has three mutually perpendicular planes of mechanical

property symmetry (a consequence of the first statement). Examples of

such materials are shown in Figs. 3.1, 3.2, and 3.3.

Cylindrically Orthotropic Carbon-Carbon Materials   For cylindrically

orthotropic carbon-carbon materials, the fiber directions are always in

cylindrical coordinate directions (i.e., radial, axial, and circumferential).

The material has three mutually perpendicular planes of mechanical pro-

perty symmetry at each point of the body, i.e., locally. Globally, the

material is axisymmetric and is often referred to as a polar weave materi-

al. An example of a cylindrically orthotropic carbon-carbon is the 3-D

weave in Fig. 3.12.

3.3.2 Material Model Validation Tests for ATJ-S Graphite

In contrast to the various carbon-carbon materials, ATJ-S graphite

is a transversely isotropic material with the plane of isotropy perpen-

dicular to the axis of symmetry of the bodies in which ATJ-S graphite is

used. Accordingly, ATJ-S graphite is a much simpler material to model

and to conduct experiments on than any of the carbon-carbon materials.

The model of ATJ-S graphite was constructed from information on mechanical

behavior (i.e., stress-strain curves) in the principal material directions

and at 45° to principal material directions. Thus, validation of the

model is performed by conducting tests to obtain response independent of

the behavior used to construct the model. Three types of laboratory-

quality tests were performed for ATJ-S graphite:

(1) Uniaxial Off-Axis Mechanical Loading   Specimens of graphite

were subjected to either tension or compression loading in

directions at an angle of 70° to the principal material

directions. The Jones-Nelson-Morgan model was used to predict

the corresponding strain response which was in excellent agreement with the measured response in the stress direction, but not as good in the direction transverse to the stress direction [2.3-9 and 2.3-14].

(2) <u>Biaxial Mechanical Loading in Principal Material Directions</u> Internal pressure and axial tension or compression were applied to a tubular specimen of ATJ-S graphite. The tube axis coincided with the direction perpendicular to the plane of isotropy; hence, the loading, which leads to axial and circumferential stresses, is in principal material directions. The axial and circumferential strains predicted with the Jones-Nelson-Morgan model in the SAAS IIIM computer program are in excellent agreement with the measured strains at room temperature. The experimental device is not as reliable at elevated temperatures as it is at room temperature, so correlations between predicted and measured strain response are not as good as at room temperature [2.3-5 and 2.3-14].

(3) <u>Biaxial Thermal Loading in Principal Material Directions</u> A graphite circular disk with a central hole (i.e., an annular disk) is rapidly heated on its outer circumference with induction heating coils. An axisymmetric state of thermal stress results because of the thermal gradient and the fact that the plane of isotropy of the material coincides with the plane of the disk. Excellent agreement is obtained between predicted and measured central hole diameter change as a function of time [2.3-20]

Important observations from the foregoing discussion of model validation

71

tests for ATJ-S graphite are:

(1) The uniaxial off-axis mechanical loading test can be performed for any material, although various kinds of coupling such as shear coupling can arise in addition to the usual Poisson effects because of anisotropy or apparent anisotropy in nonprincipal material directions. Moreover, response predictions can be made for any material provided the minimum number of mechanical properties is available to determine the material model coefficients (of which there are more for orthotropic and anisotropic materials than for transversely isotropic materials). Specimen size is of concern only when the influence of shear coupling, etc. must be eliminated in a gage section.

(2) The Biaxial Tube Test can be performed for materials from which a tube can be machined. However, the characteristics of the loading response are different for the various types of carbon-carbon considered. For axisymmetric response, the circular cross section of the tube must remain circular, and the only way for that to happen is for the material to have an axis of symmetry coincident with the tube axis; otherwise the response is asymmetric. Tube wall thickness can be a problem. The grain size of ATJ-S graphite is somewhat smaller than the .050 in. tube wall thickness used by Jortner [17]. However, that small a wall thickness might not allow a representative amount of carbon-carbon fibers to be subjected to load. Thus, the micro-mechanical response might overhwelm the desired uniform macro-mechanical response.

(3) The SoRI Thermal Stress Disk Test can be performed for materials

72

from which an annular disk of about 2 inches in outer dia-
meter and .5 inch in inner diameter can be machined. These
size limitations arise because of power limitations for
generation of the heat on the outer circumference (but have
been relaxed somewhat because of acquisition of a large power
supply). That is, the size of specimen is related to the
maximum power available to create the thermal gradients which
lead to high enough thermal stresses to fracture the specimen.

3.3.3 Possible Material Model Validation Tests for Carbon-Carbon Materials

The possible application of the ATJ-S graphite hierarchy of valida-
tion tests to various kinds of carbon-carbon is examined to determine the
suitability of this use. Each test is separately addressed to compare its
limitations to the characteristics of each of the kinds of carbon-carbon.

(1) Uniaxial Off-Axis Loading Test

This test can be performed for any carbon-carbon with only two
conditions to meet: (1) the length of the specimen must exceed
that required for the various kinds of coupling such as shear
coupling to not influence the stiffness measurement being made
and (2) the specimen length must be short enough that the
geometry of the carbon-carbon fiber array does not vary within
the specimen. The latter restriction is significant for polar
weave C-C in the plane of the polar weave. An off-axis speci-
men in the plane of the polar weave obviously has a variable
direction of circumferential fibers with length; such a varia-
tion is generally unacceptable except for the crudest of
evaluation tests and certainly is not suitable for a model

73

verification test. Note also that even the basic circum-
ferential mechanical properties are difficult to measure with
a straight uniaxial tension test specimen; instead, a ring or
hoop is usually subjected to internal pressure. However, the
NOL ring test is not at all geometrically suited to an off-
axis loading specimen for obvious geometric reasons. Problems
similar to polar weave C-C <u>can</u> occur for general configurations
of anisotropic C-C. However, no limitations exist on applica-
tion of the uniaxial off-axis loading test to rectangularly
orthotropic C-C.

(2) Biaxial Tube Test

The first limitation encountered for the biaxial tube test is
the fact that a tubular specimen must be machined from the
material. For solid materials such as anisotropic, rectangu-
larly orthotropic, or quasi-isotropic C-C, which are made in
solid billets, this limitation is not important except for
possible limitations on thinness of tube relative to repre-
sentative cell size of the material microstructure. However,
polar weave C-C is not made as a solid billet, but instead
has a central hole. This central hole exists because of the
way polar weave is made and because of the usual application
to rocket nozzles which have a central hole, by definition,
and so no excess material is created in the billet that
would just have to be wastefully machined away. Moreover, the
central hole is on the order of several inches to tens of
inches in diameter. Thus, the usual biaxial tubular specimen
of about an inch in inner diameter, length of four inches, and

74

wall thickness of .050 inch simply cannot be made from polar
weave C-C. Back to the possible limitation of thinness of
tube wall for other C-C materials: the typical fiber spacings
in all directions are not negligible relative to the tube
wall thickness of .050." Thus, we should expect difficulty in
capturing the macroscopic behavior of these materials without
the adverse influence of microscopic behavioral characteristics
such as fiber pull out. This latter problem could be cured by
increasing the specimen size with corresponding increases in
loading device capacity and multitudenous other cost increas-
ing factors.

The second limitation of the biaxial tube test is the ability
to easily predict the response only when it is axisymmetric.
Asymmetric response can be predicted if either a 3-D stress
analysis or a psuedo 3-D stress analysis like ASAAS [35] is
used. Both possibilities are more expensive than axisymmetric
analysis with the 3-D stress analysis being the most expensive.
Asymmetric response occurs for anisotropic and rectangularly
orthotropic C-C, but axisymmetric response occurs for polar
weave C-C (recall that a tube cannot, however, be made from
polar weave C-C).

(3) The SoRI Thermal Stress Disk Test

Polar weave C-C is not available with a central hole in the
billet small enough to make an annular disk for the SoRI test.
The response to an axisymmetric thermal gradient would be
axisymmetric and hence readily predictable if only the capacity
to impose such a thermal loading were available.

75

Rectangularly orthotropic C-C has been subjected to thermal loading in the SoRI Thermal Stress Disk Test, and the resulting response is asymmetric. Thus, predicted response can be obtained if we are willing to pay the price of psuedo-3-D or 3-D finite element analysis. Anisotropic C-C falls in essentially the same category as rectangularly orthotropic C-C. However, there is a difference between the two material classes in the finite element model needed to treat the behavior. For rectangularly orthotropic materials, two planes of symmetry exist perpendicular to the disk plane. Then, if $E_x = E_y$, the response can be modeled with a disk segment that is $\frac{1}{8}$ of the disk that must be modeled depends on the symmetries that do exist in the mechanical properties.

Thus, the sequence of theoretical-experimental correlation followed for ATJ-S graphite is difficult to follow for carbon-carbon materials. The uniaxial off-axis loading test can be meaningfully performed, but the biaxial tube test must be substantially modified to treat larger specimens than at present for anisotropic and rectangularly orthotropic materials, and probably cannot be applied to polar weave materials. The SoRI Thermal Stress Disk Test can obviously be used for anisotropic and rectangularly orthotropic carbon-carbons, but the difficulty in obtaining accurate response predictions is high because of the necessity to use 3-D or perhaps pseudo-3D finite element programs. And, polar weave carbon-carbons have too large a central hole in the billet to obtain a disk specimen that is small enough to be stressed and fractured in the SoRI Thermal Stress Disk Test. Moreover, polar weave carbon-carbon specimens cannot be made arbitrarily small because the material cannot be scaled down in fiber spac-

ings, etc. without inherently changing the material itself. Scaling down the material might enable us to validate a model for the same class of materials, but would involve a specifically different material.

The obvious question now is: can tests be devised that are suitable for validation of carbon-carbon material models? The different characteristics of the various carbon-carbons lead to different response and specimen characteristics. As we have seen, rectangularly orthotropic carbon-carbon which is used for reentry vehicle nosetips is quite different from polar weave carbon-carbon used for rocket nozzles. And, our objective is not to address all carbon-carbon analysis problems, but to concentrate on the problems inherent to the proper development of material models for rocket nozzle carbon-carbons. Thus, we are interested in polar weave and rosette carbon-carbons in solid body and shell configurations under axisymmetric thermal and mechanical loading that can be cyclic in nature because of firing, cease firing, firing sequences. Accordingly, a sequence of laboratory quality experiments should be developed to progressively validate the various features of the material model. That is, uniaxial off-axis behavior and biaxial behavior under mechanical loading plus biaxial behavior under thermal loading must be separately examined. We cannot hope to predict the complicated response of an object as complex as a rocket nozzle without first being certain that our model is valid for response of simpler bodies. Our situation is precisely that we must learn to crawl before we walk and walk before we run with the only exception being that we now have more stages to grow through and each is more complex than the last to a higher degree than in the crawl-walk-run analogy. To attempt to correlate new material model response directly with rocket nozzle behavior without first validating

the material model would be somewhat akin to playing pin the tail on the donkey!

An even more basic problem is the lack of measured mechanical property data to characterize a model, much less to validate it. AVCO MOD 3a carbon-carbon is the only material for which even uniaxial off-axis loading tests are available to validate the models. Tests at angles other than 45° must be performed for all carbon-carbon materials of interest.

3.4 CARBON-CARBON NONLINEAR MULTIMODULUS MATERIAL MODEL

The carbon-carbon material modeled in this report is AVCO Mod 3a, a rectangularly orthotropic material constructed of woven fibers in the xy-plane with pierced fibers in the z-direction. An equal number of fibers exists in the x-direction as in the y-direction on the average because the woven layers in the xy-plance are laid down with the warp and fill directions alternating from layer to layer. The mechanical behavior of Mod 3a is reported by Starrett, Weiler, and Pears [23] for room temperature and several elevated temperatures. The behavior at room temperature will be addressed because it appears to be more consistent data than exist at elevated temperatures. Other carbon-carbor materials could be modeled but stress-strain curves essential to the validation of those models are not available. Thus, AVCO Mod 3a is the only carbon-carbon material which we can both model and validate. The modeling with the Jones-Nelson-Morgan model will be described in this section, and the model validation will be addressed in the next two sections.

The Jones-Nelson-Morgan nonlinear multimodulus material model is basically an expression of the secant moduli of a material as a function of strain energy density in the form

$$\text{Mechanical Property}_i = A_i\left[1 - B_i\left(\frac{U}{U_o}\right)^{C_i}\right] \tag{3.7}$$

where the strain energy density (hereafter abbreviated as strain energy) is

$$U = (\sigma_x\epsilon_x + \sigma_y\epsilon_y + \sigma_z\epsilon_z + \tau_{yz}\gamma_{yz} + \tau_{zx}\gamma_{zx} + \tau_{xy}\gamma_{xy})/2 \tag{3.8}$$

and the constants A_i, B_i, and C_i are the initial value of the mechanical property, the initial curvature of the stress-strain curve, and the rate of change of curvature of the stress-strain curve, respectively. The

subscript i in Eq. (3.7) is used to distingush which mechanical property is addressed, and U_0 is used to nondimensionalize the term in brackets in Eq. (3.7).

The specific mechanical properties which must be modeled for AVCO Mod 3a are

$$E_x, \ E_z, \ \nu_{xz}, \ \nu_{xy}, \ E_{xz}^{45}, \ E_{xy}^{45}$$

in both tension and compression. The behavior in the x-direction is identical to that in the y-direction because of the way in which Mod 3a is made. The 45° off-axis properties are pure tension or pure compression properties instead of the inherently mixed tension and compression character of shear behavior. The transformations from principal material directions to principal stress directions in the Jones-Nelson-Morgan nonlinear multimodulus material model take place with either tension or compression properties. A "tension shear modulus" (i.e., for use in transformations of tension mechanical properties) is back-calculated from the other properties with a relation of the form

$$1/G_{xz_t} = 4/E_{xz_t}^{45} - (1/E_{x_t} + 1/E_{z_t} - 2\nu_{xz_t}/E_{x_t}) \tag{3.9}$$

Similar relations exist for G_{xy_t}, G_{xz_c}, and G_{xy_c}. However, these tension and compression shear moduli do not exist, i.e., they cannot be measured. They are only an artifice in the multimodulus formulation.

The constants A, B, and C are determined from measured stress-strain data which are converted to mechanical property vs. strain energy data. The mechanical property vs. strain energy curve corresponding to Eq. (3.7) is forced to be a good fit of the measured mechanical property vs. strain energy data as shown schematically in Fig. 3.13 by use of a nonlinear regression scheme developed by Jones and Morgan [2.3-22]. However,
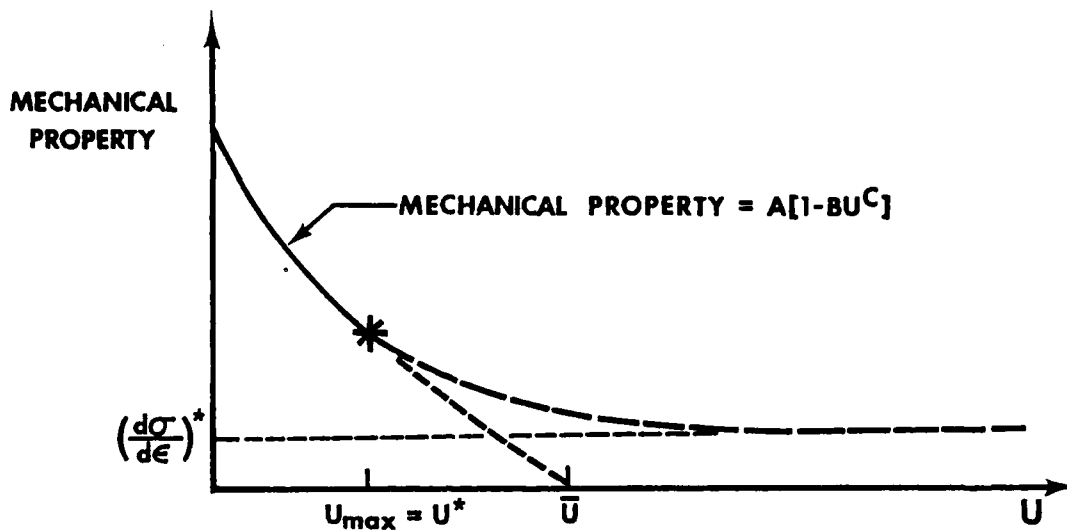
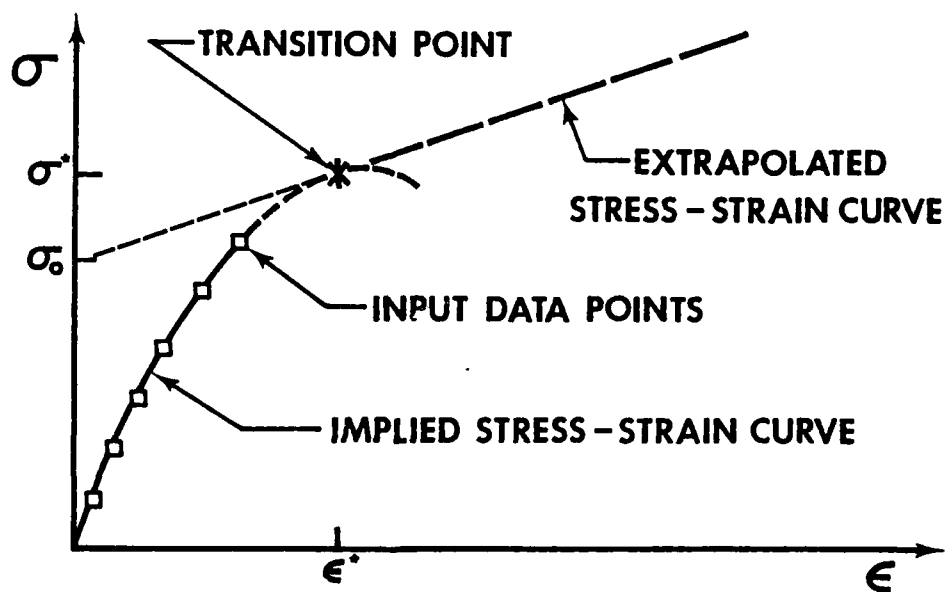FIGURE 3.13 MECHANICAL PROPERTY VERSUS STRAIN ENERGY CURVE EXTRAPOLATION

FIGURE 3.14 STRESS-STRAIN CURVE EXTRAPOLATION

81

measured stress-strain data, and hence mechanical property vs. strain energy data, do not exist for all strain energies corresponding to all possible multiaxial loading conditions (recall that mechanical properties are usually measured in uniaxial loading states). Thus, the mechanical property expression in Eq. (3.7) is valid only up to the last measured value of strain energy, i.e., up to strain energy U* in Fig. 3.13. Above that strain energy, the measured stress-strain data must be extrapolated so that the mechanical properties are defined nonzero quantities for all values of strain energy.

In the Jones-Nelson-Morgan model, the stress-strain data are extrapolated by adding a linear extension to the implied stress-strain curve corresponding to the mechanical property expression in Eq. (3.7) as shown in Fig. 3.14. That is, for strains less than ε* in Fig. 3.14, the stress-strain data are approximated with Eq. (3.7), and for strains greater than ε*, the stress-strain behavior is extended as the straight line. The portion of the mechanical property vs. strain energy curve to the right of U* in Fig. 3.13 corresponds to the linear extension of the stress-strain curve data in Fig. 3.14. This extrapolation of the mechanical property vs. strain energy data approaches a constant nonzero value as the strain energy increases. For carbon-carbon, the linear extension of the stress-strain curve is necessary to fit the measured data directly (without extrapolation). That is, the shape of many carbon-carbon stress-strain curves is quite similar to Fig. 3.14.

The numerical values for the Jones-Nelson-Morgan model for room temperature behavior of AVCO Mod 3a carbon-carbon are obtained with the JNMDATA program [2.3-18], and are given in Table 3.1. The mechanical property vs. strain energy curves are displayed in Figs. 3.15 - 3.18, and

82

TABLE 3.1 JONES-NELSON-MORGAN MATERIAL MODEL CONSTANTS FOR AVCO MOD 3a CARBON-CARBON

MECHANICAL PROPERTY[†]	$A^{\dagger\dagger}$,10^6psi(GN/m²)	B	C	U^*,psi(μN/m²)	E^*,10^6psi(GN/m²)	σ_0,psi(MN/m²)
E_{x_t}	1.70(11.7)	.197	.341	31.1(214)	.159(1.10)	4620(31.9)
E_{z_t}	13.4(92.4)	.713	.121	26.4(182)	3.25(22.4)	904(6.23)
ν_{zx_t}	.05	0	1.	0	0	0
ν_{xy_t}	.11	0	1.	0	0	0
$E_{xz_t}^{45}$	1.26(8.69)	.268	.619	3.86(26.6)	0	1930(13.3)
$E_{xy_t}^{45}$	1.44(9.93)	.162	.583	9.66(66.6)	.0300(.207)	3130(21.6)
E_{x_c}	1.49(10.3)	.0721	.457	57.8(399)	.351(2.42)	5430(37.4)
E_{z_c}	2.40(16.5)	.0316	.907	6.86(47.3)	.184(1.27)	4700(32.4)
ν_{zx_c}	.05	0	1.	0	0	0
ν_{xy_c}	.11	0	1.	0	0	0
$E_{xz_c}^{45}$	.801(5.52)	.169	.462	15.8(109)	.0541(.373)	2620(18.1)
$E_{xy_c}^{45}$	1.35(9.31)	.0505	.795	20.5(141)	0	4950(34.1)

[†]The value of U_0 is 1 psi (6.895 μN/m²)

[††]The Poisson's ratios are dimensionless

the stress-strain curves are shown in Figs. 3.19 - 3.22. Note the significantly different behavior in tension than in compression. This type of behavior is the primary motivation for the multimodulus aspect of the Jones-Nelson-Morgan model. The requirement for a nonlinear model is obvious. The stress-strain behavior in the x-direction in Figs. 3.15 and 3.19 is modeled with Eq. (3.7) until the last data point whereupon the slope at the last data point is used. The behavior in the z-direction in tension in Figs. 3.16 and 3.20 is modeled the same, but in compression a straight line is used to model the actual behavior (the solid line in Figs. 3.16 and 3.20 instead of the dashed line). The slope and intercept of the straight line are hand-calculated to fit the data rather than being obtained automatically from the JNMDATA computer program. The compression behavior at 45° to the x-direction in the xz-plane in Figs. 3.17 and 3.21 is modeled with Eq. (3.7) until the last data point is reached, and then a straight line with the slope at the last data point is used. In tension in Figs. 3.17 and 3.21, the behavior in Eq. (3.7) is continued until a zero slope is reached, and then a horizontal straight line is used. The same approach is used for the compression behavior at 45° to the x-direction in the xy-plane in Figs. 3.18 and 3.22. For the tension behavior in Figs. 3.18 and 3.22, the straight line extension is used to fit the last five data points. All J-N-M model fits of the data are quite good as can be seen in Figs. 3.16 - 3.22.

The Poisson's ratios data are not entirely satisfying. Starrett and Pears [34] report

$$\nu_{xy_c} = .11 \qquad\qquad \nu_{xz_c} = .03 \qquad\qquad \nu_{zx_c} = .05$$

and felt "that these values are adequate for both tension and compression." However, ν_{xz} should be obtainable from the reciprocal relation
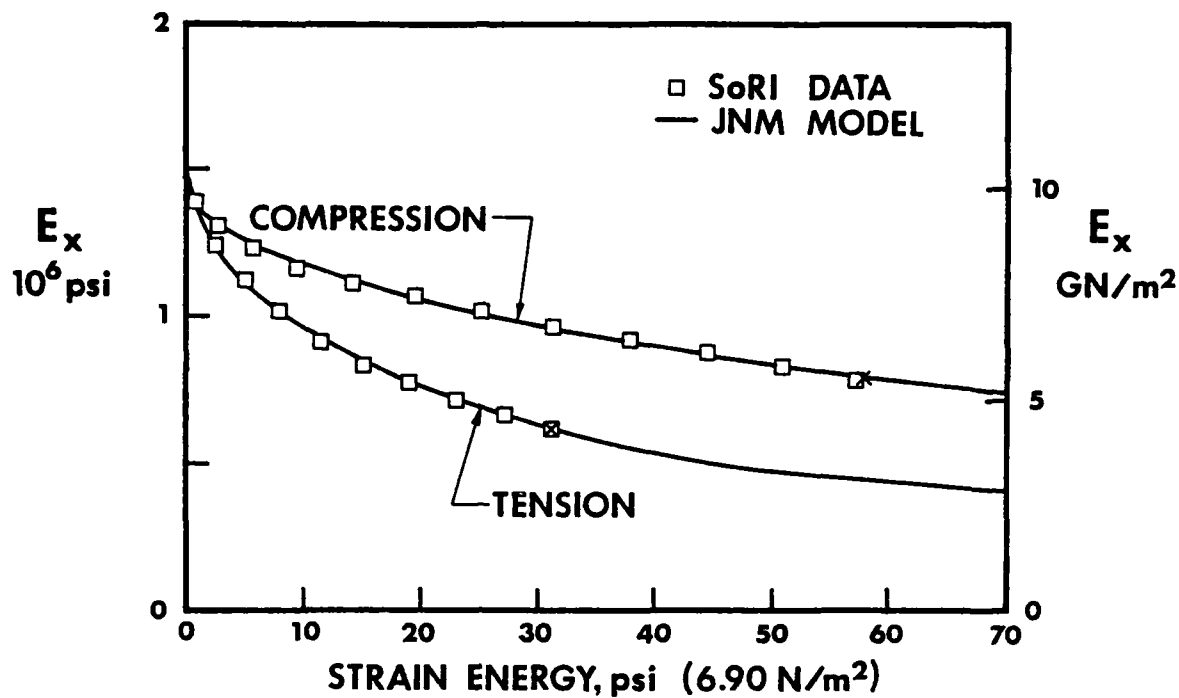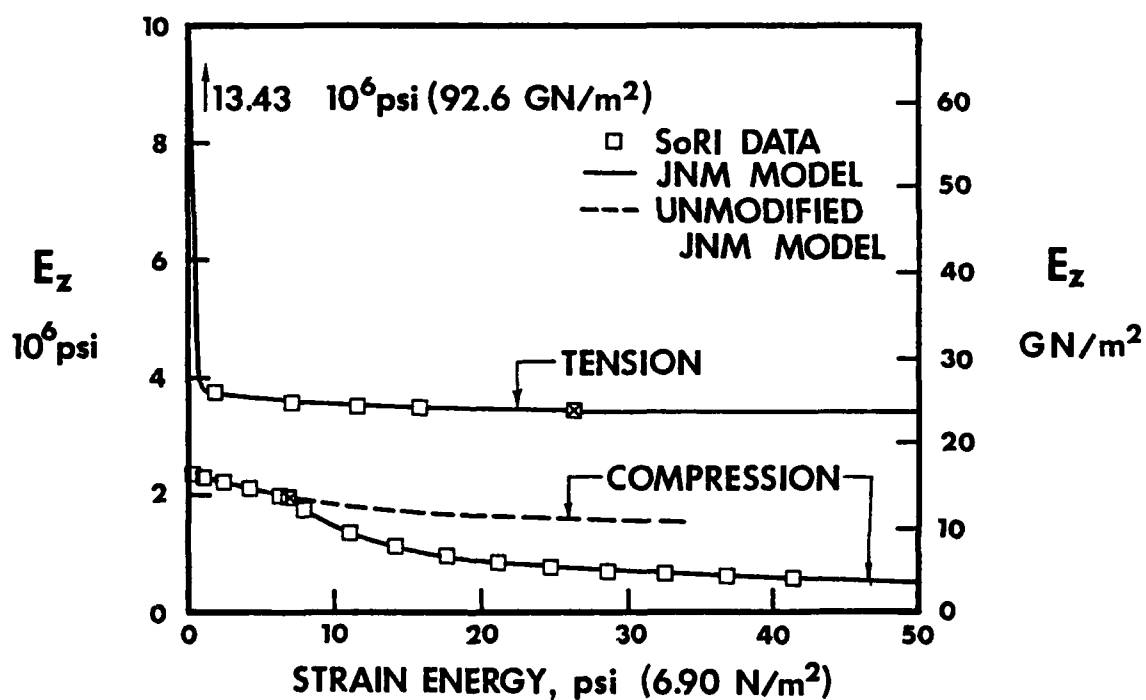
84

FIGURE 3.15 E_x VERSUS STRAIN ENERGY

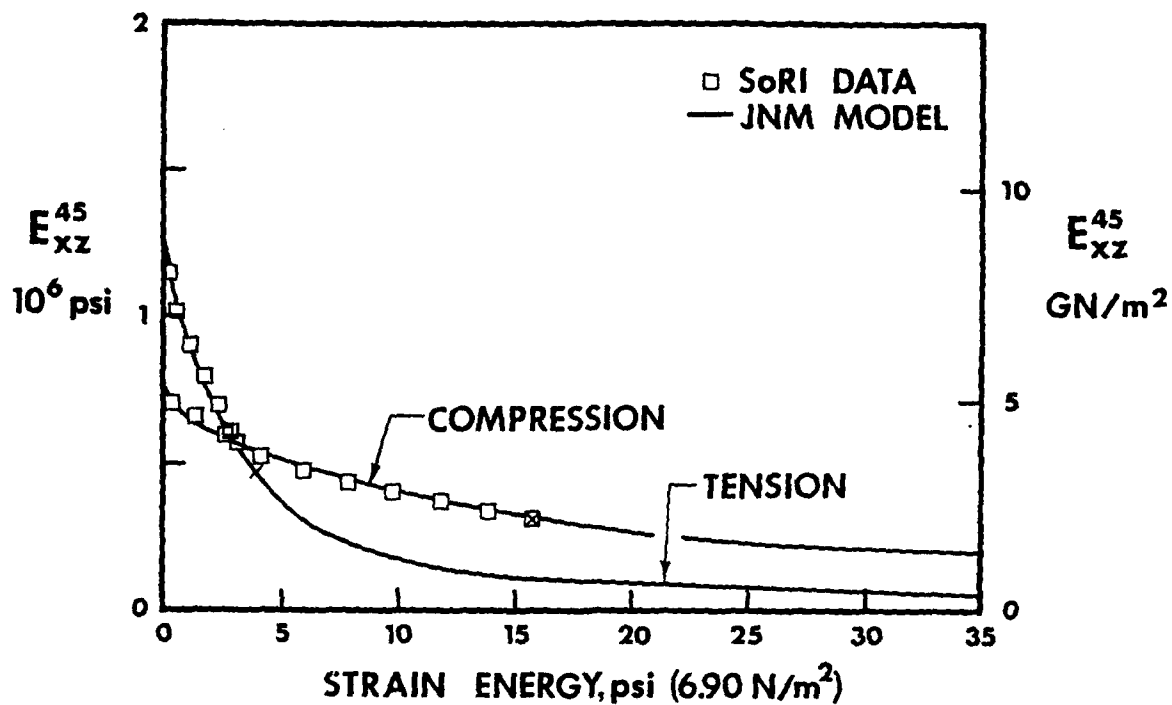

FIGURE 3.16 E_z VERSUS STRAIN ENERGY

85

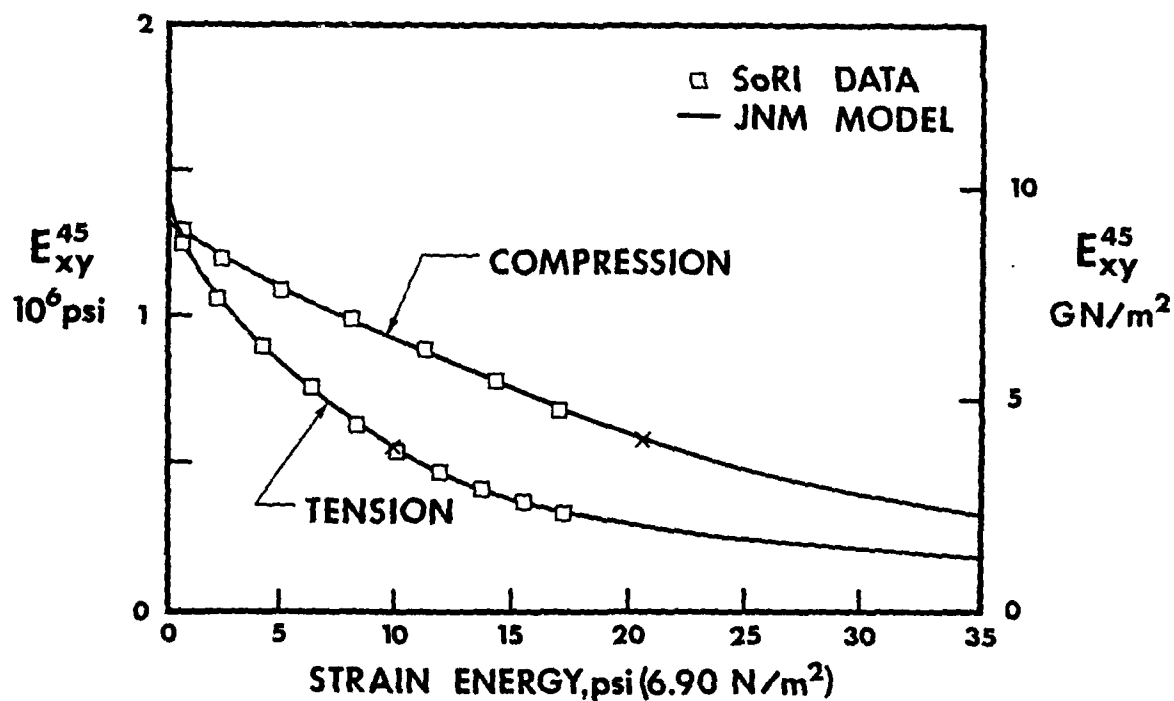FIGURE 3.17 E_{xz}^{45} VERSUS STRAIN ENERGY

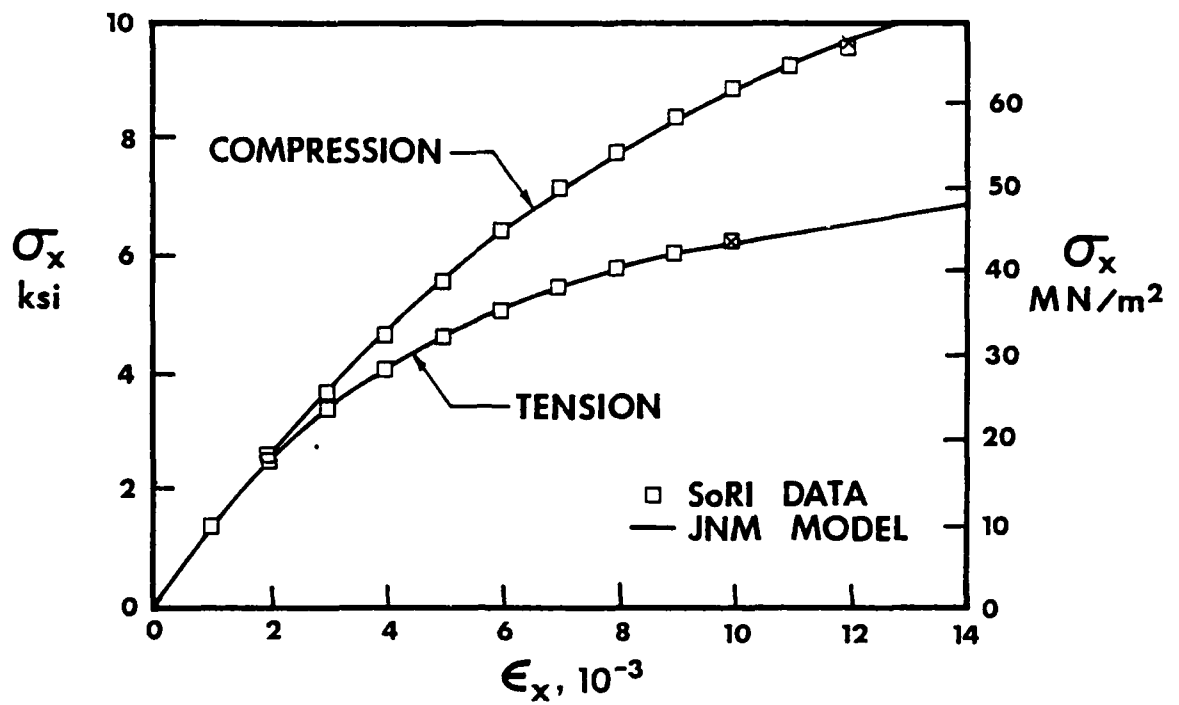FIGURE 3.18 E_{xy}^{45} VERSUS STRAIN ENERGY

86

FIGURE 3.19   STRESS-STRAIN BEHAVIOR IN THE x-DIRECTION
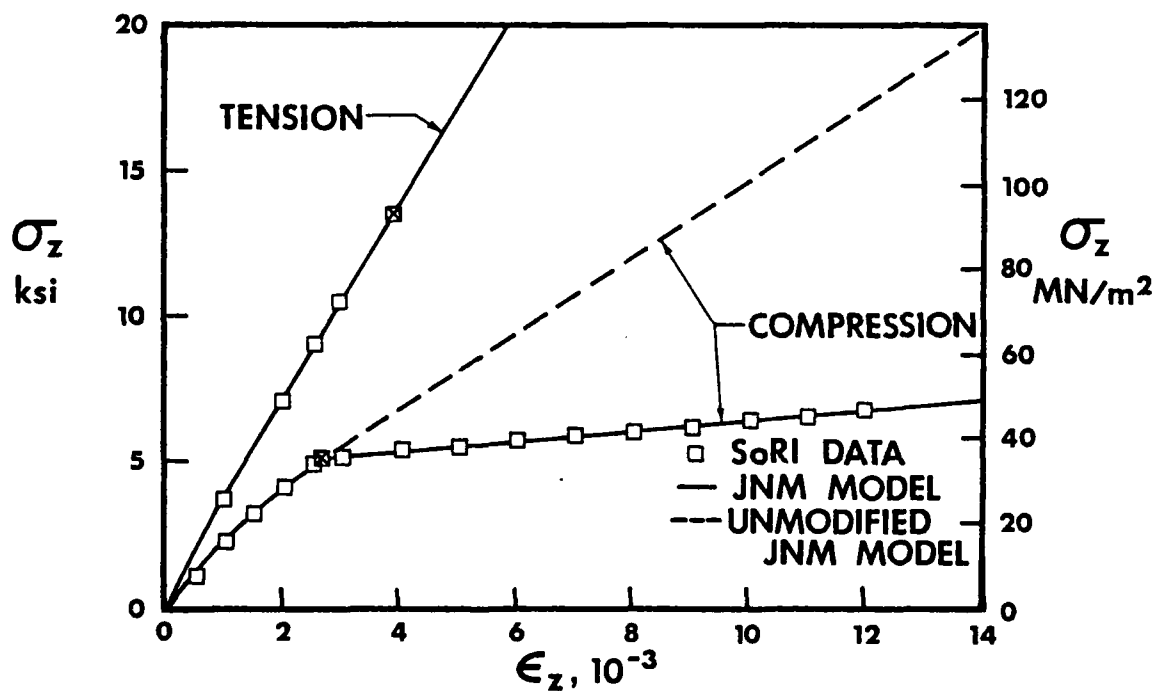

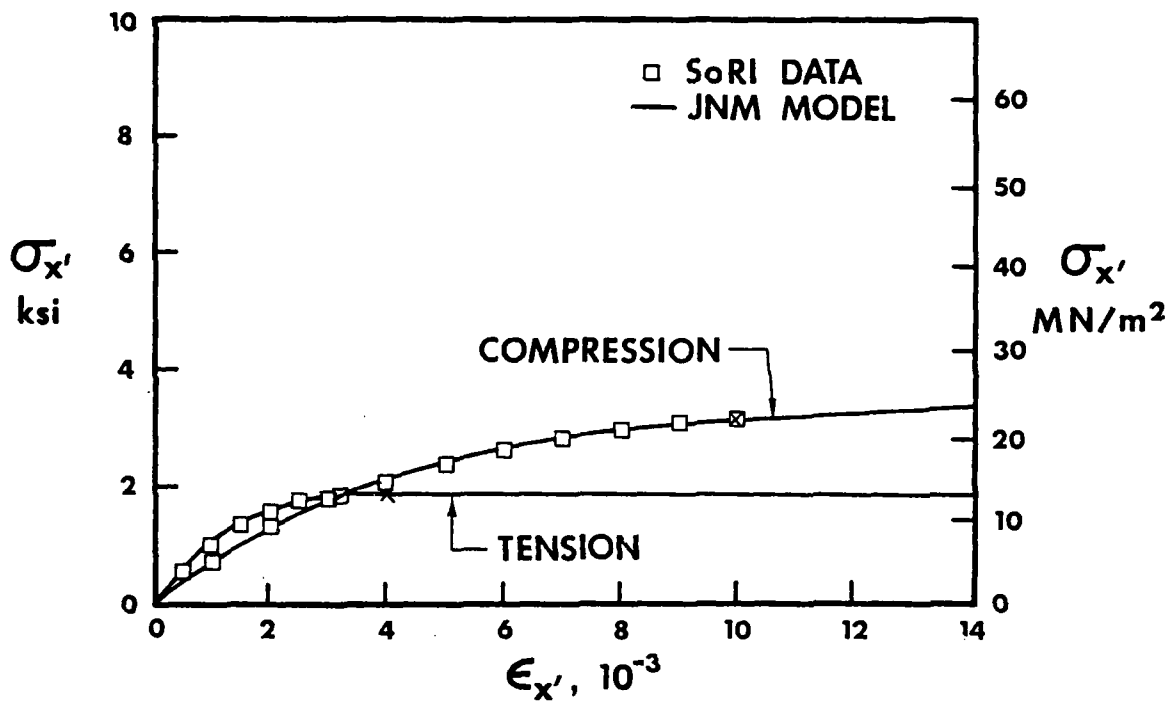FIGURE 3.20   STRESS-STRAIN BEHAVIOR IN THE z-DIRECTION

87

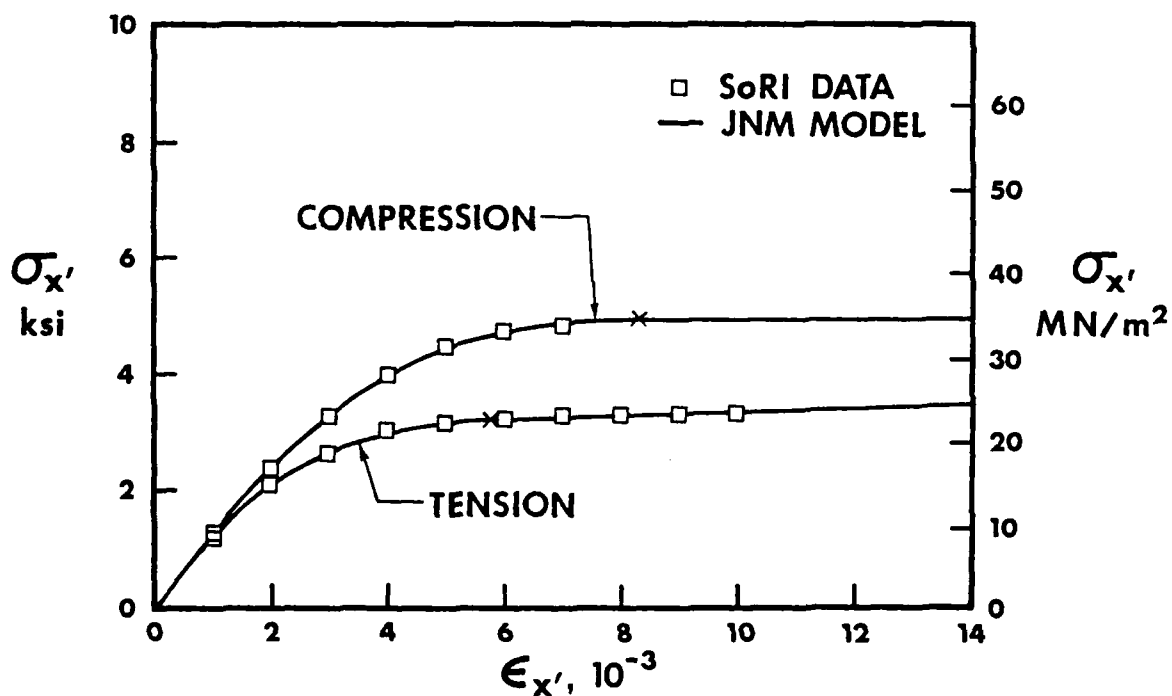FIGURE 3.21 STRESS-STRAIN BEHAVIOR IN THE xz-PLANE AT 45° TO x-AXIS

FIGURE 3.22 STRESS-STRAIN BEHAVIOR IN THE xy-PLANE AT 45° TO x-AXIS

88

$$\nu_{xz} = \nu_{zx} \frac{E_x}{E_z}$$

For compression properties, ν_{xz} does turn out to be .03. However, for tension properties, ν_{xz} is .02 or even as small as .006 if the values of A are used in the calculation. Moreover, the Poisson's ratios are not reported to be a function of stress level as would be expected for properties of a material with highly nonlinear stress-strain behavior. These are the reasons for some uneasiness about the values of Poisson's ratios in Table 3.1.

The data reported by Starrett, Weiler, and Pears [23] are in the form of "most probable value" curves to attempt to represent the amalgamation of many billets of Mod 3a carbon-carbon. That is, the billet-to-billet variation of mechanical properties is quite high. However, the most probable value curves are not sufficiently well established statistically to render good comparisons between theory and experiment valid nor to render unsatisfactory comparisons invalid. Accordingly, because of the discomforting nature of the Poisson's ratios data and the statistically unsatisfying nature of the other mechanical property data, complete confidence that a model has been established for AVCO Mod 3a carbon-carbon cannot be claimed. However, the quality of this model is higher than can be obtained for any other carbon-carbon because the data base for all other materials is even less satisfactory!

After the model is obtained, predictions of strains for specified multiaxial stress states can be made. However, the mechanical properties in Eq. (3.7) depend on the stresses and strains through the strain energy. Also, the stresses are related to the strains through the mechanical properties. Thus, for a given multiaxial loading condition, the stresses, strains, and mechanical properties are interdependent in transcendental

relationships. Accordingly, the iteration procedure due to Jones and Nelson [2.3-13] is used to find the correct stresses, strains, and mechanical properties for a given loading state.

3.5 EFFECT OF SHEAR COUPLING ON UNIAXIAL OFF-AXIS LOADING

The strains for a specified uniform stress state can be predicted by
use of the MULTIAX computer program. These predictions can be
made for materials with nonlinear stress-strain behavior by use of the
Jones-Nelson-Morgan nonlinear material model. However, actual test speci-
mens under off-axis loading are in constrained states of strain which do
not coincide with the usual objective for a test specimen of a uniform
state of strain and stress. As discussed in Section 3.2, the ends of a
uniaxial test specimen are usually forced to remain parallel by clamping
devices at each end. Thus, the shearing deformation that would otherwise
develop is partially prevented unless the observation is made at the center
portion of a very long slender test specimen. The bounds on such behavior
are shown in Fig. 3.8; there, a short wide specimen (length over width
effectively zero) is shown to exhibit an effective or apparent modulus of
$\bar{Q}_{11}$ whereas a long narrow specimen (length over width effectively infinite)
exhibits the actual modulus $E_{x'}$. Pagano and Halpin [36] analyze the
strains that exist in a simple rectangular tension (or compression) speci-
men of length L and width w (hence, their specimen is intermediate to the
bounding cases on L/w just described). Their material behavior is linear
elastic but orthotropic in principal material directions. However, the
material behavior of present interest is nonlinear and orthotropic. Thus,
their analysis must be modified or their results must be reinterpreted to
account for the material nonlinearity. Then, the results of the new
analysis for AVCO Mod 3a carbon-carbon will be examined.

3.5.1 Adaptation of Elastic Analysis for Shear Coupling to Nonlinear Materials

For a rectangular specimen L long and w wide, Pagano and Halpin
[36] obtain an apparent off-axis Young's modulus from their solution for

the strains as

$$E^*_{x'} = \frac{\sigma_{x'}}{\epsilon_{y'}} = \left(\frac{1}{1-\eta}\right)\frac{1}{\bar{S}_{11}} \qquad (3.10)$$

where

$$\eta = 3\bar{S}^2_{16}\bigg/\left\{\bar{S}_{11}\left[3\bar{S}_{66} + 2\bar{S}_{11}\left(\frac{L}{w}\right)^2\right]\right\} \qquad (3.11)$$

and the $\bar{S}_{ij}$ are the transformed compliances of an orthotropic material (see Jones [37]). As L/w approaches infinity (a long slender specimen), η approaches zero, so $E^*_{x'}$ approaches $E_{x'} = 1/\bar{S}_{11}$, the Young's modulus in a uniform stress and strain state. On the other hand, as L/w approaches zero (a short wide specimen),

$$E^*_{x'} = \frac{\bar{S}_{66}}{\bar{S}_{11}\bar{S}_{66} - \bar{S}^2_{16}} \qquad (3.12)$$

which can be shown to be less than $\bar{Q}_{11}$ of Eq. (3.2) and Fig. 3.8. For AVCO Mod 3a carbon-carbon, the results for $E^*_{x'}$, $E_{x'}$, and $\bar{Q}_{11}$ are shown as a function of off-axis angle in Fig. 3.23. Obviously, $E^*_{x'}$ is well above the actual modulus $E_{x'}$, but not as much above as is $\bar{Q}_{11}$. For a specific applied stress $\sigma_{x'}$, the implication of shear coupling for a specimen of length L and width w is that the axial strain $\epsilon_{x'}$ is smaller than without shear coupling and is obtained by multiplying the uniform stress and strain state strain by the factor $(1-\eta)$:

$$\epsilon_{x'_{actual}} = (1-\eta)\epsilon_{x'_{uniform}} \qquad (3.13)$$

or, if the modulus factor is defined as $1/(1-\eta)$, then we divide the uniform stress and strain state strain by the modulus factor.

Similarly, Pagano and Halpin obtain the lateral and shear strains along the specimen centerline as
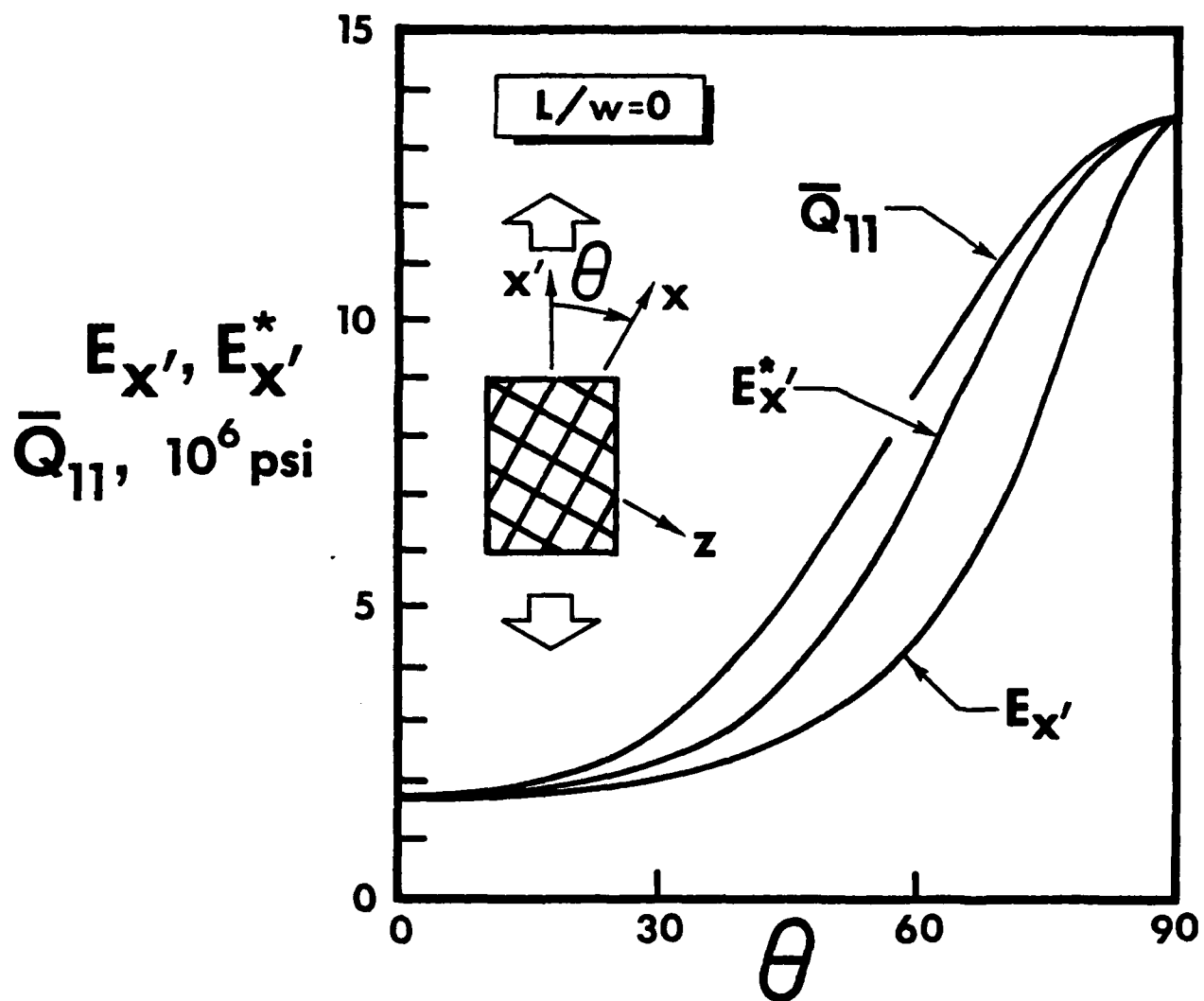
92

FIGURE 3.23   APPARENT MODULI FOR AVCO MOD 3a CARBON-CARBON
OFF-AXIS TEST SPECIMENS WITH L/w = 0

$$\varepsilon_{y'} = \left[\frac{3\bar{S}_{11}\bar{S}_{66} + 2\bar{S}_{11}^2\left(\frac{L}{w}\right)^2 - 3\bar{S}_{11}\bar{S}_{16}\bar{S}_{26}/\bar{S}_{12}}{3(\bar{S}_{11}\bar{S}_{66} - \bar{S}_{16}^2) + 2\bar{S}_{11}^2\left(\frac{L}{w}\right)^2} \right] \frac{\bar{S}_{12}}{\bar{S}_{11}} \varepsilon_{x'} \qquad (3.14)$$

$$\gamma_{x'y'} = \left\{ \frac{1}{\frac{3}{2}\left(\frac{w}{L}\right)^2\left[\frac{\bar{S}_{66}}{\bar{S}_{11}} - \left(\frac{\bar{S}_{16}}{\bar{S}_{11}}\right)^2\right] + 1} \right\} \frac{\bar{S}_{16}}{\bar{S}_{11}} \varepsilon_{x'} \qquad (3.15)$$

For long slender specimens ($L/w \rightarrow \infty$), Eqs. (3.14) and (3.15) reduce to

$$\varepsilon_{y'} = \frac{\bar{S}_{12}}{\bar{S}_{11}} \varepsilon_{x'} \qquad (3.16)$$

$$\gamma_{x'y'} = \frac{\bar{S}_{16}}{\bar{S}_{11}} \varepsilon_{x'} \qquad (3.17)$$

i.e., the uniform stress and strain state strains. However, for short wide specimens ($L/w \rightarrow 0$), Eqs. (3.14) and (3.15) reduce to

$$\varepsilon_{y'} = \frac{\bar{S}_{12}\bar{S}_{66} - \bar{S}_{16}\bar{S}_{26}}{\bar{S}_{11}\bar{S}_{66} - \bar{S}_{16}^2} \varepsilon_{x'} \qquad (3.18)$$

$$\gamma_{x'y'} = 0 \qquad (3.19)$$

which for the shear strain is the same as the simple solution for the short wide specimen. However, for the transverse strain, Pagano and Halpin obtain larger values than for the simple solution. In fact, for AVCO Mod 3a carbon-carbon, the lateral strain is a substantial fraction of the axial strain for off-axis angles near 60° in Fig. 3.24. For actual specimens of length L and width w, the actual shear strain is always less than the uniform stress and strain state shear strain, and can be obtained by multiplying the uniform strain state strain by the term in braces in Eq. (3.15). Similarly, the actual transverse strain is obtained by multi-
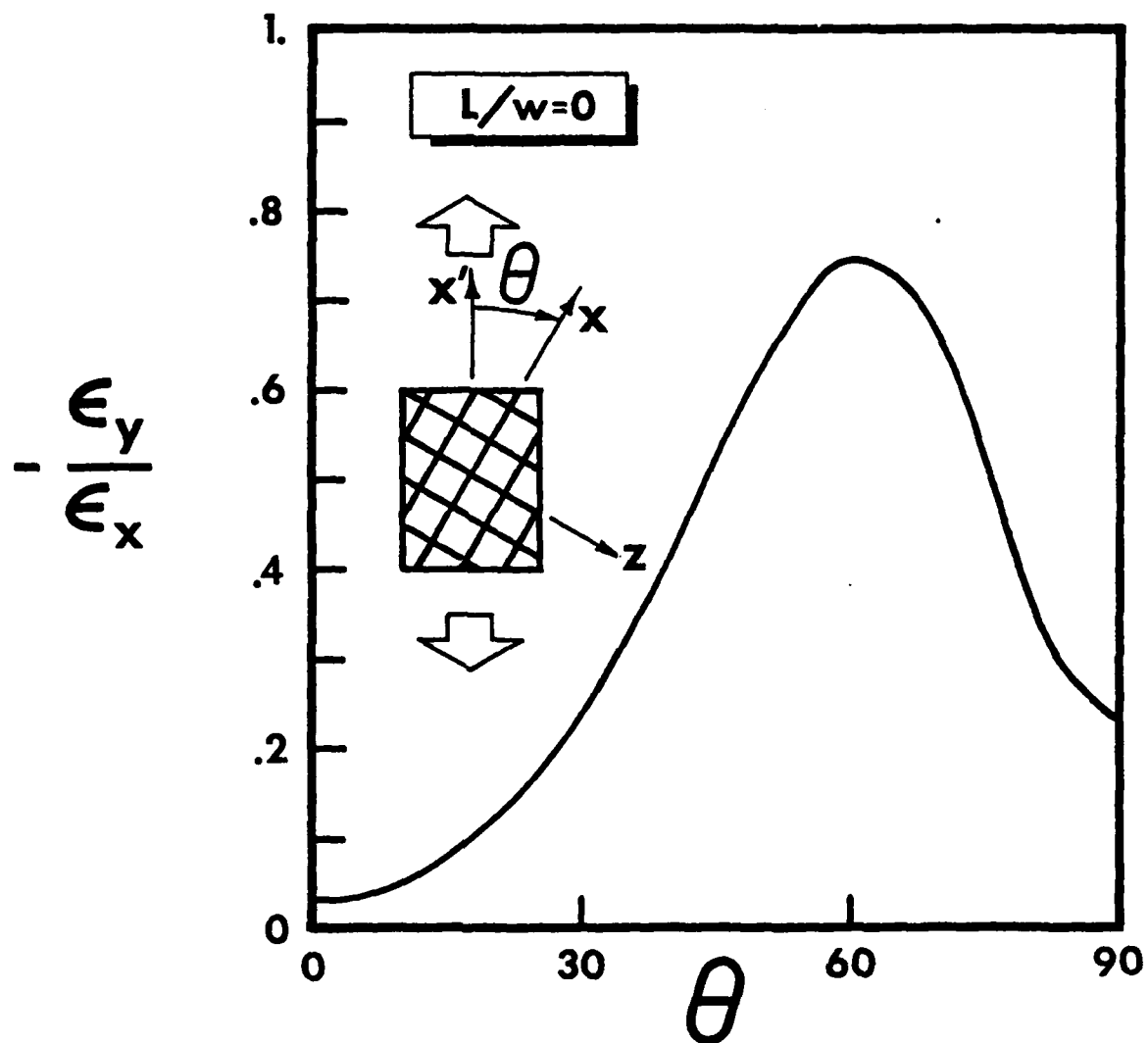
94

FIGURE 3.24   LATERAL STRAIN FOR AVCO MOD 3a CARBON-CARBON
OFF-AXIS TEST SPECIMENS WITH L/w = 0

plying the uniform strain state strain by the term in brackets in Eq. (3.14).

The key issue now is how can the foregoing analysis be used in the analysis of materials with nonlinear stress-strain behavior? The Pagano and Halpin analysis is adapted to treat nonlinear material behavior by using the compliances as a function of stress levels in all the preceding equations. That is, secant moduli are used to calculate the compliances in a deformation theory of orthotropic plasticity (the Jones-Nelson-Morgan model). As the stress level increases in an off-axis test, the compliances grow larger and the moduli get smaller. Thus, the modulus reduction factors and strain reduction factors can be calculated for use in modifications of the MULTIAX strain predictions for off-axis loading.

3.5.2 Strains for Off-Axis Loading in the xz-plane of AVCO Mod 3a Carbon-Carbon

The uniform stress and strain state strains obtained with MULTIAX for off-axis tension and compression loading in the xz-plane of AVCO Mod 3a carbon-carbon are shown in Figs. 3.25 to 3.28 for several stress levels. The off-axis normal strains are largest near $\theta = 45°$ and increase rapidly with increasing stress. The off-axis shear strains are largest near $20°$ and $60°$ and are zero near $45°$ (and, of course, are zero at $\theta = 0°$ and $90°$).

The magnitudes by which these uniform strain state strains must be adjusted to obtain reasonable approximations of actual test specimen behavior are plotted for several L/w ratios as modulus factors in Figs. 3.29 and 3.30 and as shear strain reduction factors in Figs. 3.31 to 3.33. The tension modulus increase (reciprocal of the normal strain decrease) in Fig. 3.29 is negligible for off-axis angles less than $50°$ and greater
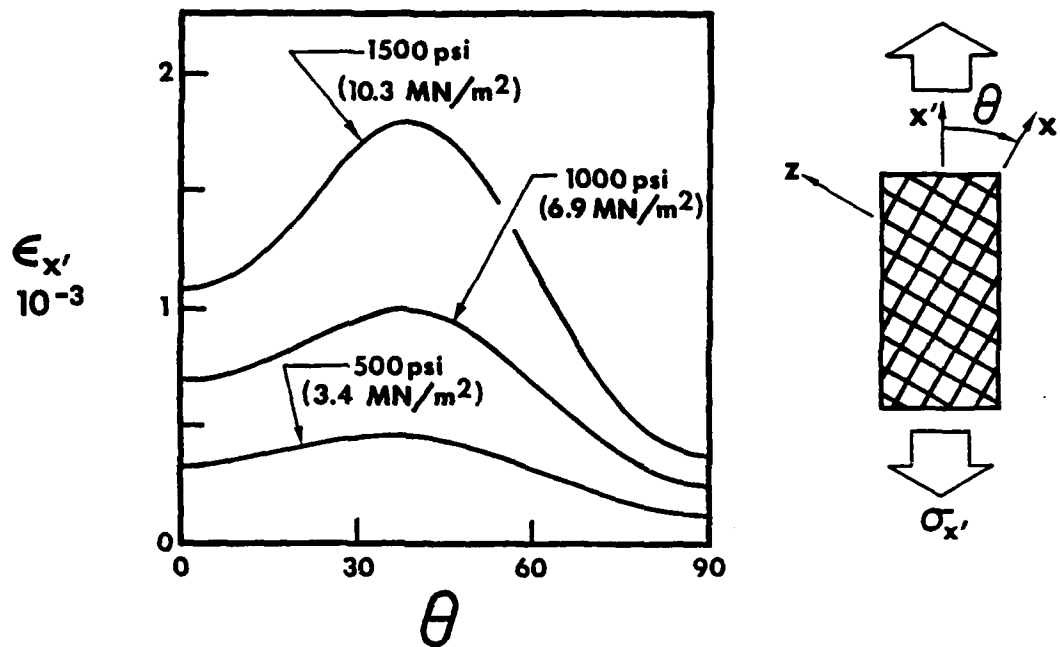
96

FIGURE 3.25   NORMAL STRAIN UNDER OFF-AXIS TENSION LOADING IN xz-PLANE
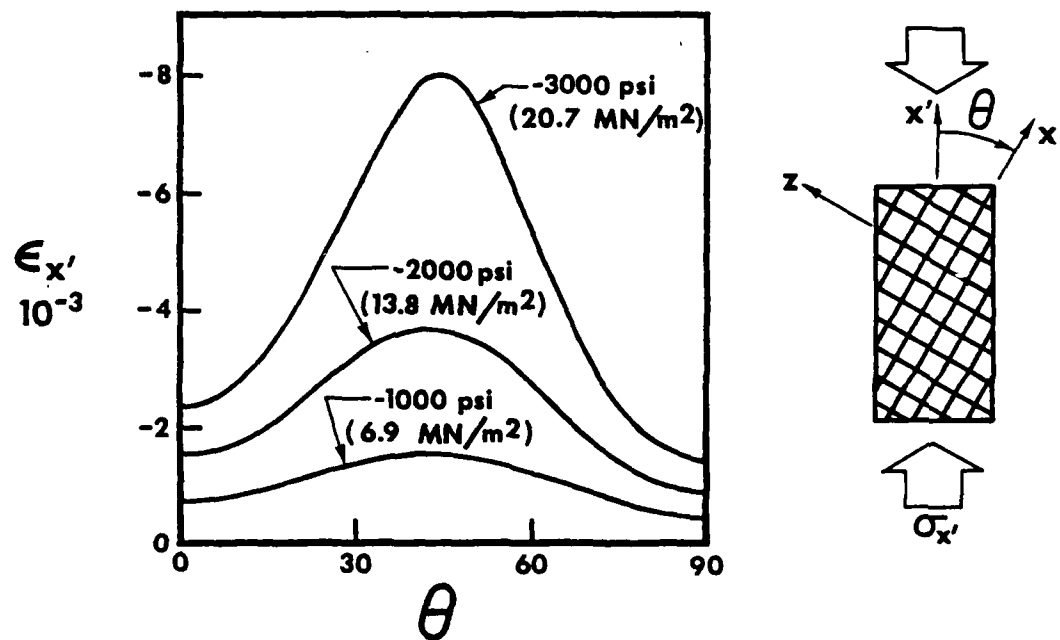

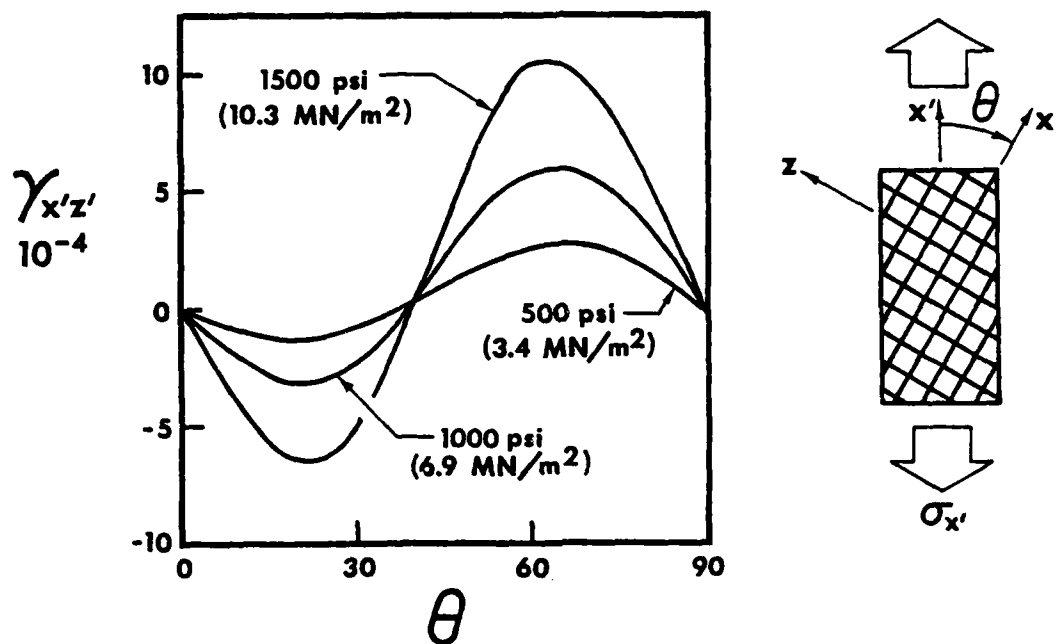FIGURE 3.26   NORMAL STRAIN UNDER OFF-AXIS COMPRESSION LOADING IN xz-PLANE

97

FIGURE 3.27   SHEAR STRAIN UNDER OFF-AXIS TENSION LOADING IN xz-PLANE
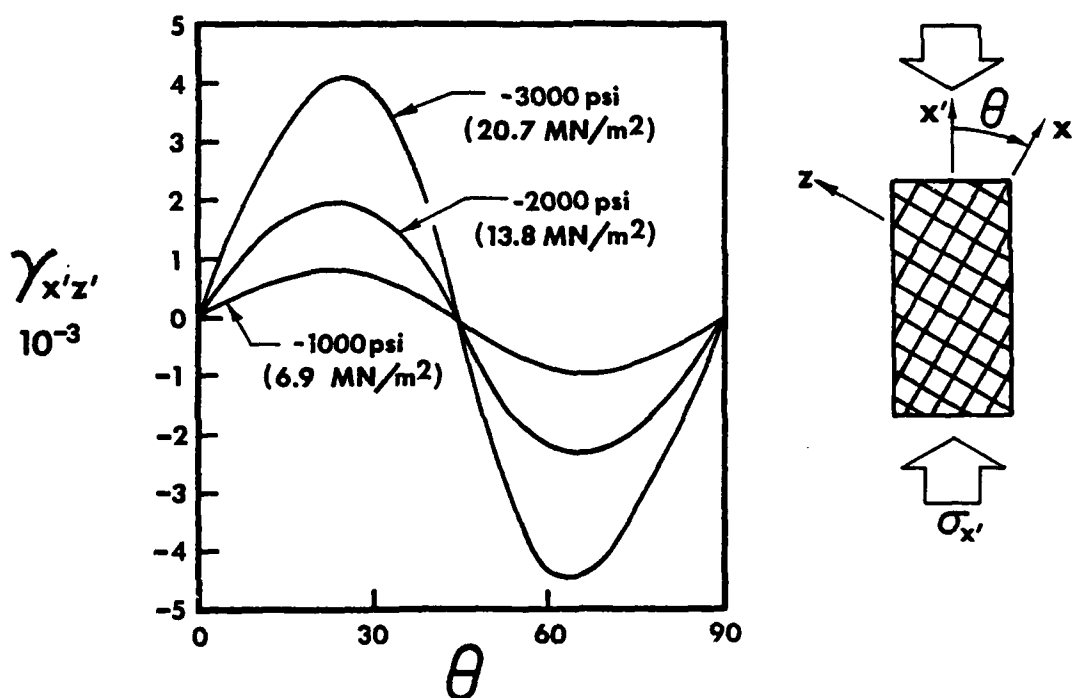

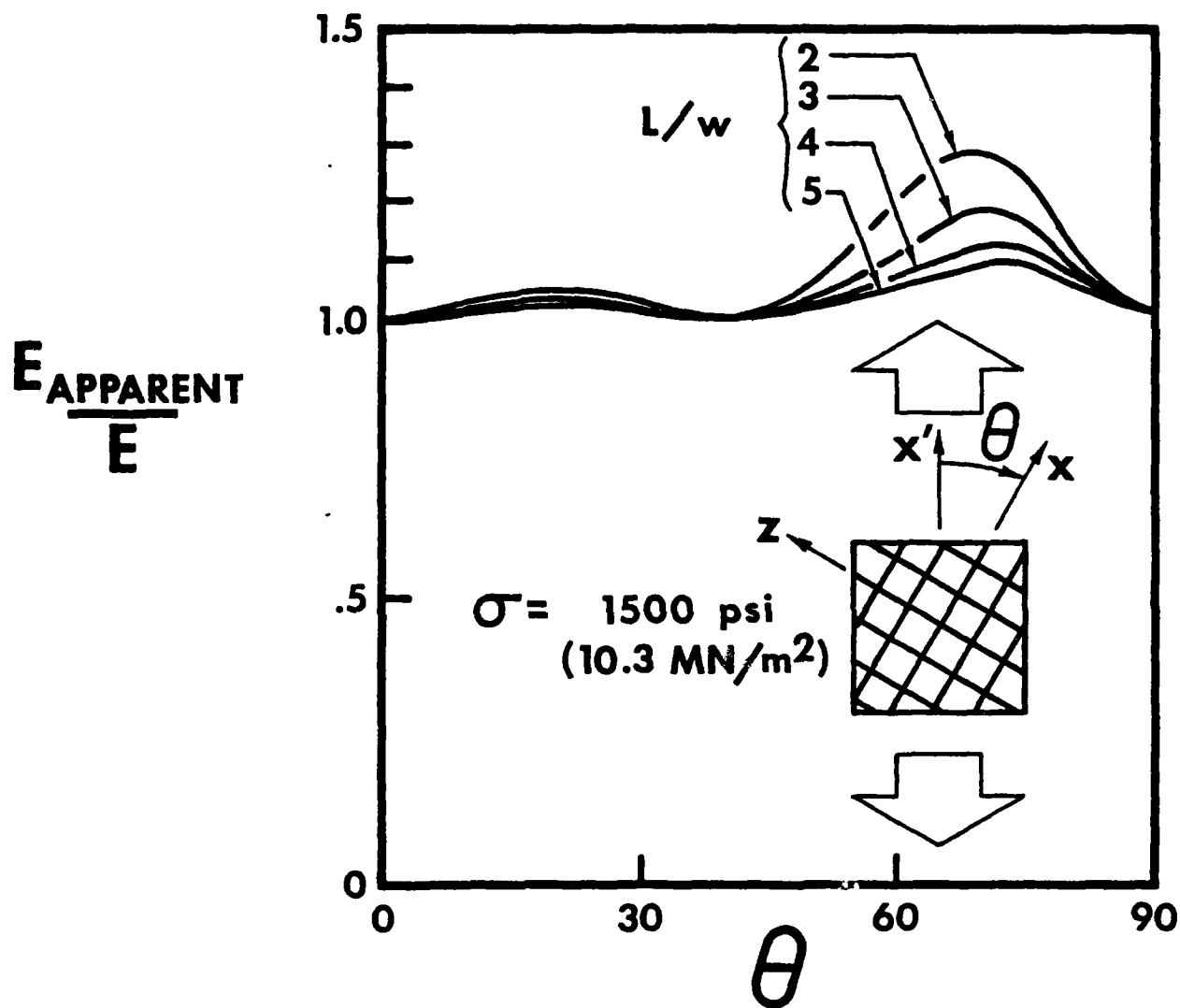FIGURE 3.28   SHEAR STRAIN UNDER OFF-AXIS COMPRESSION LOADING IN xz-PLANE

98

FIGURE 3.29   EFFECTIVE TENSION MODULUS INCREASE
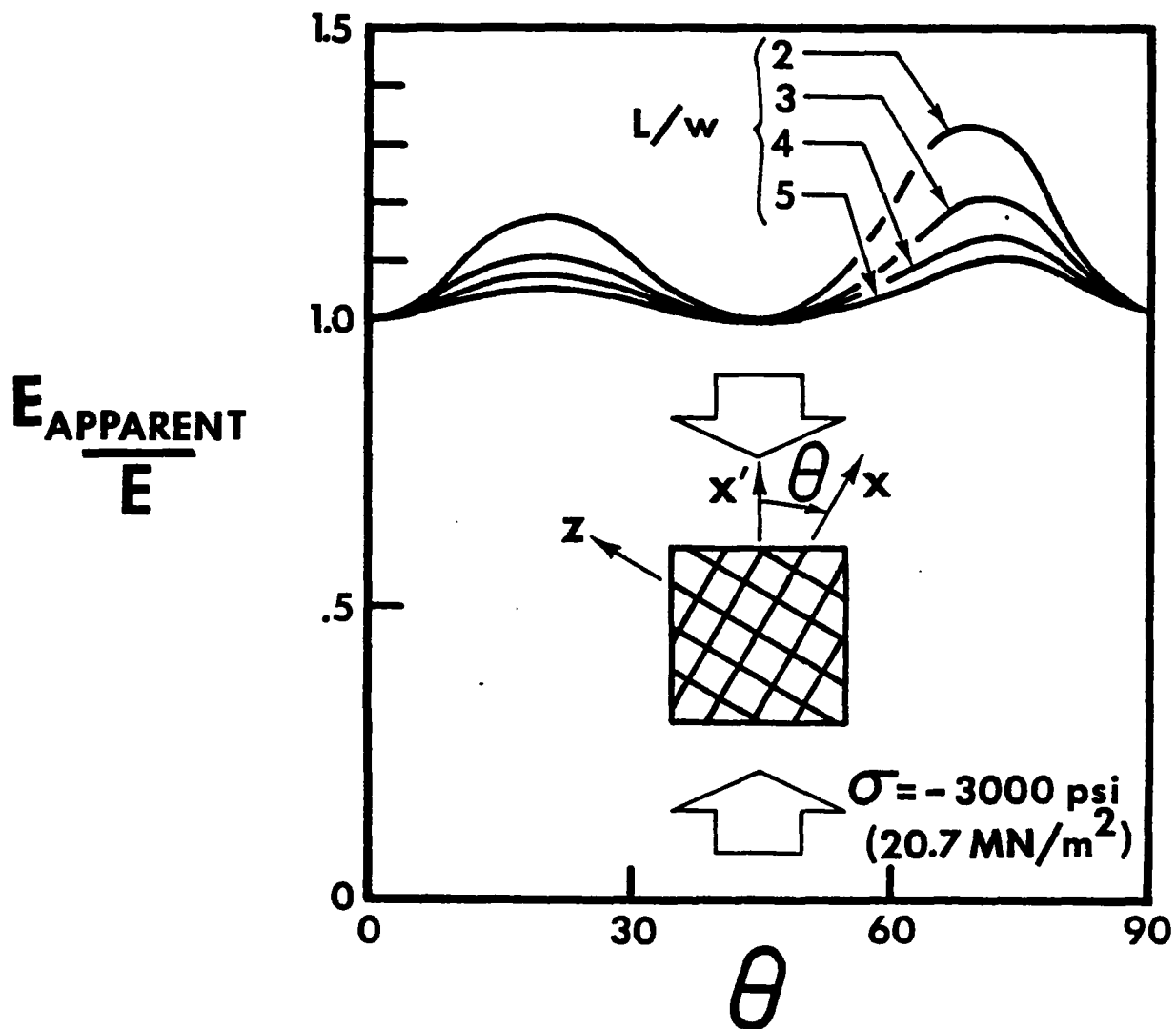UNDER OFF-AXIS LOADING IN xz-PLANE

99

FIGURE 3.30 EFFECTIVE COMPRESSION MODULUS INCREASE
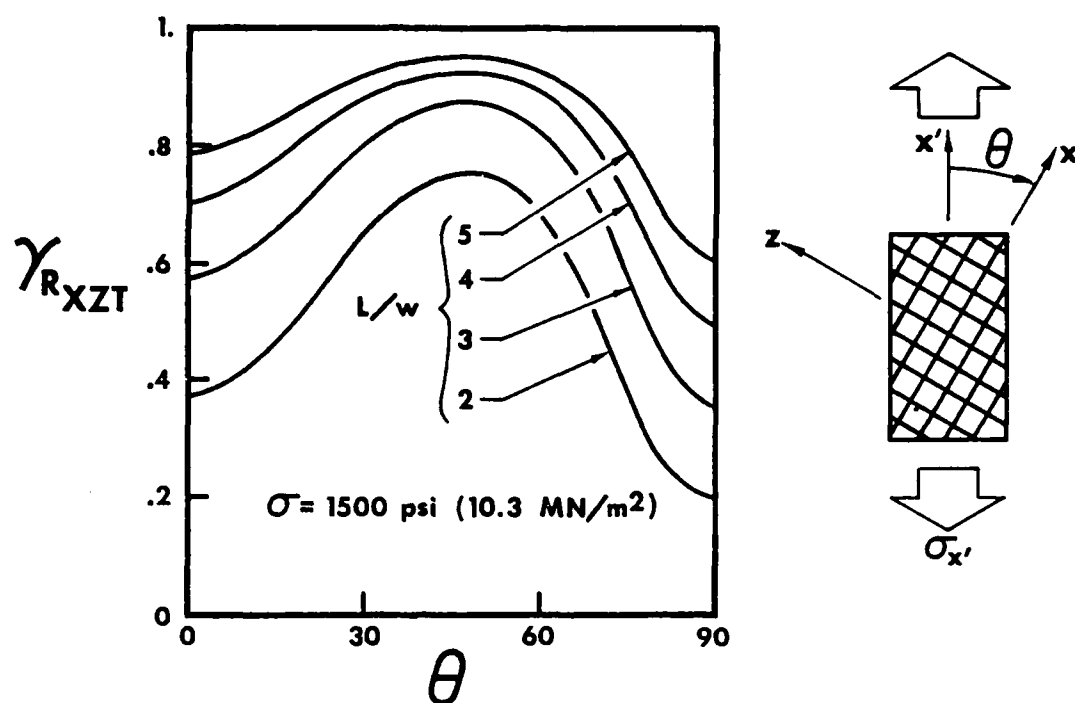UNDER OFF-AXIS LOADING IN xz-PLANE

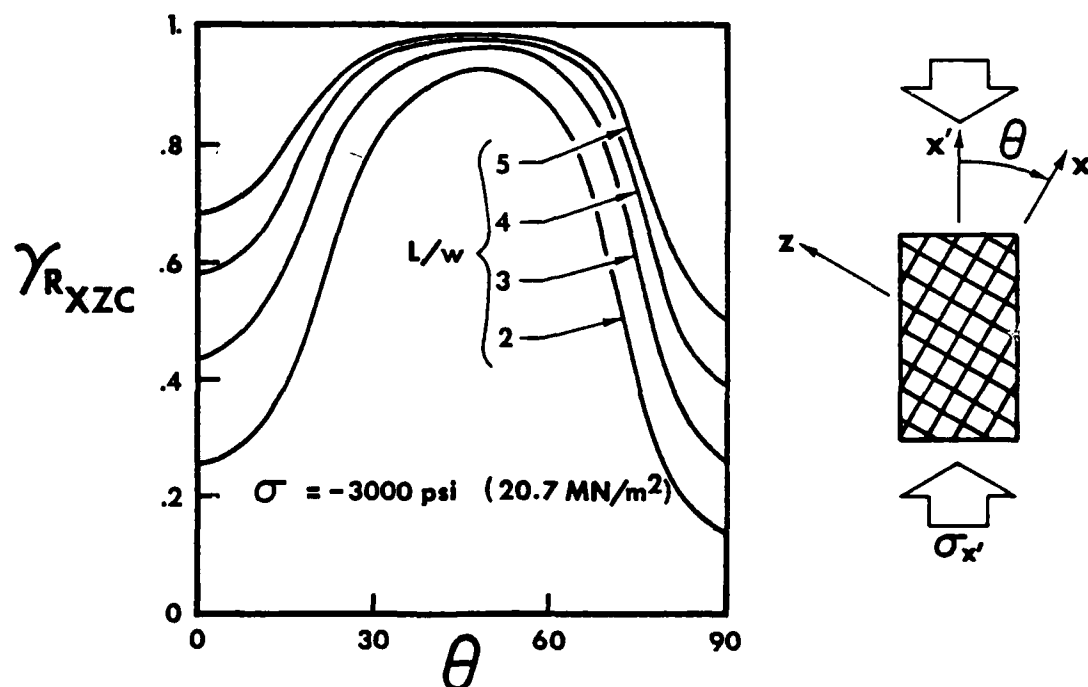FIGURE 3.31   SHEAR STRAIN REDUCTION FOR OFF-AXIS TENSION LOADING IN xz-PLANE

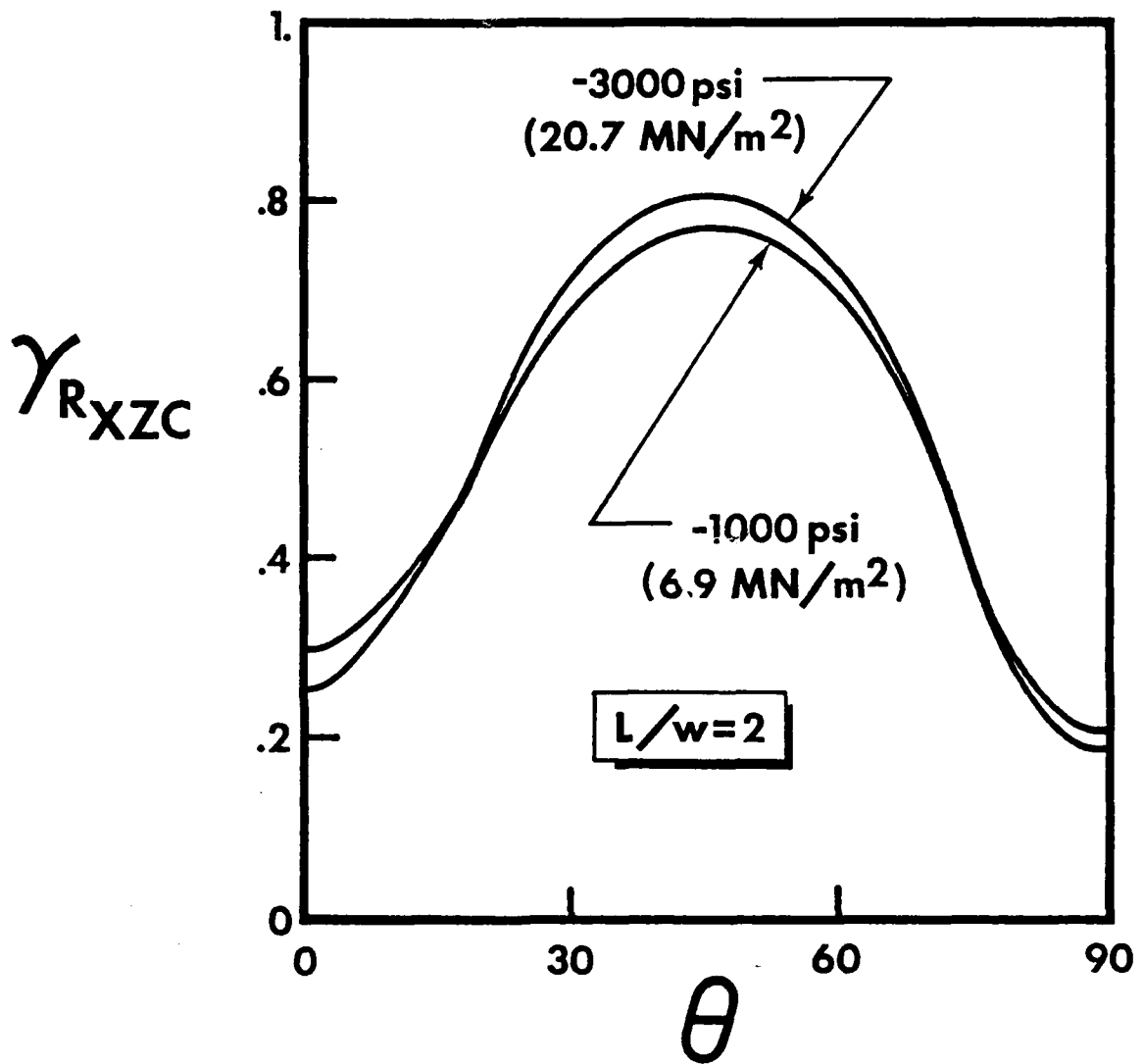FIGURE 3.32   SHEAR STRAIN REDUCTION FOR OFF-AXIS COMPRESSION LOADING IN xz-PLANE

101

FIGURE 3.33   SHEAR STRAIN REDUCTION AS A FUNCTION OF STRESS LEVEL
UNDER OFF-AXIS COMPRESSION LOADING IN xz-PLANE

than 85°. However, between those angles, the increase can be up to 30% for a very short specimen, but is about 10% for usual specimen geometries of L/w = 4 or 5. The compression modulus increase in Fig. 3.30 is generally larger than the tension modulus increase, especially for off-axis angles between 10° and 30° but also for angles between 50° and 85°. The shear strain reduction factor γ_R is shown as a function of off-axis angle for several common values of L/w in Fig. 3.31 for tension loading and for compression loading in Fig. 3.32. The smallest reductions occur near 45° where we have seen the shear strain is zero or very close to zero. The largest reductions occur at $\theta = 0°$ and 90° where the shear strains are identically zero. Thus, the practical reductions are still quite large at, for example, off-axis angles of 30° or 60°. The shear strain reduction factors are a weak function of stress level as shown in Fig. 3.33.

3.5.3 Strains for Off-Axis Loading in the xy-plane of AVCO Mod 3a Carbon-Carbon

The uniform stress and strain state strains obtained with MULTIAX for off-axis tension and compression loading in the xy-plane of AVCO Mod 3a carbon-carbon are shown in Figs. 3.34 to 3.37. Only 45° of off-axis angle needs to be investigated because of the mechanical property symmetry about $\theta = 45°$ (because the properties in the x-direction are the same as those in the y-direction). The off-axis normal strains are largest at $\theta = 45°$ and increase rapidly with increasing stress. The off-axis shear strains are largest near $\theta = 25°$ and are zero at $\theta = 45°$ (as well as at 0° and 90°).

The magnitudes by which these uniform strain state strains must be adjusted to obtain reasonable approximations of actual test specimen behavior in the xy-plane are plotted for several L/w ratios in Figs. 3.38
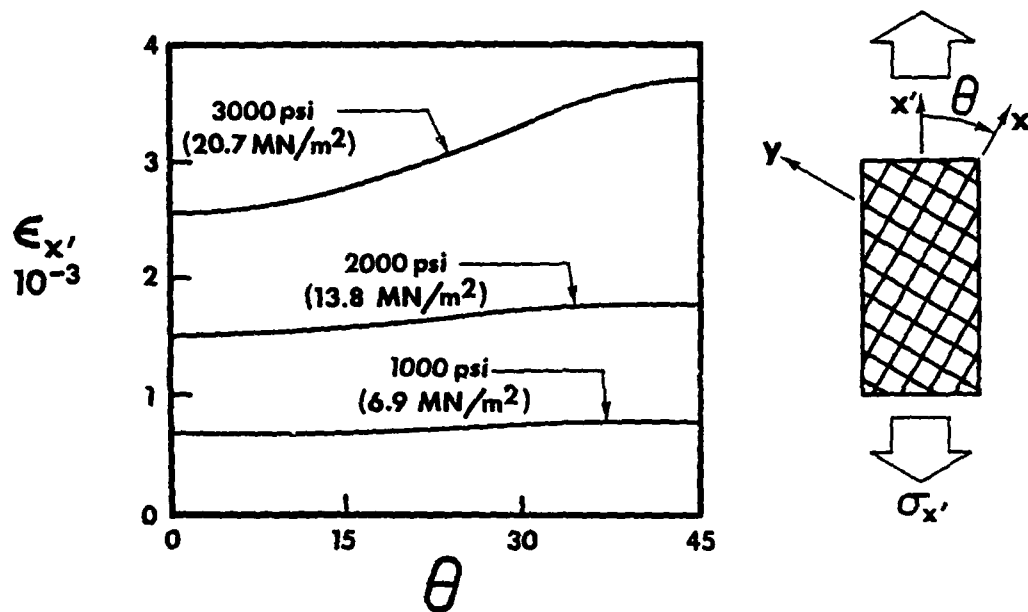
103

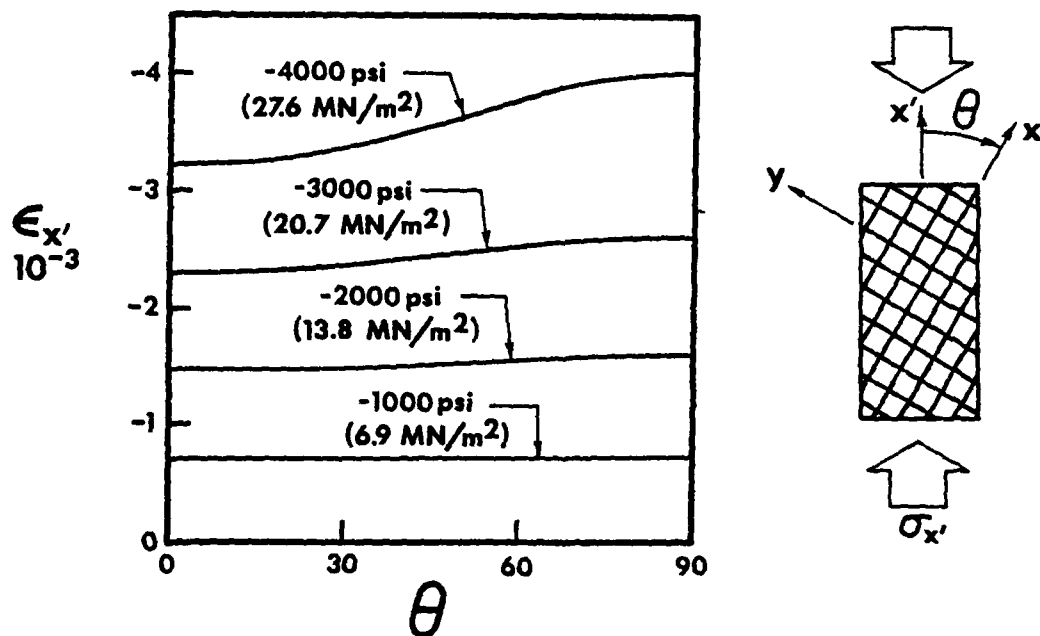FIGURE 3.34   NORMAL STRAIN UNDER OFF-AXIS TENSION LOADING IN xy-PLANE

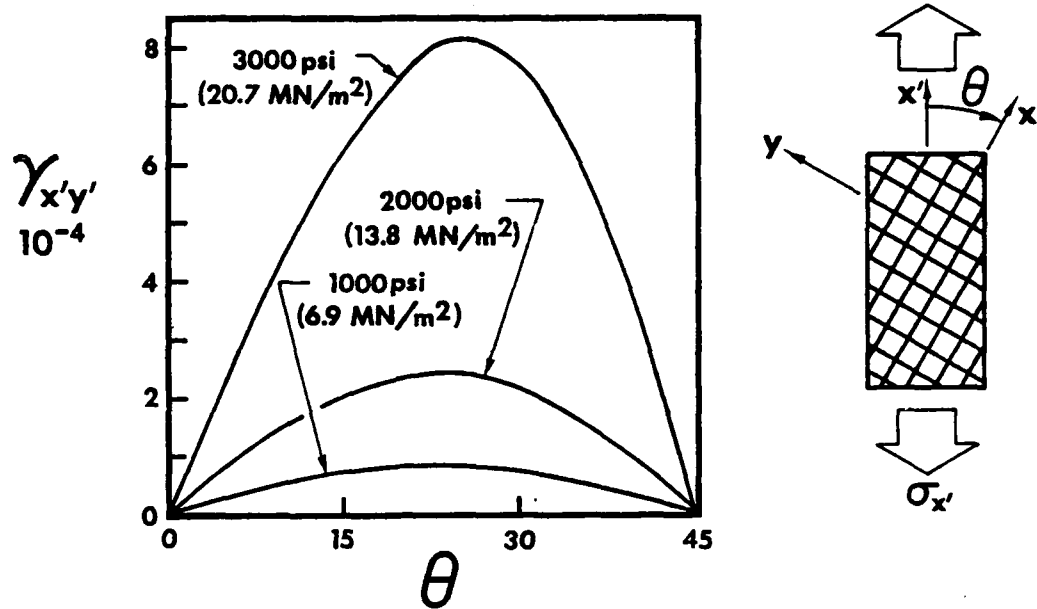FIGURE 3.35   NORMAL STRAIN UNDER OFF-AXIS COMPRESSION LOADING IN xy-PLANE

104

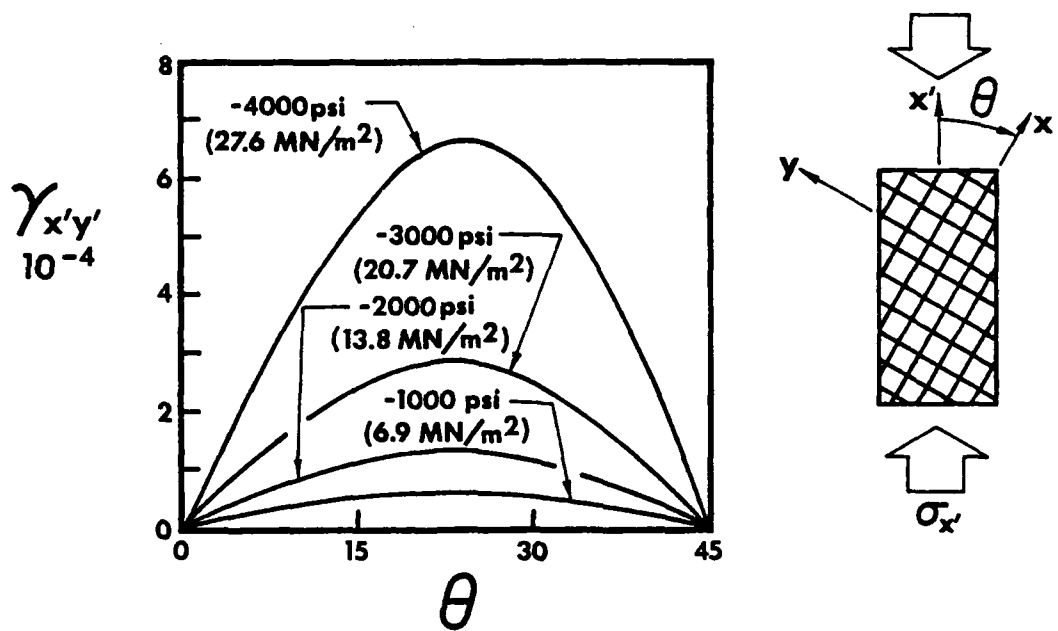FIGURE 3.36 SHEAR STRAIN UNDER OFF-AXIS TENSION LOADING IN xy-PLANE

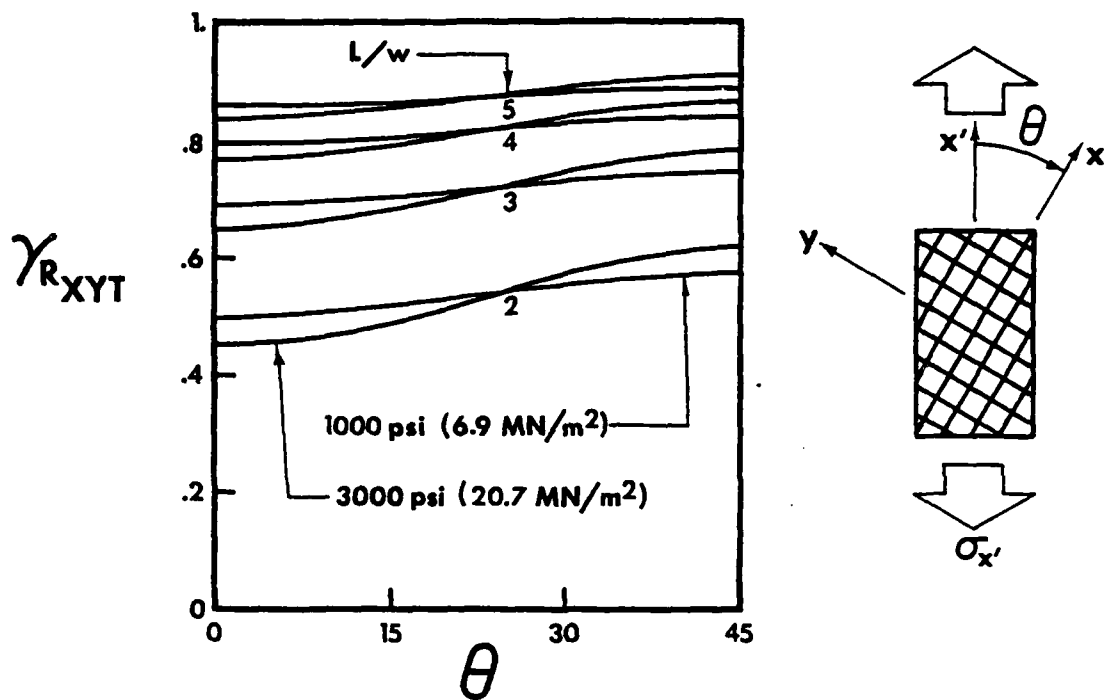FIGURE 3.37 SHEAR STRAIN UNDER OFF-AXIS COMPRESSION LOADING IN xy-PLANE

FIGURE 3.38   SHEAR STRAIN REDUCTION FOR OFF-AXIS TENSION LOADING IN xy-PLANE
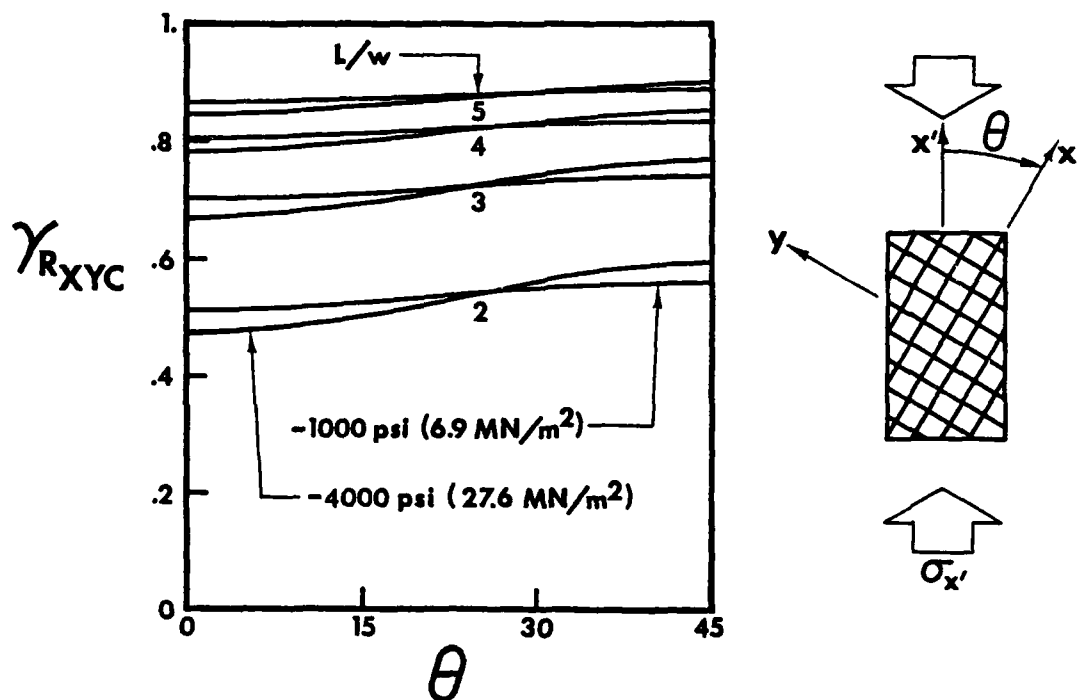
FIGURE 3.39   SHEAR STRAIN REDUCTION FOR OFF-AXIS COMPRESSION LOADING IN xy-PLANE

and 3.39. Actually, the tension and compression modulus factors are essentially one, so no adjustment is necessary for normal strains. For shear strains, the reductions are shown for tension loading in Fig. 3.38 and for compression loading in Fig. 3.39 where we see that the reductions depend mainly on the value of L/w. That is, the reductions are a weak function of stress level and of off-axis angle.

3.6 COMPARISON OF PREDICTED AND MEASURED STRAIN RESPONSE FOR UNIAXIAL OFF-AXIS LOADING OF AVCO MOD 3a CARBON-CARBON

Starrett, Weiler, and Pears subjected specimens of AVCO Mod 3a carbon-carbon to uniaxial tension and compression off-axis loading in the xy- and xz- planes. Their specimens have length-to-width ratios of approximately four and five (approximate because of specimen fillets). The Jones-Nelson-Morgan nonlinear multimodulus material model developed in Section 3.4 is used in the MULTIAX computer program to predict uniform strain state strains under the off-axis loading applied to the test specimens. Also in the MULTIAX program are strain corrections caused by shear coupling for the length-to-width ratios of the actual test specimens as described in Section 3.5.

Following are the predicted and measured strain response for these specimens used to validate the Jones-Nelson-Morgan material model. Generally, the uniaxial loading is applied at $22\frac{1}{2}°$ to the x-direction in the xy-plane and in the xz-plane. In only one case is response at $67\frac{1}{2}°$ to the x-direction measured. Shear loading is also applied, and the results are used as another independent validation of the Jones-Nelson-Morgan model predictions. The word independent is used because no shear behavior is used to define or construct the Jones-Nelson-Morgan model.

The xy-plane tension stress-strain behavior is shown in Fig. 3.40 where the x-direction behavior (identical to the y-direction behavior) is displayed along with the behavior at 45° to the x-direction (the 45xy curve). Those two curves are part of the behavior used to define the Jones-Nelson-Morgan material model in Section 3.4. The model is used to predict the response at $22\frac{1}{2}°$ to the x-direction which is very close to the measured response. A similar set of curves is shown for the xy-plane compression behavior in Fig. 3.41. However, the Jones-Nelson-Morgan
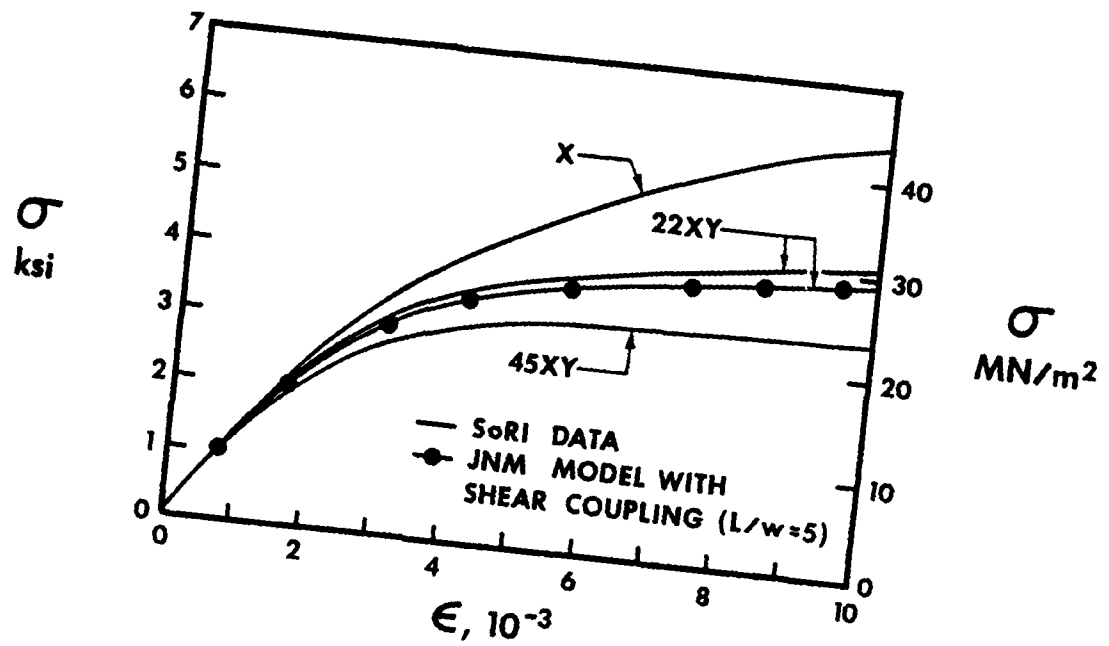
108

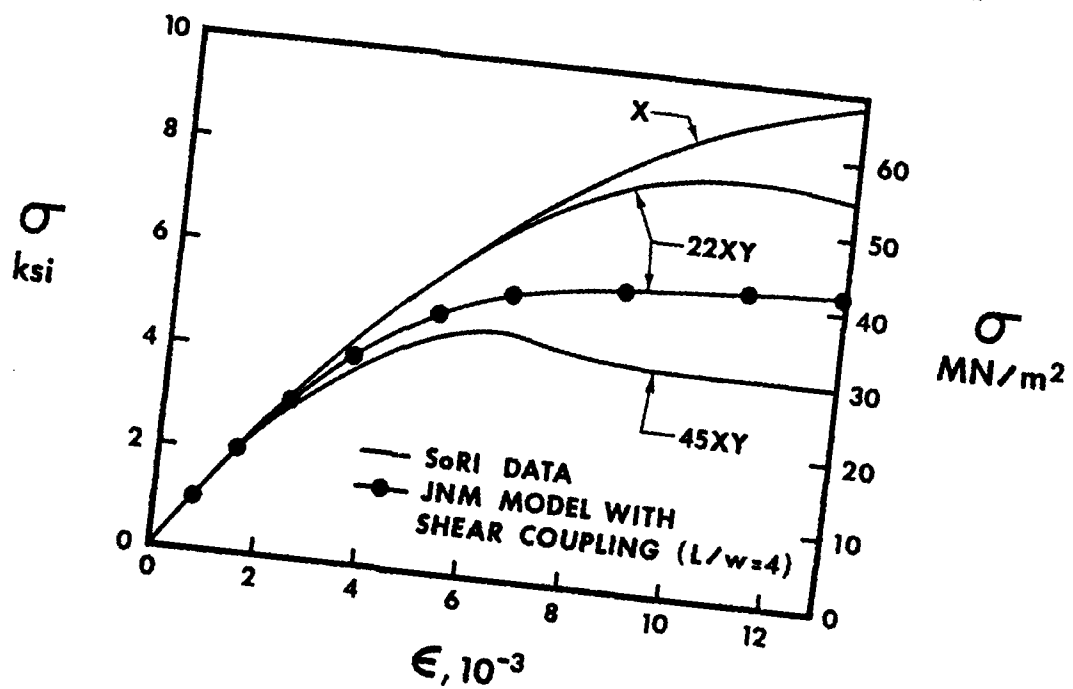FIGURE 3.40   TENSION STRESS-STRAIN BEHAVIOR IN xy-PLANE

FIGURE 3.41   COMPRESSION STRESS-STRAIN BEHAVIOR IN xy-PLANE

109

model is not forced to dip as low as the actual 45xy curve does. Even so, the predicted response at 22½° is well below the measured response. However, the measured response looks quite high in that it seems to be too close to the x-direction behavior and not close enough to the behavior at 45° to the x-direction.

The xz-plane tension behavior is shown in Fig. 3.42 where the x-direction behavior, z-direction behavior, and the behavior at 45° to the x-direction (the 45xz curve) are displayed. Those three curves are part of the behavior used to define the Jones-Nelson-Morgan material model in Section 3.4. The model is used to predict the response at 22½° and 67½° to the x-direction. The predicted response at 22½° (the 22xz curve) is quite close to the measured behavior. On the other hand, the predicted response at 67½° (the 67xz curve) is above the measured behavior. However, the measured 67½° response appears a bit low, i.e., it would seem reasonable for the measured response to be closer to the z-direction response that occurs. A similar set of curves is shown for the xz-plane compression behavior in Fig. 3.43. There, the predicted response at 22½° to the x-direction is below the measured response. The predicted 22½° response does not rise significantly when the z-direction behavior is modeled as a continuously rising curve instead of the broken curve in Fig. 3.43. That is, even if we ignore whatever physical reason that causes the broken curve and assume it won't happen in off-axis loading, we don't obtain a higher 22xz predicted response.

The measured and predicted xy-plane shear response is shown in Fig. 3.44. There, we see that the predicted response is somewhat below the measured response. For the xz-plane in Fig. 3.45, the predicted response is first higher and then lower than the measured response. In both cases, the predicted response is reasonably close to the measured response,
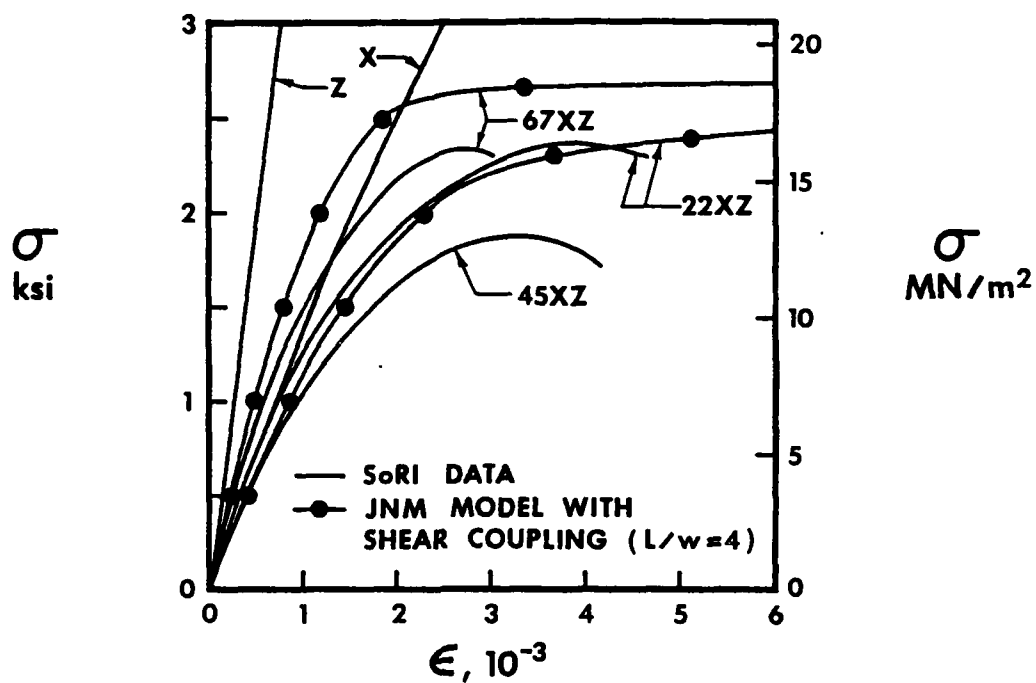
110

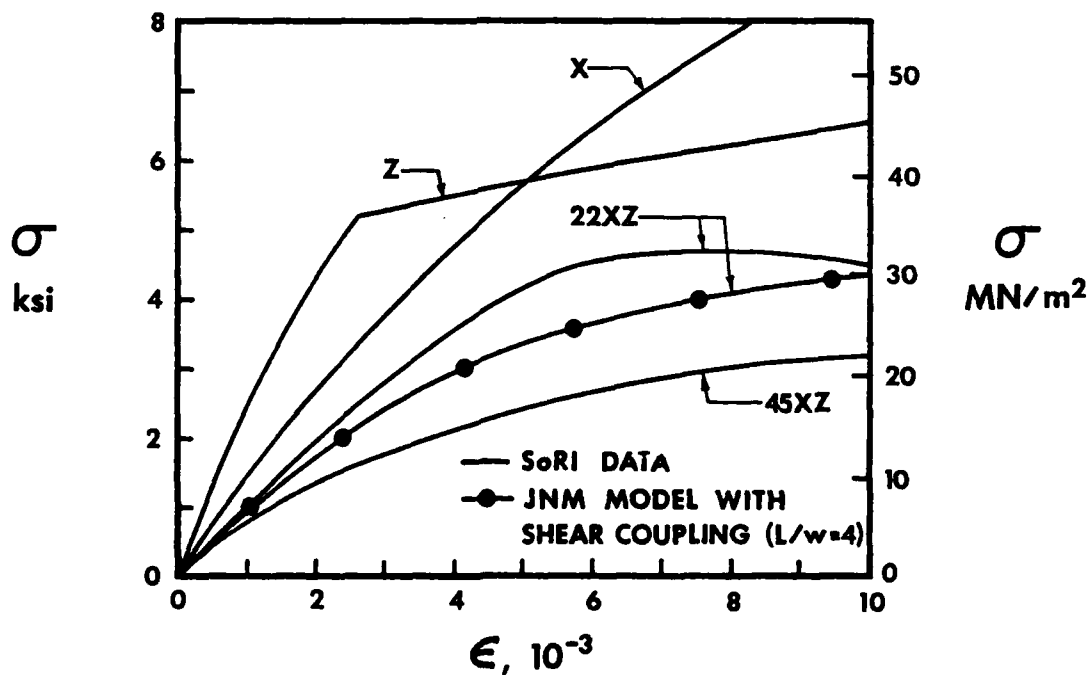FIGURE 3.42   TENSION STRESS-STRAIN BEHAVIOR IN xz-PLANE

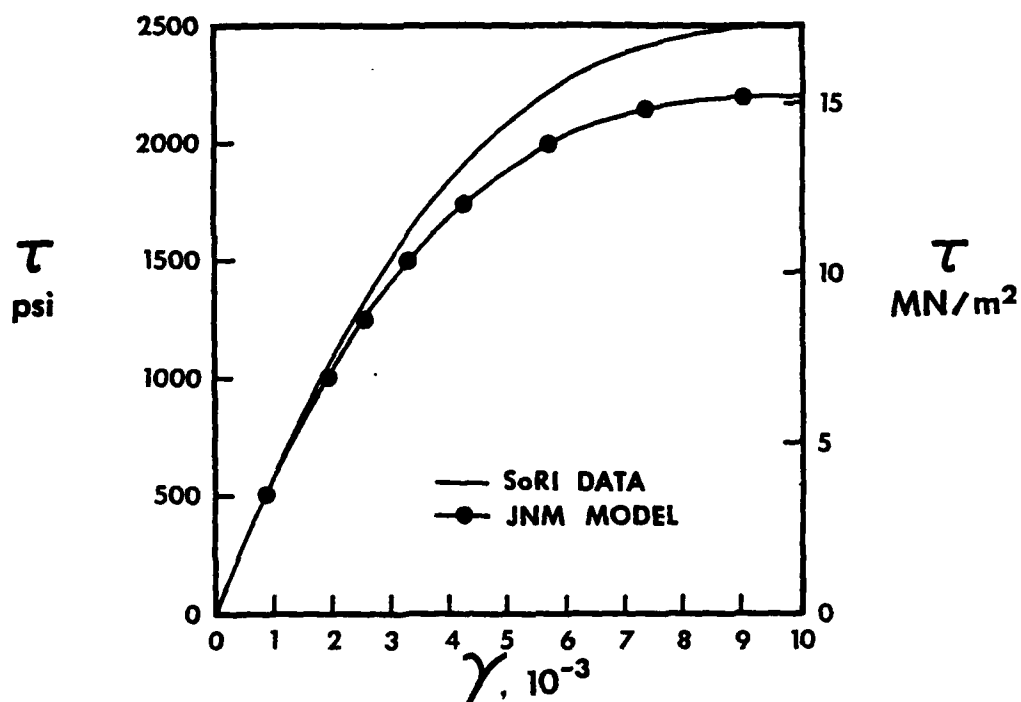FIGURE 3.43   COMPRESSION STRESS-STRAIN BEHAVIOR IN xz-PLANE
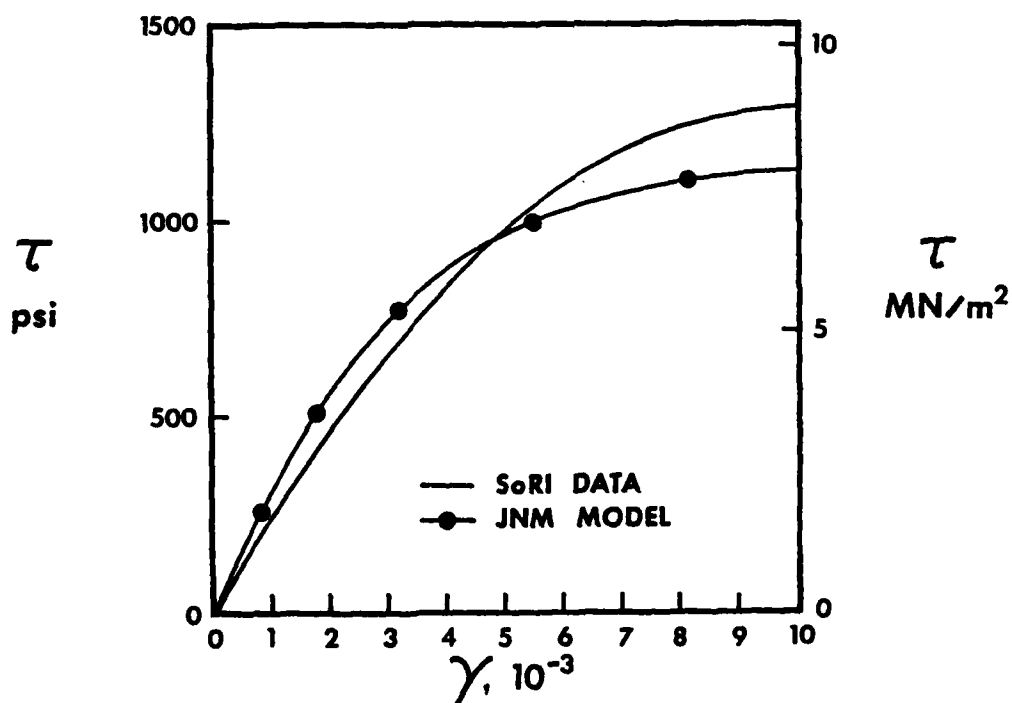
FIGURE 3.44   SHEAR STRESS-STRAIN BEHAVIOR IN xy-PLANE

FIGURE 3.45   SHEAR STRESS-STRAIN BEHAVIOR IN xz-PLANE

112

especially when we consider the imperfect nature of the shear test [38].

3.7 CONCLUDING REMARKS

The class of fiber-reinforced composite materials called carbon-carbon is investigated from the standpoint of mechanical response to loading. This class is found to have many characteristics that require modeling and analysis techniques well beyond in complexity those used for simpler materials. The possible efforts for correlation between predicted and measured response are discussed in order to begin to define a plan for the rational development and validation of suitable material models to be used in design analysis of rocket nozzles and other carbon-carbon applications. Then, a specific material model is developed for a representative carbon-carbon, namely AVCO Mod 3a, a rectangularly orthotropic material. Next, a single response measurement, the uniaxial off-axis loading test, is discussed from the standpoint of how to account for the shear coupling which for orthotropic materials is inherent to that test. A method for adjusting predicted strain response to account for the shear coupling is developed. Then, strain response predictions for off-axis loading in two planes of AVCO Mod 3a carbon-carbon are compared with measured response. The response predictions are quite reasonable when we consider the fact that stress-strain data used to define the Jones-Nelson-Morgan model are based on "most probable value" curves. "Most probable value" curves are an approximate (but statistically incomplete) representation of a collection of somewhat inconsistent and highly variable (from billet to billet) stress-strain curves. Thus, agreement between predicted and measured response is no guarantee of material model validity nor is disagreement necessarily an indication of material model invalidity. However, the Jones-Nelson-Morgan nonlinear multimodulus material model

appears to be a reasonable representation of carbon-carbon behavior, although the model must be validated for more complex strain response than the present uniaxial off-axis loading test.

4. SUMMARY

The Jones-Nelson-Morgan nonlinear material models have been developed and employed for several materials of interest for aerospace structures as listed in Table 4-1. There, the material modeling capability is seen to be most highly advanced for carbon-carbon and ATJ-S graphite as evidenced by the fact that the most sophisticated material model, a nonlinear multi-modulus material model, has been developed and used. The multimodulus characteristics of boron-epoxy, graphite-epoxy, and boron-aluminum have been investigated with a linear model. Also, nonlinear behavior of boron-epoxy, graphite-epoxy, and boron-aluminum has been investigated. However, the nonlinear and multimodulus characteristics of these materials have not been investigated simultaneously because the potential interaction between those characteristics should be small due to the low level of multimodulus behavior.

The types of correlations between experimental measurements of behavior and theoretical predictions are shown for the materials of interest in Table 4-2. ATJ-S graphite is the most comprehensively studied material. A representative set of configurations with various stresses excited relative to principal material directions has been examined for both thermal and mechanical loadings. Moreover, one of the ultimate applications of the material, a reentry vehicle nosetip with thermal and mechanical loading resulting in a multiaxial stress state is examined in Ref. 20. Experimental-theoretical correlation is somewhat sparse for the other materials.

Basically, significant multimodulus effects have been observed for granular composite materials such as ATJ-S graphite. On the other hand,

TABLE 4.1   LEVEL OF MATERIAL MODEL FOR VARIOUS COMPOSITE MATERIALS

MATERIAL	TYPE OF MATERIAL	NUMBER OF NONLINEARITIES		MATERIAL MODEL		
		TENSION	COMPRESSION	MULTIMODULUS ELASTIC	NONLINEAR	NONLINEAR MULTIMODULUS
ATJ-S GRAPHITE	TRANSVERSELY ISOTROPIC	5	5			✓
BORON-EPOXY	ORTHOTROPIC LAMINA	1	1	✓	✓	
GRAPHITE-EPOXY	ORTHOTROPIC LAMINA	1	1	✓	✓	
BORON-ALUMINUM	ORTHOTROPIC LAMINA	3	3		✓	
CARBON-CARBON	ORTHOTROPIC LAMINA AND ANISOTROPIC 3-D WEAVE	4-9	4-9			✓

TABLE 4.2   COMPARISONS BETWEEN PREDICTED AND MEASURED BEHAVIOR FOR VARIOUS COMPOSITE MATERIALS

MATERIAL	COMPARISON WITH EXPERIMENT				
	UNIAXIAL		BIAXIAL		
	PMD*	OFF-AXIS	TUBE	DISK	LAMINATE
ATJ-S GRAPHITE	✓	✓	✓	✓	N/A
BORON-EPOXY	✓	✓			✓
GRAPHITE-EPOXY	✓	✓			
BORON-ALUMINUM	✓				✓
CARBON-CARBON	✓	✓			

*PMD = PRINCIPAL MATERIAL DIRECTIONS

116

the importance of multimodulus effects for fiber-reinforced composite materials is somewhat mixed. The epoxy-based composites (boron-epoxy and graphite-epoxy) do not exhibit strong multimodulus or nonlinear effects under rcom temperature and normal humidity conditions, but are expected to have enhanced effects at elevated temperatures and humidities. Carbon-carbon composites exhibit strong multimodulus and nonlinear effects. Irrespective of the specific material, both multimodulus effects and nonlinear effects have been demonstrated to be susceptible to rational analysis which leads to material models suitable for use in design analysis.

5. REFERENCES

1. J. William Davis and N. R. Zurkowski, Put the Strength and Stiffness Where You Need It, Report T-STDB(101.05)R, Reinforced Plastics Division, Minnesota Mining and Manufacturing Company.

2. Structural Design Guide for Advanced Composites Applications, Vol. I, Material Characterization, 2nd Edition, Air Force Materials Laboratory, January 1971.

3. K. M. Kratsch, J. C. Schutzler, and D. A. Eitman, "Carbon-Carbon 3-D Orthogonal Material Behavior," AIAA Paper No. 72-365, AIAA/ASME/SAE 13th Structures, Structural Dynamics, and Materials Conference, San Antonio, Texas, 10-14 April 1972.

4. E. J. Seldin, "Stress-Strain Properties of Polycrystalline Graphites in Tension and Compression at Room Temperature", Carbon, 1966, pp. 177-191.

5. H. S. Starrett and C. D. Pears, Probable and Average Properties of ATJ-S(WS) Graphite, Southern Research Institute, AFML-TR-73-14, Volume 1, February 1973.

6. S. A. Ambartsumyan, "The Axisymmetric Problem of a Circular Cylindrical Shell Made of Material with Different Stiffness in Tension and Compression", Izvestiya adademii nauk SSSR, Mekhanika, No. 4(1965), pp. 77-85, Translation available from STAR as N69-11070.

7. S. A. Ambartsumyan and A. A. Khachatryan, "Basic Equations in the Theory of Elasticity for Materials with Different Stiffness in Tension and Compression", Inzhenernyi zhurnal, Mekhanika tverdogo tela, No. 2(1966), pp. 44-53. Translation available as LRG-67-T-12, The Aerospace Corporation El Segundo, California.

8. S. A. Ambartsumyan, "Equations of the Plane Problem of the Multimodulus Theory of Elasticity", Izvestiya akademii nauk armianskoi SSR, Mekhanika Vol. 19, No. 2(1966), pp. 3-19. Translation available as LRG-67-T-14, The Aerospace Corporation, El Segundo, California.

9. S. A. Ambartsumyan and A. A. Khachatryan, "Theory of Multimodulus Elasticity", Inzhenernyi zhurnal, Mekhanika tverdogo tela, No. 6 (1966), pp. 64-67. Translation available from STAR as N67-27610.

10. Farhad Tabaddor, "Two Dimensional Bi-Linear Orthotropic Elastic Materials," Journal of Composite Materials, October 1969, pp. 725-727.

11. Robert M. Jones, "Buckling of Circular Cylindrical Shells with Different Moduli in Tension and Compression", AIAA Journal, January 1971, pp. 53-61.

12. S. A. Ambartsumyan, "Basic Equations and Relations in the Theory of Elasticity of Anisotropic Bodies with Differing Moduli in Tension and Compression", Inzhenernyi zhurnal, Mekhanika tverdogo tela, No. 3 (1969), pp. 51-61. Translation available as LRG-70-T-1, The Aerospace Corporation, El Segundo, California.

13. Robert M. Jones and Dudley A. R. Nelson, Jr., "A New Material Model for Inelastic Biaxial Behavior of ATJ-S Graphite," AIAA Paper No. 74-396, AIAA/ASME/SAE 15th Structures, Structural Dynamics, and Materials Conference Las Vegas, Nevada, April 1974. Journal of Composite Materials, January 1975, pp. 10-27.

14. Hong T. Hahn and Stephen W. Tsai, "Nonlinear Elastic Behavior of Unidirectional Composite Laminae," Journal of Composite Materials, January 1973, pp. 102-118.

15. James M. Whitney, Informal presentation at Air Force Workshop on Durability Characteristics of Resin Matrix Composites, Columbus, Ohio, 30 September - 2 October 1975.

16. James G. Crose and Robert M. Jones, <u>SAAS III, Finite Element Stress</u>
    <u>Analysis of Axisymmetric and Plane Solids with Different Orthotropic,</u>
    <u>Temperature-Dependent Material Properties in Tension and Compression,</u>
    TR-0059(S6816-53), The Aerospace Corporation, San Bernardino,
    California, June 1975.

17. J. Jortner, <u>Multiaxial Behavior of ATJ-S Graphite</u>, McDonnell-Douglas
    Astronautics Company - West, Huntington Beach, California, Air Force
    Materials Laboratory Technical Report AFML-TR-71-253, December 1971.

18. C. D. Pears and H. S. Starrett, <u>Polygraphites Subjected to Temperature</u>
    <u>Stress Loadings</u>, Southern Research Institute, Birmingham, Alabama,
    Air Force Materials Laboratory Technical Report AFML-TR-73-59, March
    1973.

19. H. S. Starrett and C. D. Pears, <u>Probable and Average Properties of</u>
    <u>ATJ-S (WS) Graphite</u>, Southern Research Institute, Birmingham,
    Alabama, Air Force Materials Laboratory Technical Report AFML-TR-73-14,
    Volume I, February 1973.

20. Robert M. Jones, <u>Nonlinear Multiaxial Modeling of Graphitic and</u>
    <u>Carbon-Carbon Materials</u>, Southern Methodist University, Dallas, Texas,
    Air Force Materials Laboratory Technical Report AFML-TR-76-215,
    December 1976.

21. Frank C.Weiler, <u>DOASIS, A Computer Program for the Deformation Plastic,</u>
    <u>Orthotropic, Axisymmetric (and Plane) Solution of Inelastic Solids,</u>
    Volumes I-III, Weiler Research, Inc., Mountain View, California, Air
    Force Materials Laboratory Technical Report AFML-TR-75-37, September
    1975.

22. B. W. Cole and R. B. Pipes, <u>Filamentary Composite Laminates Subjected</u>
    <u>to Biaxial Stress Fields</u>, IIT Research Institute, Chicago, Illinois

and Drexel University, Philadelphia, Pennsylvania, Air Force Flight
Dynamics Laboratory Technical Report AFFDL-TR-73-115, June 1973.

23. H. S. Starrett, F. C. Weiler, and C. D. Pears, Thermostructural
Response of Carbon-Carbon Materials Under High Heat Flux Environments,
Southern Research Institute, Birmingham, Alabama, AFML-TR-74-232,
June 1975.

24. J. M. Whitney and A. W. Leissa, "Analysis of Heterogeneous Anisotropic
Plates", Journal of Applied Mechanics, June 1969, pp. 261-266.

25. Bo O. Almroth, "Influence of Edge Conditions on the Stability of
Axially Compressed Cylindrical Shells", AIAA Journal, January 1966,
pp. 134-140.

26. K. M. Kratsch, J. C. Schutzler, and D. A. Eitman, "Carbon-Carbon
3-D Orthogonal Material Behavior", AIAA Paper No. 72-365, AIAA/
ASME/SAE 13th Structures, Structural Dynamics, and Materials Con-
ference, San Antonio, Texas, 10-14 April 1972.

27. J. K. Legg, H. S. Starrett, H. G. Sanders, and C. D. Pears, Mechan-
ical and Thermal Properties of Mod 3, Southern Research Institute,
Birmingham, Alabama, Air Force Materials Laboratory Technical Re-
port AFML-TR-73-14, Volume IV, September 1973.

28. James G. Crose, Structural Assessment of Carbon-Carbon Materials
for the Carbon-Carbon Assessment Program (CCAP), Prototype Develop-
ment Associates, Inc., Costa Mesa, California, PDA Report No.
1011-00-01, January 1974.

29. H. S. Starrett, F. C. Weiler, and C. D. Pears, Thermostructural
Response of Carbon-Carbon Materials under High Heat Flux Environ-
ments, Southern Research Institute, Birmingham, Alabama, Air Force
Materials Laboratory Technical Report AFML-TR-73-255, Volume I,
February 1974.

30. Eric M. Ross, The Carbon-Carbon Assessment Program, Air Force Materials Laboratory Technical Report AFML-TR-74-39, September 1974.

31. J. K. Legg and C. D. Pears, Mechanical and Thermal Properties of Mod 3a, A Pierced Fabric Carbon-Carbon Material, Southern Research Institute, Birmingham, Alabama, Air Force Materials Laboratory Technical Report AFML-TR-74-211, December 1974.

32. J. K. Legg, H. G. Sanders, H. S. Starrett, W. T. Engelke, and C. D. Pears, The Carbon-Carbon Assessment Program, Supplement I (Appendix A), Materials Characterization, Southern Research Institute, Birmingham, Alabama, Air Force Materials Laboratory Technical Report AFML-TR-74-39, Supplement I, January 1975.

33. J. K. Legg, H. G. Sanders, H. S. Starrett, W. T. Engelke, and C. D. Pears, The Carbon-Carbon Assessment Program, Supplement 5 (Appendix E), Failure Analysis, Southern Research Institute, Birmingham, Alabama, Air Force Materials Laboratory Technical Report AFML-TR-74-39, Supplement 5, January 1975.

34. H. S. Starrett and C. D. Pears, Elastic Compliances for ATJ-S Graphite and Mod 3a Carbon-Carbon, Southern Research Institute, Birmingham, Alabama, Air Force Materials Laboratory Technical Report AFML-TR-74-271, February 1975.

35. James G. Crose, ASAAS, Asymmetric Stress Analysis of Axisymmetric Solids with Orthotropic Temperature-Dependent Material Properties that can Vary Circumferentially, TR-0172(S6816-15)-1, The Aerospace Corporation, San Bernardino, California, December 1971.

36. N. J. Pagano and J. C. Halpin, "Influence of End Constraint in the Testing of Anisotropic Bodies", Journal of Composite Materials, January 1968, pp. 18-31.

122

37. Robert M. Jones, <u>Mechanics of Composite Materials</u>, McGraw-Hill, 1975.

38. Nicolae Iosipescu, "New Accurate Procedure for Single Shear Testing of Metals", <u>Journal of Materials</u>, September 1967, pp. 537-566.